DOCTORAATSPROEFSCHRIFT

2008 | Faculteit Wetenschappen

A MIP, Molecularly Imprinted Polymer, based impedimetric sensor for the detection of small MW molecules

Proefschrift voorgelegd tot het behalen van de graad van
Doctor in de Wetenschappen, richting natuurkunde, te verdedigen door:

Ir. Ronald THOELEN

Promotor: prof. dr. Patrick Wagner
Copromotor: prof. dr. Thomas J. Cleij

universiteit hasselt

INSTITUUT VOOR MATERIAALONDERZOEK

DOCTORAATSPROEFSCHRIFT

2008 | Faculteit Wetenschappen

A MIP, Molecularly Imprinted Polymer, based impedimetric sensor for the detection of small MW molecules

Proefschrift voorgelegd tot het behalen van de graad van
Doctor in de Wetenschappen, richting natuurkunde, te verdedigen door:

Ir. Ronald THOELEN

Promotor: prof. dr. Patrick Wagner
Copromotor: prof. dr. Thomas J. Cleij

universiteit hasselt

INSTITUUT VOOR
MATERIAALONDERZOEK

Acknowledgements

Throughout my work that led to this thesis I had the opportunity and pleasure to meet, collaborate and interact with several persons. I would like to thank these persons in this short foreword…

Prof. dr. Patrick Wagner, Paddi, mijn promotor, bedank ik natuurlijk als eerste. Jij hebt mij de kans gegeven om na mijn master stage, een doctoraat te beginnen. Bedankt voor je vele suggesties en dat je altijd klaar stond met een brede glimlach om me verder te helpen. Ik vond het dan ook plezant als ik iets kon terug doen door je te helpen met je presentaties te maken op de computer. Vielen herzlichen Dank für alles.

Daarnaast Prof. dr. Thomas J. Cleij, mijn copromotor, bedankt voor al jouw hulp. Jij stond altijd gewapend met een blikje cola klaar om mijn chemische vragen te beantwoorden en onze MIP groep in het juiste spoor te houden. Ook tijdens de laatste fase, bij het corrigeren en het redigeren van de teksten heb ik heel veel van jou geleerd.

Mijn mede bureau-bewoners, Peter, Sylvia en Pieter, het BIOS-groepje, we hebben ons mannetje gestaan ten opzichte van de andere groepen op het IMO. Dankzij onze goede begeleiding van masterstudenten hebben we ons BIOS-groepje zelfs kunnen uitbreiden. Het was plezant en leerrijk om met jullie samen te werken. Ik zal die tijd nooit vergeten.

Ik mag natuurlijk ook niet mijn scheikundige collega's vergeten. Jan en Frederik, ik ken niemand die betere MIPs kunnen maken als jullie. Dankzij jullie is mijn kennis van de chemie er ook deftig op vooruit gegaan. Ik herinner mij onze MIP

vergaderingen, de viering van onze prijzen en de dagdromen achteraf over hoe we een MIP spin-off gingen oprichten. Als die er ooit komt, je weet me te vinden.

Voor de fluorescentiemetingen kon ik steeds rekenen op de steun van dr. Martin vandeVen en Prof. dr. Marcel Ameloot. Bedankt voor altijd een luisterend oor te zijn tijdens de PhD vergaderingen.

In deze thesis mag ik niet vergeten een heel aantal studenten te bedanken die aan dit onderzoek hebben meegewerkt. Dit zijn Rob Vansweevelt, Jamie Drossaerts, Tim Vangansewinkel, Karel Knez, Kasper Eersels, Lars Grieten, Jan Alenus, Danniëlle Benning en Kelly Houben. Ik vond het plezant om jullie te mogen begeleiden en ik hoop dat ik jullie wat heb bijgeleerd.

Verder heb ik veel hulp gehad bij de eerste stap naar een miniaturisatie van de sensor opstelling van Ward, Jan en Lieven. Jan, Bart en Kris mag ik ook niet vergeten, jullie vonden altijd wel een gaatje om wat SEM fotootjes te maken. Als er iets met de computer scheelde stond Erik altijd paraat, bedankt. Johnny, jij was er als ik een of ander technisch probleem had en maakte de tekeningen voor de werkplaats. Ook Johan van de werkplaats, mag ik niet vergeten, hij zette mijn hersenspinsels in iets tastbaar om. Hilde en Christel, jullie zorgden dat alles vlotjes verliep in de labo's. Ik wil ook nog het secretariaat, Lea, Relinde, Marina, Els, bedanken om tijdens mijn doctoraat alle administratieve zaken vlotjes te laten verlopen.

Wouter en Rob mijn carbuddies, carpoolen samen met jullie was niet gewoon carpoolen. Onze roadkills, La Chouffe in de kaf, een ritje door de bos, de grapjes op het werk, de ambi, 60 baantjes, jingle bells... het zijn maar een aantal kernwoorden van de vele leuke herinneringen. Jullie zijn vrienden voor het leven, deze tijd vergeet ik nooit meer.

Ik kan voor iedereen van het IMO wel een leuke herinnering ophalen maar dan zou mijn voorwoord te uitgebreid worden. Ik ga jullie met een paar woorden samenvatten en de herinneringen die halen we wel op bij een flesje La Chouffe.

Rob M (de gekke van Dilsen), Michael (alwetende), Ilse (dat is gek), Evi (shake it), Koen (droog maar zo goed), Sabine (seg), Lars (eagle eye), Jan (Ironman), Bert (real girls), Oliver (sweet),...

Jan ik wens je veel succes met de verderzetting van dit werk. Ik zal zeker nog wel langskomen om eens te horen wat de laatste nieuwe ontwikkelingen zijn. Het is fijn om te weten dat mijn onderzoek in goede handen is.

Mama, papa, en Severine, jullie mag ik ook niet vergeten. Het is een drukke periode geweest: mijn doctoraat, de bouw, ... Jullie waren er altijd voor me. Het was fijn te weten dat ik altijd op jullie kon rekenen.

Tot slot Ann, mijn schatje, we wonen nu een aantal weekjes in ons huisje. Ik vind het super. 2008 zal een jaar worden dat ik niet snel zal vergeten, mijn thesis, de verhuis, ... bedankt om deze schitterende momenten samen met mij te beleven en er te zijn voor mij. Jij bent er één uit de duizend.

"If we knew what it was we were doing,

it would not be called research, would it?"

Albert Einstein

Table of contents

Abstract

Currently there is an increasing demand for sensors for medical, environmental and industrial applications with strong requirements concerning selectivity, sensitivity and selectivity. Ordinary biosensors make use of biological systems, such as antibodies, enzymes, cells, etc., as recognition element. These bio-molecules posses a high selectivity and affinity, however they are not available for any target molecule and are not resistant against hostile environments, e.g. high temperatures, high and low pH or organic solvents. As proof of principle, a MIP, molecularly imprinted polymer, based sensor for L-nicotine, $C_{10}H_{14}N_2$, has been developed. Furthermore, the first step was made for detecting a more medical relevant molecule, histamine, a mediator.

The imprinting technique is based on the development of a non-covalent complexes formed between the target molecule and suitable functional monomers, being methacrylate (MAA). Subsequently cross-linker, ethylglycol dimethacrylate (EGDM) is added to this mixture to form a matrix in which the complexes are fixed. After extraction of the target molecule from this matrix, a tailor-made highly selective synthetic receptor is created which can rebind the anlyte according to its shape and functionality. For further processing the bulk monolith of the polymer is mechanically grinded to small micro-particles. Besides the MIP, a non-imprinted polymer, NIP, is synthesized. This acts as a reference material to be able to distinguish non-specific adsorption of the target to the surface of the MIP or NIP.

Optical batch-rebinding experiments showed specific binding of nicotine and a clear difference could be made between L-nicotine en L-cotinine, the oxidized

form of nicotine, which only differs one oxygen atom. Due to the heterogeneous character of the binding sites of the MIP the Freundlich isotherm was used to model the binding characteristics.

To obtain a sensing device the micro particles were glued on a metal electrode using a conjugated polymer OC_1C_{10}-PPV, allowing electronic detection based on the impedance principle. The surface coverage was investigated using optical microscopy and scanning electron microscopy. The coverage of the samples was about 20%.

As a second reference technique fluorescence spectroscopy was used. The idea was, when the binding site would be close enough to the conjugated polymer chain the fluorescence of the conjugated polymer would be quenched. However, the measurements revealed no indication whether L-nicotine or L-cotinine could quench the fluorescence.

Impedance spectroscopy is used to obtain an electronic read out. By measuring the impedance in the lower frequency range, below 1 kHz, small changes at the interface of the electrode and the solution can be visualized. The impedance is measured time-resolved for four different channels inside the measurement device. The measurements are carried using an impedance analyzer. Also, the first step is made towards a hand-held device. A apparatus was developed which could track impedance changes of eight different channels at a fixed frequency. Upon introduction of L-nicotine an impedance increase was visualized. This increase was also visible for the reference channels, NIP and blank polymer, but here the rise was less. This augmentation is probably due to non-specific adsorption at the surface of the material. The impedance sensor shows to be very sensitive for the target molecule L-nicotine and insensitive for the resembling molecule L-cotinine. The response time was only a few minutes with a detection limit of 0.3 ng/ml within a linear range of 2 to 5 nM for the L-nicotine MIP-based sensor.

The gravimetric principle can also be applied to investigated the binding properties of the MIP sensor. A quartz crystal is functionalized in the same way as with the impedance sensing technique. In this way a microbalance is obtained. The resonance frequency of the quartz is dependent on the mass

loading of the surface. When L-nicotine is bound to the MIP a frequency decrease is visualized. In this way a MIP based quartz crystal microbalance, QCM, was created which was sensitive for the presence of L-nicotine, while showing little affinity for the resembling L-cotinine. The NIP based QCM sensor showed a lower affinity for both molecules. These results confirmed the conclusion from the impedance measurements. This method allowed also for the possibility of flushing the measurement cell. This showed the possibility of regeneration the MIP sensor when flushed with distilled water. The first tests were also performed towards a more medical relevant sensor. A histamine MIP was used instead of the L-nicotine MIP. Histamine is a molecule which is involved in different biochemical processes. For example it plays an important role in the gastrointestinal tract, where it is in indicator for stress. This sensor showed a higher affinity compared to the L-nicotine sensor.

This project initiated the further research towards a MIP based impedimetric sensor. Using a relative easy method, a cheap and fast sensor was developed with high sensitivity, enabling it to measure small molecules for pharmaceutical, environmental, diagnostic or biotechnical applications. The suggestion for further work in this field is therefore, trying to develop a MIP based impedimetric sensor for molecules with a large field of applications. Next, the miniaturization of the sensor has to be further investigated making the step to a hand-held device.

Nederlandse samenvatting

Vandaag de dag is er een stijgende vraag naar sensoren voor toepassingen in verschillende gebieden zoals geneeskunde, milieu en voeding. Er worden steeds hogere eisen gesteld aan de sensitiviteit, selectiviteit en stabiliteit van sensoren. In veel sensoren worden natuurlijk voorkomende macromoleculen, zoals antilichamen en enzymes, gebruikt als herkenningslaag voor de sensor. Deze macromoleculen bezitten een zeer grote selectiviteit en affiniteit maar zijn niet voor elk doelmolecule beschikbaar en niet bestand tegen vijandige omgevingen zoals hogere temperaturen, hoge of lage pH of organische solventen. Een oplossing hiervoor is te werken met een synthetische herkenningslaag op basis van molecularly imprinted polymers (MIPs). Om de werking van de sensor aan te tonen, is er sensor ontworpen voor het detecteren van L-nicotine. Verder is er ook de eerste stap gezet naar een sensor met meer biomedische toepassingen, namelijk een MIP-sensor voor de detectie van histamine.

De imprinting techniek is gebaseerde op het vormen van niet-covalente complexen tussen het doelmolecule en het geschikte functionele groepen, zijnde in dit geval methacrylaat (MAA) Een crosslinker, te weten ethylglycol dimethalcrylaat (EGDM) zal dit pre-polymerisatie complex vernetten. Na verwijdering van het doelmolecule blijft een holte achter in het polymeer waarin het terug kan binden volgens vorm en functionaliteit. Voor verdere metingen werd het bulk polymeer fijngemalen tot microdeeltjes. Als referentiemateriaal is er ook een niet-geïmprint polymeer, NIP, gesynthetiseerd. Deze NIP werd op dezelfde manier vervaardigd behalve dat het doelmolecule niet is toegevoegd aan het polymeermengsel.

Optische batch-rebindingexperimenten hebben aangetoond dat de microdeeltjes zeer specifiek L-nicotine kunnen binden, en dat ze zelfs het onderscheid kunnen maken tussen L-nicotine en L-cotinine, een geoxideerde vorm van L-nicotine met slecht één zuurstof atoom verschillend. De metingen vertoonden een heterogene distributie van de bindingsplaatsen welke met behulp van het Freundlich model kon worden benaderd.

Deze MIPs zijn vervolgens geïmplementeerd in een sensor. De herkenningslaag bestaat uit moleculair geimprinte PMAA micropartikels die vastgezet zijn op een metaalelektrode in een dunne film van een halfgeleidend polymeer, OC_1C_{10}-PPV. De bezetting van de sensor is nagegaan met behulp van optische en electronenmicroscopie. De bezetting van de electrode bedroeg ongeveer 20%.

Als bijkomende karakterisatie methode werd geprobeerd de binding van het doel molecule met behulp van fluorescentie te detecteren. Helaas volgde uit de metingen dat L-nicotine geen invloed uitoefende op de fluorescentie van het halfgeleidende polymeer.

Impedantie spectroscopie werd gebruikt als elektronische uitlezing. Door de impedantie te volgen in het lage frequentie gebied, beneden 1 kHz, kunnen heel gevoelig veranderingen aan het oppervlak van de sensor waargenomen worden. Er werd een meetcel ontworpen die voor vier verschillende kanalen de impedantie simultaan kon volgen in de tijd. Er werden metingen uitgevoerd met een impedantieanalyzer, maar er werd ook een huisgemaakte impedantietoestel gebruikt welke de impedantie voor een vaste frekwentie vlugger en nauwkeuriger kon volgen. Bij het toevoegen van nicotine werd er steeds een impedantie verhoging vastgesteld. Deze verhoging trad ook op voor het kanaal met NIP deeltjes en het blanko halfgeleidend polymeer, maar slechts in mindere mate. Dit is te wijten aan niet specifiek adsorptie aan het oppervlak van de zowel NIP als het halfgeleidend polymeer. De sensor bleek ook ongevoelig te zijn wanneer deze werd blootgesteld aan het gelijkaardige molecule, L-cotinine. De detectie limiet was 0.3 ng/ml in een bereik van 2 nM to 5 nM voor de MIP gebaseerde L-nicotine sensor.

De kwarts kristal microbalans, QCM, kon ook gebruikt worden om de binding van de sensor te onderzoeken. Deze techniek laat toe heel gevoelig massa

verandering waar te nemen. Een kwartskristal werd gefunctionaliseerd op dezelfde methode als bij de impedantiemetingen. Naarmate dat er massa gaat binden op het oppervlak van het kristal zal de resonantie frekwentie gaan veranderen. Deze verandering kan dan omgerekend worden naar een massa toename. Deze techniek liet toe om de MIP bloot te stellen aan een achtergrond stroming van gedestilleerd water en dan om bepaalde tijdstippen concentraties van L-nicotine of L-cotinine toe te voegen. Hierdoor was het ook mogelijk de sensor te spoelen met gedestilleerd water na de meting waardoor de regeneratie succesvol kon getest worden. De meetresultaten van de kwarts microbalans konden eveneens met het Freundlich model vergeleken worden. De eerste tests met deze techniek toonden aan dat L-nicotine specifiek herkend kon worden van L-cotinine. De NIP gefunctionaliseerde kristallen gaven een kleinere massa toename in vergelijking met de MIP gefunctionaliseerde ksitallen. Dit bevestigde de resultaten van de impedantie metingen. Er werd met deze techniek ook de eerste stap gezet naar een meer medische toepassing door een MIP te meten die gevoelig is voor histamine. Een biochemische stof die betrokken is bij verscheidene fysiologische processen. Het speelt bijvoorbeeld een rol in het maagdarmkanaal, waar het een indicator is voor stress. De histamine sensor toonde een hogere affiniteit, vergeleken met de L-nicotine sensor.

Dit werkt toonde de eerste aanzet voor verder onderzoek naar de MIP gebaseerde impedimetrische sensor. Met een relatief eenvoudige methode verkregen we een sensor die goedkoop en snel is en gevoelig genoeg om bepaalde ziektemarkers, giftige stoffen of andere relevante molecules op te kunen sporen. Dit zal dus ook een suggesties zijn de opvolging van dit werk om verder MIP sensoren te ontwikkelen met een grotere toepasbaarheid. Verdere optimalisatie zal ervoor zorgen dat de sensor meer reproduceerbaarder wordt. Hiernaast kan de verdere miniaturisatie van de sensor plaatsvinden met het oog op een hand-held device voor de toekomst.

Chapter 1 - Introduction to bio- and chemo-sensors

During the last decades, research and development in the field of sensors has expanded exponentially in terms of financial investment, the published literature and the number of active researchers. Sensors provide information on our physical, chemical and biological environment. Since the chemical and physical properties of polymers may be tailored for particular needs, they gained importance in the construction of sensor devices. In this introduction chapter, different aspects of the sensor will be discussed. First the need for fast, label-free assays will be mentioned and next the 'new' materials used for these sensors, the different receptor layers and purposes of the devices are discussed. This chapter concludes with the aim of this study.

1.1 The need for fast, label-free assays

Imagine drug tests, which can be performed much quicker, metal ions or other polluting molecules, which are detected faster in the river nearby or different proteins, which are biomarkers for cancer or cardiovascular problems are traced immediately in a droplet of blood. These key problems in the society stress an urgent need in the diagnostics laboratories for accurate, fast and inexpensive devices, which can be routinely used. In this context, bio- or chemosensors are considered to provide viable solutions to the problems posed by healthcare industry. The biosensor market describes a wide area of interest. These sensors can have their use in bio-warfare, food quality control, environmental problems,

and pharmaceutical industry or to be used for medical point-of-care devices. In Figure 1-1 a classification of the wide variety of possible assays is given.
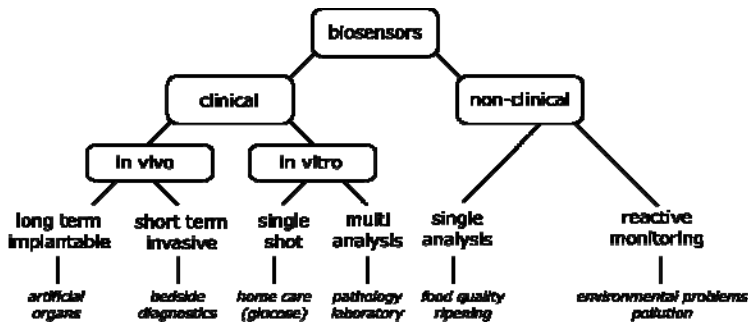
Figure 1-1: Variety of applications of bio- or chemosensors. [1]

The viability of developing such bio- or chemosensors commercially depends on many factors. There are besides technical barriers also economic obstacles. The devices should be amongst others robust, easy-to-use and have a reasonable shelf life. When these goals are obtained, a market should be chosen with a large outlet. There are some excellent examples of biosensors that made it to a commercial product. There is the pregnancy test, which consists of a qualitative detection, and the glucose sensor for diabetics, which is the first quantitative sensor. With the increasing knowledge about bio- and chemosensing and 'new' materials, which are currently entering the market, the possibility of increasing the number of commercial biosensors becomes more realistic. These sensors are not a replacement for the current expensive lab equipment, which handles typical blood or water samples. The fast and label-free assays are needed to make these tests more accessible for a broad public. This makes the early tracking of a certain disease or pollution much easier and faster. For example, novel sensor technology can play a pivotal role in early detection of breast cancer where the quick diagnosis plays an essential role in a happy ending for the patient. There are much more similar examples where bio- or chemosensors will play an important role in the near future.

1.2 Sensing devices

The word biosensor means according to a dictionary, 'a device that uses biological materials to monitor the presence of various chemicals in a substance' [2]. The first biosensor ever dates back to 51 BC. Cleopatra used slaves as food testers to detect poison in her food and beverages. More recently in the early days of coal mining, canaries were used to detect toxic gases in the tunnels. In Table 1-1 a brief history is given of the development of biosensing over the last decades.

Table 1-1: A brief history of biosensing. [3, 4]

1922	First glass pH electrode [5]
1956	Invention of the oxygen electrode by Prof. Leland Charles Clark Jr. [6]
1962	First biosensor: an amperometric enzyme electrode for glucose [7]
1970	Ion-selective field-effect transistor [8]
1972	First commercial biosensor: Yellow Springs Instruments glucose biosensor
1976	First bedside artificial pancreas, Miles Biostator
1980	First optic pH sensor for in vivo blood gases
1982	First fiber optic-based biosensor for glucose [9]
1983	First surface Plasmon resonance immunosensor
1984	First mediated amperometric biosensor for detection of glucose [10]
1987	Launch of the MediSense ExacTech™ blood glucose biosensor
1990	Launch of the BIACore SPR-based biosensor system
1992	i-STAT launches handheld blood analyzer
1996	Abott acquires MediSense
1998	Launch of LifeScan FastTake blood glucose biosensor
1999-2008	Academic literature reports of devices exploiting , nucleic acids, cell receptors, antibodies and intact cells, in combination with electrochemical, optical, piezoelectric and thermometric transducers

The previous table shows that the glucose sensor was the first biosensor, which reached the market. The ongoing developments and variations in detecting glucose lead the research for biosensors for different types of marker molecules. This trend is shown in Figure 1-2, where the amount of articles about biosensors is given as a function of years. We can see a booming of biosensor research starting from the 80s when the glucose sensor was introduced to the market. This discovery was a decisive step in biological analysis. The new term, biosensors, was created by combining the existing techniques, like amperometry, potentiometry, piëzo-electricity, optical, thermal, etc., with biological systems, such as enzymes, cells, chemical receptors or immunological

agents. It caused a major financial input for the developments leading to other commercial biosensing devices, all based on different measurement principles.
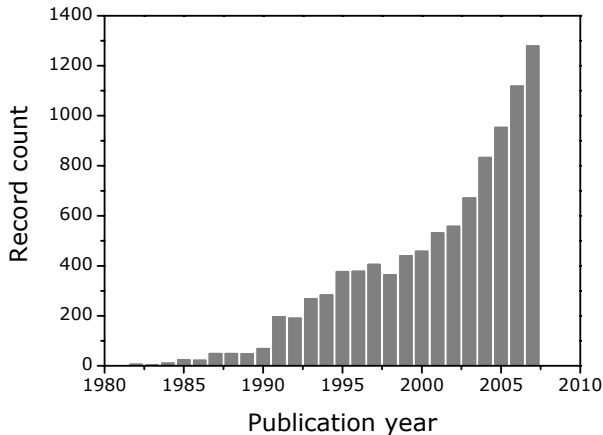
Figure 1-2: Biosensor record count in literature
according to Web of Science (search term: biosensor).

The dictionary definition used the word 'biological' materials. Why biological …, well the reason is because Nature's most important talent is the evolutionary development of systems capable of molecular recognition, distinguishing one molecule from another. In Figure 1-3 it can be seen how these two worlds come together, the one of nano-physics of the recognition event and the micro-physics of the sensor device.
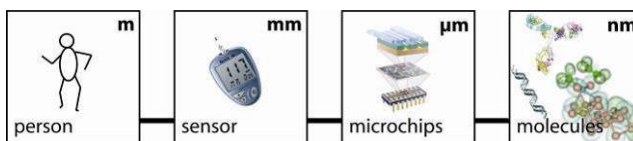
Figure 1-3: Length scale representation.

In Figure 1-4 the typical schematic layout of a biosensor is given. There are three main parts of the device: a recognition layer, the transducer layer and the read-out. The recognition element is the most important part of the sensor. This layer is able to bind, 'recognize', the target molecule in the actually to be tested

medium. This recognition is then translated by the transducer into a measurable signal.
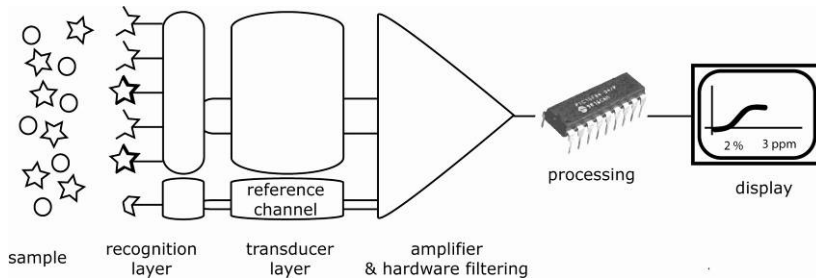
Figure 1-4: Schematic layout of a typical biosensor.

Depending on the actual type of translation, an electrochemical, optical or piëzo-electric readout is achieved. The choice of which type of transducer, recognition layer or read-out depends on the different requirements needed for the sensing device. A biosensor should respond selectively, continuously, rapidly, specifically and label free. The qualities of the sensor can be fine-tuned be choosing the right materials and readout for the right detector. For example, enzyme biosensors may respond as quickly as 30 seconds, but 15 minutes is acceptable for immunosensors. In order to define biosensors for use in the food industry, the types of biological events that might be acceptable for biosensor measurement need to be known and these may differ from the demands, which are needed for a clinical sensing device. The manner in which the recognition layer is implemented in the sensor design may dependent on the cost, life-time, implementation, etc. of the sensor. For example a disposable sensor does not require an expensive immobilization technique and sensor which are to be used multiple times need to be strongly bound.

1.2.1 Recognition layer

The classification of a biosensor is based on the receptor layer, which is chosen. The layer may consist of enzymes [11-14], antibodies [15-17], nucleic acids [18-20] or synthetic receptors [21-28]. The biological elements most used are enzymes. These can be used in purified form, or may be present in microorganisms or in slices of intact tissue. They are biological catalysts for

particular reactions and can bind themselves to a specific substrate. Antibodies have a different working principle. They will bind specifically with the corresponding antigen. They have no catalytic effect, which excludes some readout techniques. Despite this, they are capable of developing ultra-high sensitivity in biosensing. Considerable inventiveness is often needed to incorporate them into the sensor and to provide a signal for the transducer to measure. Thus far nucleic acids have been used much less. They operate selectively because of their base-pairing characteristics. They have great potential in identifying genetic disorders, cancers and viral infections. Enzymes, antibodies, nucleic acids are all biological materials. This means that they do not function well beyond typical biological conditions needed to keep the receptors active. This duality between stability and specificity is visualized in Figure 1-5.
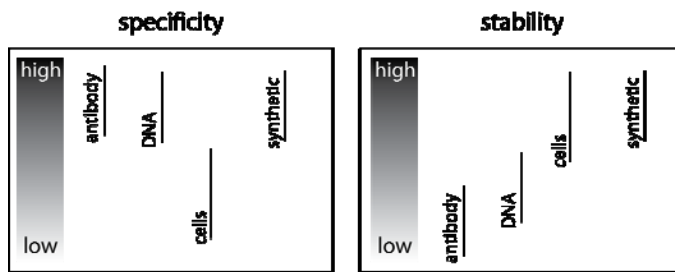
Figure 1-5: Duality between specificity and stability of a biosensor.

The basis for all biological processes associated with detection is molecular recognition, which is therefore of universal interest. This has inspired researchers to mimic the molecular recognition properties typically found for bio materials. In this way a synthetic receptor can be developed, which can operate at different conditions and can be custom made for specific target molecules.

1.2.2 Transducer

The key part of a biosensor is the transducer, which makes use of a physical change accompanying the binding event. There are several 'translations' possible as depicted in Figure 1-6.
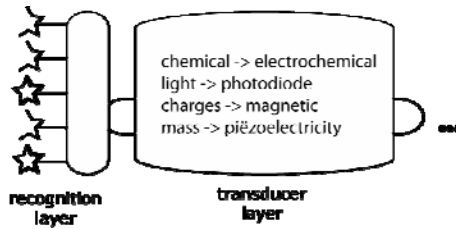
Figure 1-6: Different kinds of transductions towards a measurable signal.

When the 'translation' is caused by heat, the devices are called calorimetric biosensors. For the electrochemical biosensors, there are three possibilities. The potentiometric biosensors are based on changes in the charge distribution upon binding which causes an electrical potential. Further, amperometric devices measure movement of electrons, produced by a redox reaction. The conductimetric principle is used when the binding causes interface changes which influence the dielectric constant of the surface. These are the impedance based sensors.

Optical biosensors are based on light output produced by a binding reaction or a light absorbance difference between the reactants and products. Furthermore, when effects due to the mass of the reactants or products cause a signal, they are called microgravimetric biosensors, they are based on the piezo-electric properties of the transducer layer. Next, a pretreatment of the sample solution is possible with magnetic beads [29]. These bind specifically to the target molecules; in this case, the magnetic biosensors detect variations in the magnetic field. Based on the transduction an evolution in the generation of biosensors can be noted. In the first sensor designs, the binding reaction causes a byproduct, which diffuses to the transducer and subsequently causes a response. This is the case for the electronic glucose meters. The glucose is broken down by the enzyme, glucose oxidase, which causes the byproduct gluconic acid. This reaction consumes oxygen. The amount can be measured using the Clark electrode [6]. The next step is a sensor, which involves specific mediators between the reaction and the transducer in order to generate a signal. An example is the second-generation glucose sensor, in which redox

active species are used such as ferrocene derivatives. In this case, the oxygen is replaced by ferrocene and the concentration can be measured using an electrochemical oxidation [14]. In the third generation biosensor the reaction itself induces a response. This is the case for sensors based on the gravimetric principle were the binding directly induces a mass change.

Depending on the desired transduction, a suitable material can be chosen. In addition, a transducer material can be used as a support for another transducer material on which immobilization of receptors is easier. For example, a polymer transducer is not necessarily suitable for gravimetric detection. But a piëzo-electric material like quartz can be coated with a polymer to achieve a measurable signal. Polymers [30, 31], conjugated polymers [17, 24, 32], gold [16, 33-35], silicon [36-38], silicon oxide [39], diamond [40-44], graphite [45, 46] and carbon [47, 48] are all materials, which are being used for biosensing. There is a large choice and the number and combinations of materials is virtually infinite.

1.2.3 Immobilization of the receptor component

The choice of receptor and transducer is dependent on the application of the device. Only the method of immobilizing of the receptor to the transducer is more complex. The attachment of the receptors has to be reproducible and stable. There are several ways to connect the receptor with the transducer, as is depicted in Figure 1-7.
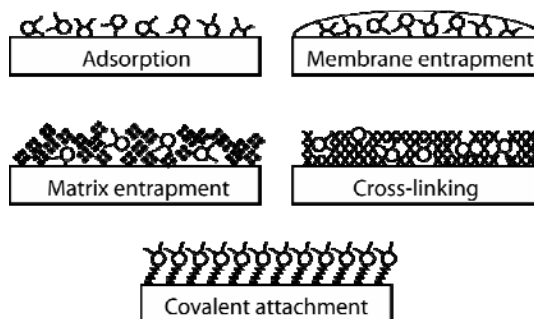
Figure 1-7: Different immobilization methods. [4]

The most straightforward way of immobilization is by adsorption onto a surface. This technique involves a minimum of preparation. There are two classes, physical and chemical adsorption. Physisorption is usually weak and occurs via the formation of van der Waals bonds, hydrogen bonds or charge-transfer forces. Chemisorption is much stronger and involves the formation of semi-covalent bonds. An example is the formation of SAMs by chemisorption of thiols onto gold surfaces.

Membrane entrapment or micro encapsulation is the word used for trapping the receptor behind a membrane. This is one of the early methods used with the glucose biosensors. It limits the contamination and biodegradation of the receptor. The membrane can be made permeable for certain compounds in order to have of preselection of molecules in the solution. Some example of membranes are cellulose acetate, which excludes proteins and slows transportation of interfering species, polycarbonate, a synthetic material which is non-permselective, collagen, a natural protein, and Teflon®, a synthetic polymer which is selectively permeable to gases such as oxygen.

Matrix entrapment is used when the receptor is trapped in a matrix of a gel or a polymer. The receptors are mixed in the transducer material, which involves close contact between receptor and transducer. Unfortunately, this can cause barriers to the diffusion of the target molecule, thus slowing the reaction. Also a part of the receptors are not accessible for the dissolved target molecules.

By the formation of strong bonds between the receptor and transducer a covalent attachment is achieved. This involves a transducer, which is tailor-made with the right functional groups. The advantage is the certainty that the receptor will not release during use. It is important to confirm that the covalent attachment does not affect the accessibility of the receptor.

By cross-linking the receptor and transducer, a bifunctional agent is used, which chemically embeds the two components. This causes also some diffusion limitations but this approach can be useful to stabilize adsorbed components to a surface.

By choosing the right immobilization method the lifetime of the biosensor is greatly enhanced. Typical lifetimes of immobilization techniques: [4]

- adsorption: 1 day,
- membrane entrapment: 1 week,
- physical entrapment: 3-4 weeks ,
- covalent binding: 4-14 months.

These values may depend also on the shelf life of the receptor, which is in turn again related to the application for which the device is used.

1.2.4 Read-out

Based on the choice of transducer a specific type of read-out is obtained. Five basic classes of read-out exist: optical, electrochemical, thermometric, gravimetric and magnetic. An electronic read-out is usually preferred. An electronic read-out is straightforward, while the sensor can be integrated in a hand-held device, with a numeric read-out and where no post processing of information is needed. However, the electronic read-out is not always the most sensitive form of read-out.

Most biosensor devices were originally based on optical detection. The binding of the target induced a change in the photometric properties of the transducer. Important techniques to measure this change are absorption spectroscopy, fluorescence spectroscopy, luminescence spectroscopy, internal reflection spectroscopy, surface plasmon resonance (SPR) and light scattering. [15, 49-51]

Electrochemical transducer systems are those that produce either an electrical signal due to a direct interaction with the recognition element or the interaction between the receptor causes a change in the dielectric properties at the interface resulting in a impedance change at the interface. These sensors are based on a bio-recognition element incorporated into or onto the electrode material. This enables for fast responses. [17, 18]

Thermometric biosensors measure the total heat energy absorbed or evolved during a biochemical reaction. This absorbed or evolved heat can be measured

by sensitive thermistors and is proportional to the molar enthalpy and to the product stoichiometry of the biochemical reaction. [52-54]

A piezoelectric read-out is obtained by using a quartz crystal microbalance, QCM, it comprises of a specifically cut thin disc of quartz crystal with electrodes plated onto either one or both of its surfaces. If this crystal is placed into an electrical circuit and the current is oscillated at a similar frequency to the fundamental mechanical oscillation frequency of the crystal then a resonant oscillation may be achieved. In simple terms, the resonant oscillatory frequency is dependent on several factors including chemical structure, density and thickness of the crystal and similar physical properties of the surrounding medium. Therefore, this frequency is also directly related to the amount or mass of material immobilized onto the surface of the crystal. [55-57]

Magnetic read-out is a very sensitive technique, which has the ability of single molecule detection. Magnetic beads are incorporated into the test solutions and bound to the target molecule. By pumping the solution through a device which measures changes in the magnetic field the amount of change is related to the concentration of target molecules. [29, 58, 59]

1.2.5 Performance factors

The most important property of a well functioning biosensor is a high selectivity, *i.e.* the ability to discriminate between different substrates. Together with selectivity, the device has to have a reasonable sensitivity range. This is usually sub-millimolar and can go down to the femtomolar range depending on the relevant concentrations of the target molecule. Conditions such as pH, temperature and ionic strength have to be considered, depending of the nature of the solution. The response time is preferably small with a not too long recovery time, if regeneration is possible. The working lifetime is determined by the lifetime and stability of the receptor and transducer layer.

1.3 The aim of the study

The main principles of biosensors have been explained in the previous sections. The goal of current biosensor research is to develop a sensor, which possesses the following properties:

- small size
- straightforward use
- manufacturability in large numbers
- fast in operation
- economical
- self calibrating
- minimal user action required

Keeping these properties in mind, the previous depicted receptors, transducers and different read-out possibilities can be scrutinized.

The sensing platform has to consist of a receptor, which is sufficiently stabile and capable of binding the target molecule in a specific and sensitive manner. It must be able to use tailor-made receptors for different types of applications, which can be implemented without interfering with the working principle of the device. The receptor chosen in this study is a synthetic receptor, a molecularly imprinted polymer, MIP. MIPs have a range of advantages when compared to natural biomolecules, see Table 1-2.

Table 1-2: Comparison of natural biomolecules used in sensors and MIPs [60].

Biomolecules (Ig's, enzymes, DNA, …)	MIPs
- Low stability	- MIPs are stable at low/high pHs, pressure and temperature
- High price of the enzymes and receptors	- Inexpensive and easy to prepare
- Generally poor performance in non-aqueous media	- MIPs can work in organic solvents
- Different natural biomolecules have different operational requirements	- Due to minimal operational requirements of MIPs, the design of MIP-based multisensor is relatively easy
- Natural receptors and enzymes exist for limited number of important analytes	- In principle, MIPs could be prepared for practically any compound
- Poor compatibility with micromachining technology and miniaturization	- Polymers are fully compatible with micromachining technology

The particular features, which make MIPs the target of this investigation, are: their high affinity and selectivity, which are comparable to those of natural receptors, their unique stability, which is superior to that of natural biomolecules, the simplicity of their preparation and the ease of adaptation to different practical applications. This method of obtaining a synthetic receptor is comparatively straightforward and readily to perform and can be extended to large-scale production. In the presence of a template molecule, functional monomers are polymerized, thus immobilizing this molecule in the polymer matrix. After polymerization, the template is removed and a nanocavity is left behind, which can rebind the target molecule by its shape and functionality. The main advantage of using MIPs in sensing devices is the possibility of synthesizing MIPs for a wide variety of compounds.. Most small-MW molecules do not posses a biological receptor and in these cases MIPs provide a viable alternative. Almost any molecule with a mass below about 5 kDa is suitable for imprinting, as such molecules can diffuse through the polymer network fast and therefore can also reach interaction sites deep within the inner structure of the MIP. For larger structures, such as many typical biomolecules, this strategy can not be applied. As an alternative, surface imprinting procedures can be used, in which these large molecules are imprinted on the surface using a stamping technique. This result is a functional surface with strong interactions with the templating species. [61]

The transducer used to immobilize the synthetic receptors is dependent on the read-out, which is desired. The read-out has to be a fast and straightforward technique capable of translating the recognition event in a measurable signal. In this study the change of the dielectric properties of the interface between the receptor and solutions is used to sense the binding of target molecules. Impedance spectroscopy is applied to investigate the influence of binding. In the experiments a specific frequency is searched where the change of the impedance represents the binding of the target molecule to the receptor. When this frequency is found a hand-held device can be developed operating at this frequency and which gives an electronic read-out relating to the concentration of target molecules in the sample being investigated.

Typical promising areas of MIP sensor applications are medical diagnostics, utilization of MIPs mimicking natural receptors for drug screening and for in vivo monitoring, environmental sensing, rapid detection of chemical and biological warfare agents, sensors for deep sea and space exploration. These applications mostly operate at harsh conditions and require high specificity and sensitivity, making them ideal application areas for synthetic sensors to operate.

Chapter 2 - Molecularly Imprinted Polymers

Molecular imprinting allows the creation of artificial recognition sites in synthetic polymers. It is based on a simple, but elegant, principle of building an own recognition site using the target molecule during polymerization. They have become an important class of synthetic materials, which mimic the molecular recognition of natural receptors. Hence, it is not surprising that the synonym for these artificial receptors is plastic antibodies [27].

2.1 Historical background

Figure 2-1 shows that the last five years witnessed a fast progress in the area of MIPs incorporated in sensing devices. However, even with this relatively new interest and research, the roots of molecular imprinting date back to the beginning of the 19th century and the pioneering work of a Soviet chemist, M. Polyakov. In 1931 Polyakov [62] published a study on the effects of drying silica in the presence of different additives on its pore structure. Another important step towards the current MIP technology was the polymerization of sodium silicate using a dye as template, presented by Dickey in 1949. [63] The first work on imprinted organic polymers came independently from two different groups in 1972. One of these studies, presented by the Klotz group [64] involved the synthesis of binding sites from methyl orange in a polyethyleneimine cross-linked network. The other study, presented by Wulff *et al.* involved an imprint that showed enantiomeric affinity for the D-form of

glycerolic acid. [65, 66] Both of the cited studies involved a covalent linkage of the template molecule to the monomers before polymerization.
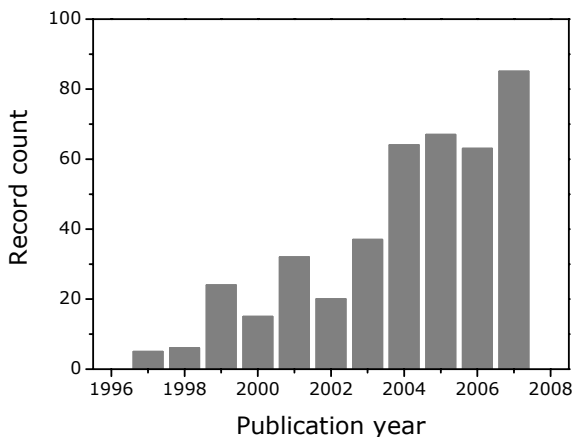
Figure 2-1: Progress in the development of MIPs used in sensing devices according to Web of Science (search term: molecularly imprinted polymers).

The most common approach today is to use non-covalent linkage of the monomers to the template molecule. This non-covalent approach for producing organic imprinted polymers was introduced in the early 1980s by the group of Mosbach and was called the non-covalent approach, *i.e.* "host-guest polymerization". [67-69] Worldwide there are about 20 research groups working on MIPs incorporated in sensors.

2.2 General principles

Selective binding of a guest molecule is among the most desirable properties of man-made antibody and receptor mimics. This is achieved allowing a template, for example, a target molecule of interest, to form complexes in solution with one or more polymerizable functional monomers that have the possibility to interact with this template in one or more ways, *e.g.* hydrogen bonds or ionic interactions, this compound is called the pre-polymerization complex.

Subsequently, a highly cross-linked polymeric matrix is formed around the template–functional monomer complexes by adding an excess of cross-linking monomer, thus "freezing" these interactions in such an arrangement that would allow subsequent rebinding of any molecule that has the correct size, shape and functionality to match the requirements of the so-called binding site. In Figure 2-2 the famous "lock-and-key" metaphor depicts how the monomer and the target molecules interact and form a molecularly imprinted polymer.
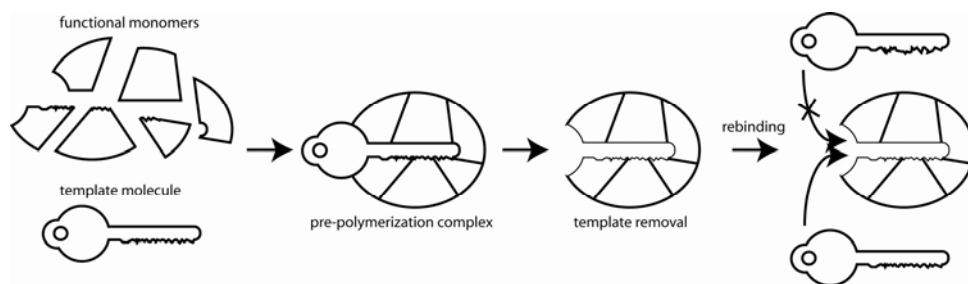
Figure 2-2: Schematic illustration of the "lock-and-key" metaphor of molecular imprinting.

Various approaches can be applied to choose how the pre-polymerization complex is formed. One approach uses monomers, which covalently bind to the target molecule, *i.e.* covalent imprinting. On the other hand, in the above description the pre-polymerization complex is formed by hydrogen bounds and ionic interactions, this is the non-covalent approach. The differences in these methods lie in the way the functional groups are linked to the target molecule. Covalent imprinting has the advantage of a strong interaction with the target molecule leading to well-defined imprint sites. The drawback is that the template binding has to be chemically cleaved in order to extract the template after polymerization. As a result, this method is limited to only a number of compound classes. This implies that the non-covalent approach is the most straightforward method.

The non-covalent approach is generally regarded as being of a more versatile nature and can be applied to almost any type of template, since there are a large number of commercially available functional monomers with diverse functionality ranging from acidic, basic or neutral to hydrophilic or hydrophobic.

Due to the very weak forces between the complexes the imprinting usually leads to a heterogeneous material with a range of binding sites with different binding affinities ranging from strong to very weak. In the process of non-covalent imprinting the number of parameters is larger; temperature, concentration of template and monomers/cross-linkers and polarity of porogenic solvent being the most important of them. In spite of these drawbacks, the non-covalent approach remains the method, which attracts the greatest number of researchers since it remains the most universally applicable. This approach will be used in the work underlying this thesis. The pro and contras of the covalent and non-covalent approaches are presented in Table 2-1.

Table 2-1: Advantages and disadvantages of covalent and non-covalent imprinting [70].

	Covalent	Non-covalent
Synthesis of monomer-template conjugate	necessary	unnecessary
Polymerization conditions	rather free	restricted
Removal of template after polymerization	difficult	easy
Guest-binding and guest-release	slow	fast
Structure of guest-binding sites	well defined	variable

2.3 Molecular imprinting

Before going further in the details of imprinting, the basic fundamentals of polymerization will be explained. A polymer is a large molecule consisting of smaller repeating units, monomers. The reaction between these monomers is called polymerization. This monomer is a building block of the polymer. Either are all monomers of the same type, in this case the polymer is a homopolymer. When the polymer is composed of two or more different monomers, it is called a copolymer. Different types of polymerization reactions can be applied. This depends on the type of monomers used, but the most widely used process for molecularly imprinted polymers is the free radical polymerization.

The free radical polymerization is a chain-growth reaction and consists of three main steps. The first step is the production of free radicals to initialize the polymerization. The radicals are usually obtained by decomposition of an initiator by UV-light or heating, producing the propagating radicals. Subsequently these initiating radicals react with the first monomer. This reaction

proceeds readily, but it is important to remove molecular oxygen from the mixture. The propagation leads to chain forming of the polymer. In the final step the process of monomer addition is terminated. This can occur when two chains recombine or by disproportioning of the reaction. The process of free radical polymerization is depicted in Figure 2-3.

$$I \xrightarrow[\text{temperature}]{\text{UV}} 2R^\bullet$$

$$R^\bullet + M \longrightarrow M_1^\bullet \qquad M_i^\bullet + M \longrightarrow M_{i+1}^\bullet$$

initiation   propagation

$$M_n^\bullet + M_m^\bullet \longrightarrow M_{n+m}$$

termination

$$M_n^\bullet + M_m^\bullet \longrightarrow M_n + M_m$$
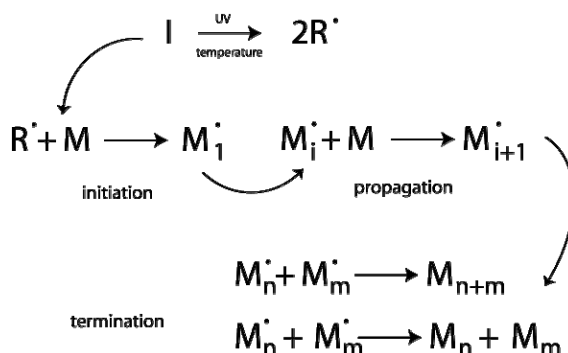
Figure 2-3: Working principle of free radical polymerization.

The basic principles of molecular imprinting have been presented. Further the experimental conditions of imprinting have to be determined. Important questions are what kinds of reagents are needed, what the reaction conditions are and which factors lead to high imprinting efficiency. In molecular imprinting most of the polymers are copolymers. The principle of molecular imprinting involves three steps as demonstrated in Figure 2-4:

1. The formation of a pre-polymerization complex between the template molecule and the functional monomers,

2. Polymerization of the formed template-monomer complex in the presence of a cross-linker,

3. Extraction of the template molecule from the polymer matrix.

The basic set of chemicals needed for imprinting are thus the functional monomers, which link to the template molecule, cross-linking agents to 'freeze' the pre-polymerization complex, solvents for the polymerization of the MIP and solvents to be able to remove the template from the MIP structure.
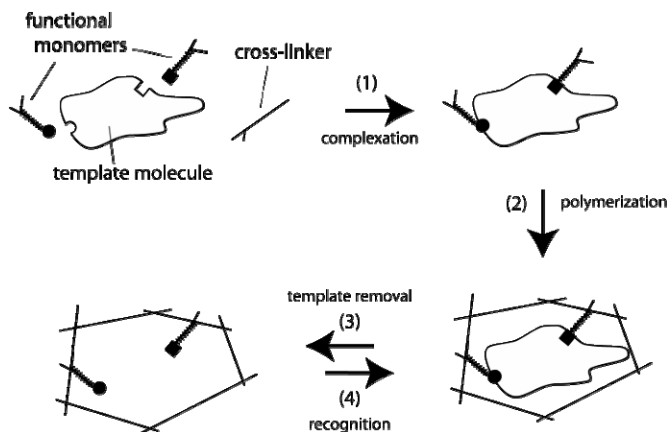
Figure 2-4: Schematic illustration of the principle of molecular imprinting [70].

The structures of a selection of typical reagents used for the preparation of MIPs are depicted in Figure 2-5. A prerequisite for imprinting is that the polymerization occurs without interfering with the pre-polymerization complex and all other compounds should remain intact. For non-covalent imprinting, vinyl monomers bearing appropriate functional groups are most suitable.
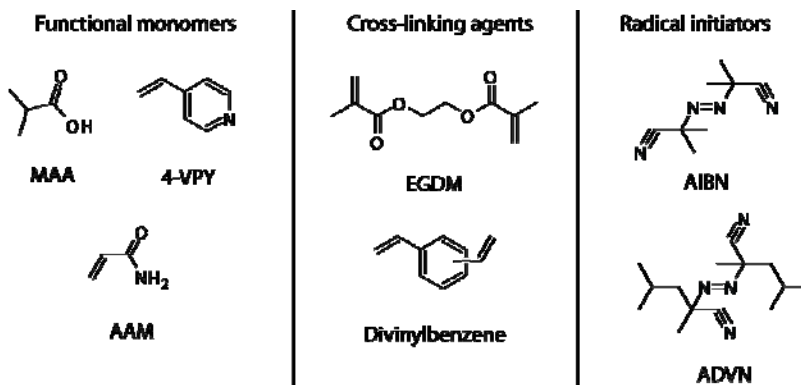
Figure 2-5: Typical reagents used to make molecularly imprinted polymers. [70]

The non-covalent linking of the template happens through hydrogen bonding, ion-pairing or π-π interactions. (Table 2-2) Furthermore, Coulombic attraction, charge transfer, induction, and dispersion contribute to the complex formation. The driving forces of ion-pairing interactions (ion-ion, dipole-ion, dipole-dipole)

are Coulombic interactions. Hydrogen bonding is a strong interaction playing an important role in naturally occurring non-covalent interactions. Complexes based on hydrogen binding typically exhibit comparatively high stability constants. Comparatively weak electrostatic interactions such as π-π stacking may occur between aromatic rings in polar solvents. In general, the molecular recognition of a guest molecule may be due to the combinations of two or more interaction modes.

Table 2-2: Types and estimated bond energies of non-covalent interactions. [71, 72]

Bond type	Bond energy (kJ/mol)	Relative strength
hydrogen bond	20[8] 4-60[9]	weak/medium
hydrophobic effects	1-3[8]	weak
ion-ion (1/r)	250[8] 100-350[9]	strong
dipole-ion (1/r²)	15[8]	weak
dipole-dipole (1/r³)	2[8] 5-50[9]	weak/medium
π-π stacking	0-50[9]	weak/medium
dispersion (1/r⁶) attractive van der Waals	2[8] <5[9]	weak
cation-π	5-80[9]	medium

The cross-linking agents, which are used in organic solvent are often ethylene glycol dimethacrylate (EGDM) or divinylbenzene. These agents fixate the guest-binding structure firmly and give a solid polymeric material. The reactivity of the cross-linking agents should be similar to that of the functional monomer in order to obtain a matrix with a random distribution of the functional residues. The ratio of cross-linking agents to the amount of template complexes is of great importance to the imprinting efficiency. When the amount is too large, binding sites are located too close together, suppressing the ability of binding a template molecule next to the specific binding site.

Also, the role of solvent is of great importance. Next to dissolving the agents for polymerization, the solvents should provide porous structures to the MIPs. During the polymerization the porogenic solvent introduces a three dimensional

network, leading to a larger binding capacity and good accessibility of binding sites. Furthermore, it plays an important role in distributing the heat of the reaction to prevent side-reactions due to local heating.

The polymerization procedure can be initiated by using thermal initiators, such as AIBN. Another method of polymerization is by UV-light irradiation. If enough UV light is absorbed, the initiator can be triggered into decomposition, thus forming radicals and initiating the polymerization of the mixture. The UV polymerization is performed without applying any heat to the mixture. This could be of interest to produce MIPs using a very volatile porogen, in which the mixture has to be cooled during the UV polymerization.

2.4 MIPs for small MW-molecules

As mentioned in section 1.3 , the aim of the study, the main goal is to detect small MW-molecules. For small molecular weight molecules often no suitable biological receptor exists and the use of MIPs as a synthetic receptor for detecting these molecules would therefore be of interest. For the studies presented here a model set consisting of two relevant target molecules is used, *i.e.* L-nicotine and Histamine. L-nicotine is used to proof the principle of electric sensing devices based on MIPs. Further, to expand the proof, the clinically more relevant histamine is used. Both molecules are shown in Figure 2-6.
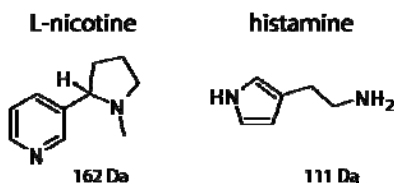
Figure 2-6: Molecule structure of Nicotine and Histamine.

Nicotine, $C_{10}H_{14}N_2$, is an organic compound, an alkaloid found naturally throughout the tobacco plant, with a high concentration in the leaves. Two stereo-isomers exits of nicotine, with L-nicotine being the naturally occurring enantiomer. It inhibits the enzyme activity of acetylcholinesterase, which

catalyzes the hydrolysis of neuron-transmitter acetylcholine, and enhances the central nerves system. It has been used as a nerve poison or pesticide. A common source of nicotine is tobacco smoking, since the nicotine adheres to small particles of tar in the smoke. In the body, the nicotine is distributed through the blood and can pass through the blood-brain barrier. Up to After intake, it takes about 7 seconds for nicotine to reach the brain. The most harmful effect of nicotine is addiction. In small quantities, it has a stimulating effect and increases the activity, alertness and memory. It causes an increase of the heart rate and blood pressure and reduces the appetite. High concentrations can produce vomiting and nausea. The LD50 (lethal dosage to kill 50% of the population) for adult humans is about 50-60 mg, which translates to a concentration of 61.6 µM in the human blood. The concentration of L-nicotine in urine is 0.3 µM for non-smokers and 8.6 µM for cigarette smokers. Various methods for the determination of nicotine have been proposed in the past few years, including methods based on radioimmunoassay [73-75], chromatography [76-78], and flame ionization [79, 80]. However, these methods are expensive and require complex operations. To solve these problems there is a need for a fast and straightforward sensing device.

Histamine is a well-known monoamine and plays important roles in relation to immune response and gastric secretion, and also as a neurotransmitter in the central nervous system. It acts as a mediator in allergies and the histamine concentration is an important parameter in the irritable bowel syndrome (IBS). IBS is a group of symptoms including abdominal pain and discomfort often reported as cramps, bloating, gas, diarrhea, and constipation. IBS has no cure, but there are some therapies or diets, which relieve the symptoms. In order to investigate the influence of relieve treatment like diet changes, medicine or stress relief, it would be favorable to measure the histamine levels instantly in the bowel [81, 82]. The bowel is not the ideal environment for biological receptors because of its low pH, which makes the use of a MIP based sensor a potentially favorable alternative. It is also important to detect the histamine concentration in seafood because histamine often causes a severe allergic reaction. Many different methods have already been proposed for measuring histamine. Most approaches use liquid chromatography (LC) or fluorometric

detection combined with anion-exchange resin treatment, which is the officially recognized method [83-85]. These methods have been employed for food analysis. However, they are inappropriate for measuring short-time events such as histamine release from mast cells. Histamine can also be found in various foods and beverages, such as wine, beer, fish and meat, normally as a result of enzymatic degradation or fermentation processes [86, 87].

2.5 Procedures and synthesis

Usually bulk polymerization procedures are used to prepare MIPs. In a typical bulk polymerization protocol the reagents for the synthesis are dissolved in the diluent together with the radical initiator. The solution is then degassed to remove oxygen and placed under UV light or heated to decompose the initiator. Subsequently, the reaction is allowed to proceed for several hours, depending on the polymerization procedure. The result is a polymeric monolith, which is crushed, milled and sieved to obtain desirable particles sizes. Finally, the polymer particles are washed to remove the template molecule and unreacted reagents.

The main drawback of the bulk method is that the resulting particles are irregular in shape, which limits their applicability and reproducibility. There are several techniques for making imprinted polymers beads, which are of a more controlled shape. The first option for the synthesis of molecularly imprinted beads is suspension polymerization [88], which has been developed using liquid perfluorocarbons, mineral oils or water as the continuous phases. Another technique that has been evaluated for the MIP production is dispersion or precipitation polymerization [89, 90]. There are also some surface modification procedures which have been developed, like grafting of MIP films on silica particles [91] and preparation of surface-modified imprinted polymers by polymerization method on seed particles [92].

The target molecules used in this work were L-nicotine and Histamine. A representative synthesis protocol for L-nicotine MIPs is given in Figure 2-7 and can be outlined as follows. To obtain the MIPs, a mixture of MAA (12.5 mmol),

EGDM (25.2 mmol) and AIBN (0.66 mmol) was dissolved in 7 ml chloroform together with the template molecule L-nicotine (6.41 mmol).
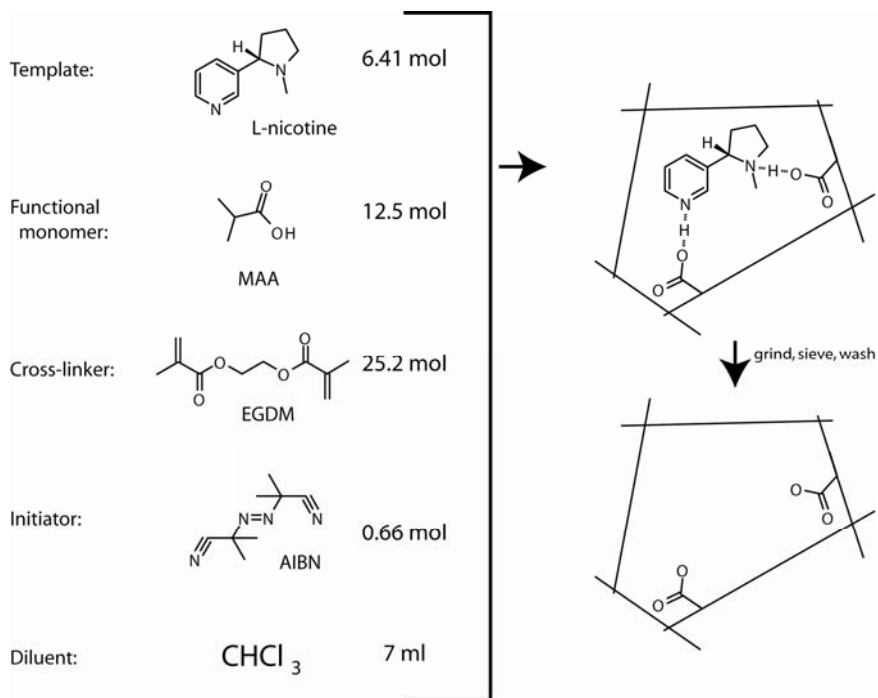
Figure 2-7: Schematic picture of the imprinting procedure for a MIP for L-nicotine.

Subsequently, the mixture was degassed for 10 min with N_2. Next, for polymerization the solution was sealed and kept in a controlled temperature water bath at 65°C for 72 hours. Alternatively, to polymerize the mixture UV hardening with an ultraviolet source (360 nm) at room temperature for 24 hours was used. The resulting monoliths were mechanically crushed and sieved to particles sizes between 25 µm and 45 µm for batch rebinding experiments, to characterize the binding properties and particle sizes smaller then 25 µm were used for the sensing experiments. After grinding, the L-nicotine was extracted from the polymer by a continuous extraction of the MIP powder with first methanol, then a mixture of acetic acid/acetonitrile (1/1) and again methanol [93]. The test the selectivity a reference material is needed with the same non-specific binding properties as the molecularly imprinted polymer. Therefore, a

non-imprinted polymer, referred to as NIP, was synthesized. The NIP is prepared in the same way using the same ingredients except without the presence of the target molecule. In this way the non-specific binding at the surface of the MIP can be investigated and eliminated when measuring in a differential way.

2.6 Testing affinity and selectivity

Once the MIPs are synthesized, they are tested for their affinity against the target molecule and the selectivity in the presence of other similar molecule structures. There are two procedures commonly proposed in the literature, chromatographic separation [94-99] or batch-rebinding experiments [100-104].

For chromatographic experiments, the MIPs are packed into stainless steel column-tubes and used as the stationary phase for high-performance liquid chromatography, HPLC. A typical HPLC chart is schematically illustrated in Figure 2-8. The major peak resulting from the target molecules has a retention time, t_g. The minor peak is that for the void marker, a standard molecule (e.g. acetic acid, acetone, or acetonitrile) which is poorly bound by the MIP, it retention time is t_0.
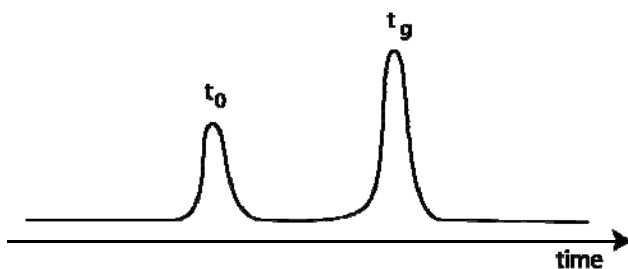
Figure 2-8: Schematic illustration of the HPLC chart.

A representation of the binding activity of a MIP towards a particular target molecule is given by the capacity factor k, which is defined by equation (2.1).

$$k = \frac{t_g - t_0}{t_0} \tag{2.1}$$

When the molecular imprinting is successful, the k value of the target molecule is much higher compared to k value of other, similar compounds. In unsuccessful imprinting, the difference between the k values of the target and the others would be negligible.

In contrast using batch rebinding experiments, the guest-binding activity of the imprinted polymer is determined by the amount of target molecules bound by the polymer. A known concentration of target molecules is exposed to an amount of MIP. This mixture is incubated until the guest binding reaches the equilibrium. Then the MIP is removed and the remaining concentration, C_f, of target molecules is measured by HPLC, UV/Vis or other analytical methods. UV/Vis spectroscopy is the technique used in this work.

From this concentration the amount of target molecules, which are bound, C_b, can be determined. The selectivity is analyzed by comparing the amount of target molecules bound by the MIP per unit weight, S_b, with those of other compounds. The curvature of the binding isotherm, which is obtained by plotting S_b versus C_f, is indicative of the presence of specific binding sites within the MIP. A straight-line suggests only the existence of non-specific binding, as depicted in Figure 2-9.
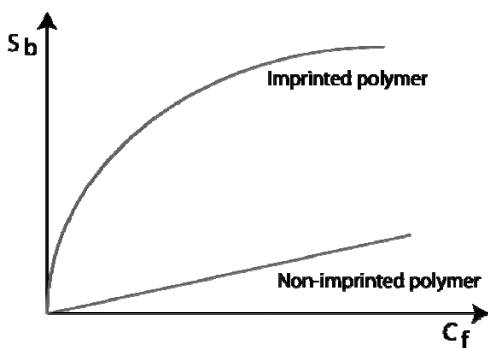
Figure 2-9: Appearance of MIP binding isotherms for imprinted and non-imprinted polymers.

More specific binding sites in the MIPs provide much higher affinities than the non-specific sites. This is reflected in changes in the curvature of the binding isotherm. Using this, the selectivity can be deduced by comparing the curvature

of the target molecule to the MIP with the curvature of the isotherm of other compounds.

2.7 Applications

A literature search yields a wide variety of applications of molecularly imprinted polymers. Not only are MIPs ideal as a synthetic receptor for sensing but they can also be found in chromatography and catalysis applications. In Figure 2-10 a schematic representation of the research areas in MIP technology are given. In the following paragraphs, a few examples will be given in order to demonstrate the use of MIPs in these fields.
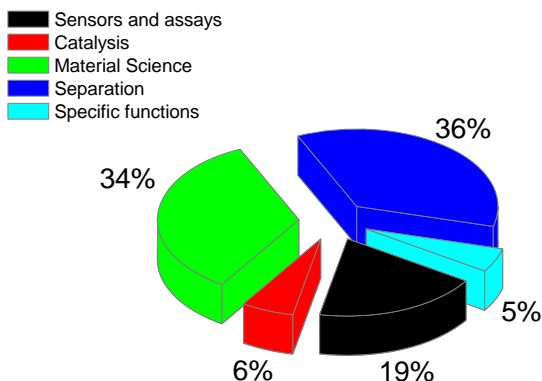
Figure 2-10: A schematic representation of research area in MIP technology [21].

During the last years, a large number of researchers explored the use of MIPs as a synthetic receptor in sensing devices [21, 60]. The target molecules investigated range from small molecules such as drug substances, amino acids steroid hormones, or metal ions to larger molecules such as peptides or proteins, viruses, bacteria and even cells. Examples of typical applications are listed in Table 2-3.

Table 2-3: Sensor applications of MIPs.

Application	Reference
- measuring a hydrolysis product of a chemical warfare agent in water	[105]
- a MIP incorporated microbalance for detecting anabolic steroid nandrolone	[106]
- a surface-imprinted sensor for tracing a plant virus in aqueous media	[107]
- a surface-plasmon sensor chip using MIPs embedded with gold nanoparticles	[108]
- an opto-electric sensor for tracking toxic pesticides and inorganics	[109]
- an impedimetric sensor for the detection of nicotine in a physiological solution	[24]
- a sensor based on surface imprinted blood cells to determine blood group	[110]

The applications of MIPs as stationary phases for chromatography is the most intensively investigated field, especially for liquid chromatography [111]. The imprinted polymers show enantio-selective properties, since the enantiomer, which was used as the template, is more strongly retained than the other enantiomer. This makes MIPs the perfect column packing material for separations of peptides [112], commercial drugs [113] and many other substances.

Since MIP materials contain spatially and functionally selective cavities for the template, they can also be applied in catalytic processes [114]. The catalytic active polymers are manufactured using transition-state analogues as template in, for example, ester hydrolysis [115] as well as ester hydrolysis including metal-ion coordination [116]. Another possible application for MIPs lays in enhanced drug loading, controlled drug delivery and drug targeting [117-119].

The above applications are selected examples of the most promising areas in which MIPs could be commercially applied. Resulting applications range from clinical point-of-care (POC) devices, water purification and waste-material treatments to rapid detection of chemical and biological warfare agents.

Chapter 3 - Concept and layout of MIP-based sensors

As mentioned in the aim of the study, the purpose is to develop a sensor for the detection of low MW molecules. The concept is immobilizing the synthetic receptors to an electrode surface, which can lead to an electrical read-out. In this chapter the two routes will be explained which are followed to obtain an electrical read-out. Next, the sensor concept and methods of immobilization, applied in this work, will be discussed. Finally, the implementation of these activated electrodes in a sensing device will be tackled. This will result in a highly sensitive and specific sensor based on molecularly imprinted polymers.

3.1 Electronic read-out

Depending on which type of electrical read-out is chosen, a suitable transducer can be selected. In this thesis two different techniques are applied to obtain an electronic read-out. One method will concentrate on the change of dielectric properties when a target molecule is bound to a receptor on the electrode surface. This implies the use of a conducting or semi-conducting transducer, which is needed to be able to measure capacitance or resistance changes of the interface. The other route is a microgravimetric sensitive device. By using a quartz crystal as sensor substrate, a quartz crystal microbalance is obtained, which can detect mass changes in the order of nanograms.

3.1.1 Impedance spectroscopy

This technique is based on measuring resistance or capacitance change of the interface. Resistance and capacitance can be summarized by the impedance. The impedance of a circuit is the complex resistance. For an ideal resistor Ohm's law applies, equation (3.1). This relation has several simplifying properties, such as the assumptions of frequency independence and the fact that AC current and voltage through the resistor are in phase with each other.

$$R = \frac{V}{I} \tag{3.1}$$

In reality, a much more complex behavior is found. The impedance replaces the simple concept of a resistor. Like resistance, impedance is a measure of the ability of a circuit to resist the flow of electrical current but it is not limited to the simplified properties.
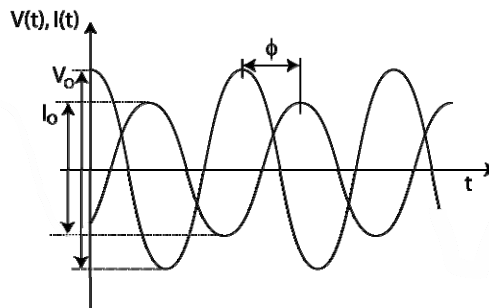
Figure 3-1: Voltage and Current signals from impedance measurement.

The impedance is measured using a small excitation voltage signal, V(t) see equation (3.2). The response is the current signal, I(t), which is slightly shifted in time resulting in a phase shift ϕ. Both signals are visualized in Figure 3-1.

$$V(t) = V_0 e^{i\omega t} \text{ and } I(t) = I_0 e^{i(\omega t - \phi)} \tag{3.2}$$

From these expressions the impedance, Z, as a function of frequency, ω, of the system can be calculated. The impedance is thus expressed in terms of Z_0 and a phase shift as mentioned in equation (3.3).

$$Z = \frac{V(t)}{I(t)} = Z_0 e^{-i\phi} = Z_0(\cos\phi + i\sin\phi) \qquad (3.3)$$

The impedance is frequency depended. The easiest way to represent the impedance as a function of frequency is the Bode plot. In Figure 3-2, the logarithm of the impedance is plotted against the logarithm of the frequency.
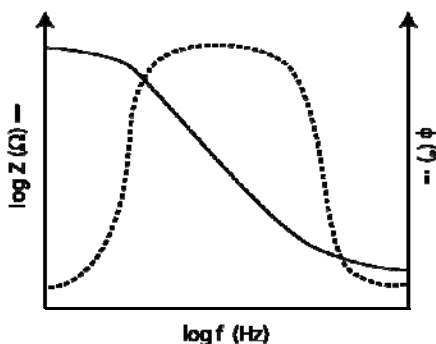
Figure 3-2: An example of a schematic Bode plot.

From equation (3.3), it can be seen that $Z(\omega)$ is composed of a real part and an imaginary part. When the real part is plotted against the negative of the imaginary part a Nyquist plot is obtained, shown in Figure 3-3.
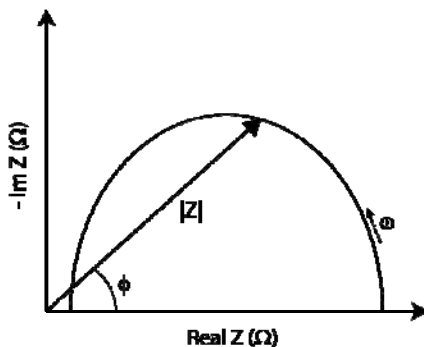
Figure 3-3: An example of a Nyquist plot from the bode plot shown in Figure 3-2.

Each point of the Nyquist plot is the impedance at a fixed frequency. For the electrochemical impedance spectroscopy (EIS) data, where impedance usually decreases as frequency increases, low frequency data are on the right side of

the plot and higher frequencies are on the left. The data can be represented as a vector of length |Z| and the angle between this vector and the x-axis is φ.

A very important aspect of electrochemical impedance spectroscopy is fitting the data. EIS data is commonly analyzed by fitting it to an equivalent electrical model circuit. Most of these circuit elements in the model are common electrical elements such as resistors, capacitors and inductors. Many circuits can be fitted to a specific measurement but to be useful the elements of the model should have a physical meaning to the system. In the following Table 3-1 the different elements are presented with their impedance contribution.

Table 3-1: Components for equivalent circuit fitting [120]

Component	Impedance	Info
R	$Z_R = R$	Resistor
L	$Z_L = i\omega L$	Inductor
C	$Z_C = \dfrac{-i}{\omega C}$	Capacitor
CPE	$Z_{CPE} = Q_0^{-1}(i\omega)^{-n}$	Constant phase element, takes into account semi-infinite diffusion, a kind of imperfect, leaking capacitor. (when n = 1, Q = C)
W	$Z_W = Y_0^{-1}(i\omega)^{-\frac{1}{2}}$	Warburg component, takes into account unrestricted diffusion to a large planar electrode. It is the same as the CPE with n = 0.5.

Besides the components mentioned above there are some others, like a Gerisher element, which describes chemical reaction at the electrodes. However these are not relevant in this work. One of the most common and simplest circuit models of electrochemical impedance is the Randles equivalent circuit.
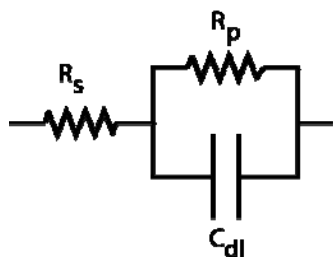
Figure 3-4: Schematic representation of the Randles circuit.

The equivalent circuit for the Randles cell is shown in Figure 3-4. It consists of a solution resistance, R_s, a double layer capacitor, C_{dl}, and a charge transfer or polarization resistance, R_p. In addition to being a useful model in its own right, the Randles cell model is often the starting point for other more complex models. [121]

The physical idea of the electrode capacitance is a double layer which is formed at the electrodes interface is depicted in Figure 3-5. At the electrode-liquid interface a translation from electronic to ionic conduction occurs. In the solution at the electrode surface this double layer is formed as soon as the metal is wetted. Within this layer the electron transfer takes place. This transition zone consists of a non-uniform distribution of charges. It can be thought of as a molecular capacitor.
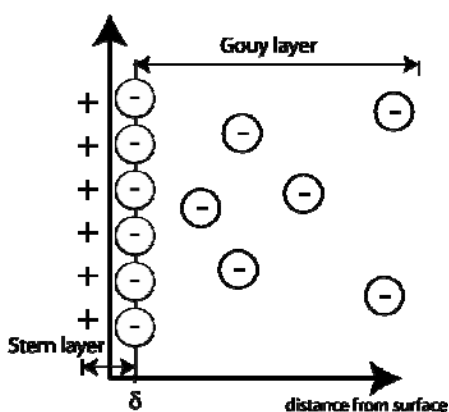
Figure 3-5: Stern's model of a diffuse electric double layer.

The formation of this layer is amongst others described by Stern. Stern combines the simple molecular plate capacitor model from Helmholtz and the Gouy-Chapman theory, which describes a diffuse double layer of counterions. Stern's model sketches a double layer, which consists of a layer of absorbed ions at the surface according to the Langmuir adsorption isotherm and a second diffuse layer of counterions at a distance δ from the surface. When the electrode is set to a positive or negative bias voltage, the negative respectively positive counterions in the electrolyte are attracted to the surface. During this process, a kind of plate capacitor is formed at the interface, being the double layer capacitance. The thickness of this layer ranges from 0.5 to 10 nm, depending on the size of the Gouy layer [121]. The charge transfer resistance is a measure on how easy the charge is transferred from the carriers in the electrolyte, being ions, to the charge carriers of the electrode, being electrons.

To measure the impedance changes, initially an impedance analyzer was used. The impedance based setup is depicted in Figure 3-6. The impedance analyzer is first connected to a multiplexer to be able to measure four different channels at once. The sensing device is placed in a temperature-controlled oven in a socket, which is connected to the multiplexer. Using this setup an impedance spectrum can be measure from 100 Hz until 1 MHz. The full range of time resolved impedance spectra can be taken every 90 seconds for all four channels.
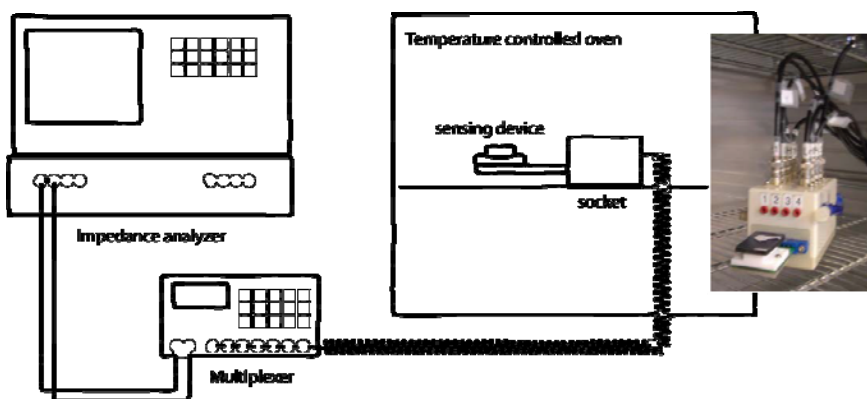
Figure 3-6: Measurement setup for impedance based sensing.

The next step, which at the same time comprised the first step towards a handheld device, consisted of a small measurement box, which could measure the impedance at a fixed frequency in function of time for two different sensing devices. This way, eight channels could be read every 4s. The whole system, shown in Figure 3-7, was homemade and PC controlled.
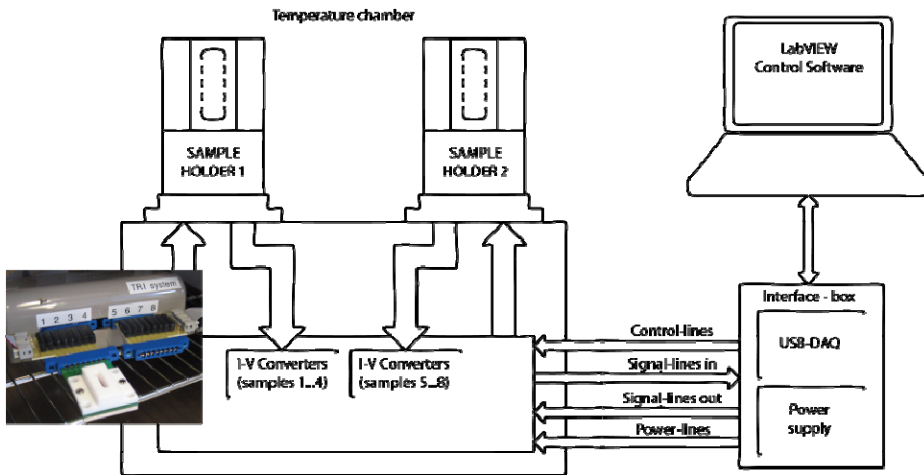
Figure 3-7: Homemade impedance based readout system.

3.1.2 Quartz Crystal Microbalance

The second route in obtaining an electrical read-out is using the quartz crystal microbalance technique, QCM. Quartz is a crystal with piezo-electric properties. Quartz is an anisotropic crystal, it has no centre of symmetry. When such types of crystals are mechanically stressed an electrical signal is generated. Otherwise, when an electrical signal is applied, the crystal will mechanically deform. When an oscillating voltage is applied, an oscillation deformation will take place. Each crystal has its natural resonant frequency of oscillation. This frequency is dependent on the mass of the crystal and the coated material around it. This principle can be applied to sense small mass changes on the substrate. A quartz crystal microbalance is an extremely sensitive sensor capable of measuring mass change in the nanogram/cm² range with a wide dynamic range extending into the hundred microgram/cm² range.

In 1959, G. Sauerbrey [122] was the first to recognize the potential usefulness of the technology and demonstrated the extremely sensitive nature of these piezo-electric devices towards mass changes at the surface of the QCM electrodes. His work resulted in the development of the equation (3.4), which correlates the change in resonance frequency of the crystal with the mass deposited on it.

$$\Delta f = -\frac{2f_0^2}{A\sqrt{\rho_q \mu_q}} \Delta m \qquad (3.4)$$

Where

f_0	=	the resonant frequency of the crystal (Hz)
Δf	=	the frequency change (Hz)
Δm	=	the mass change (g)
A	=	the piezo-electrically active crystal area (m²)
ρ_q	=	the density of quartz (2.648 g/cm³)
μ_q	=	the shear modulus of a quartz AT-cut crystal (2.947·10¹¹ g/cm·s²)

The most common types used in sensing devices are AT-cut quartz crystals. These are crystal slices, which are cut at an angle of 35°10' from the optical axis of the quartz crystal, see Figure 3-8. The AT-cut produces a resonator, which is around room temperature almost insensitive for temperature variations. Due to the nature of the cut this resonator operates in thickness shear mode.
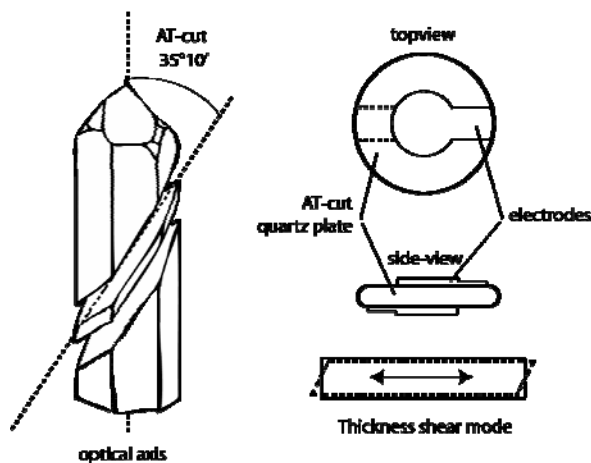
Figure 3-8: Schematic representation of a quartz AT-cut crystal. [123, 124]

These ultra-sensitive microbalances have a wide field of applications. They are used for thin film thickness monitoring, biotechnology, functionalization of surfaces, thin film formation, liquid plating, etc.

The piezo-electric read-out is performed using a phase lock oscillator, PLO. The PLO uses an internal voltage controlled oscillator to drive the crystal. The crystal current is monitored and the frequency of the oscillator adjusted until there is zero phase between the crystal voltage and current. The piezo electric setup is shown in Figure 3-9. The PLO is connected to a frequency counter to monitor the resonant frequency and a voltmeter to measure the crystal resistance.
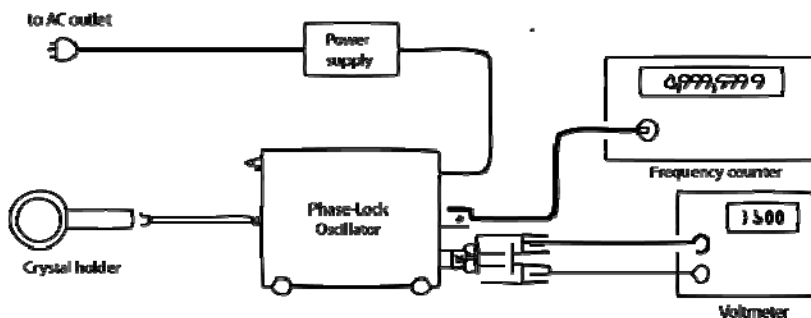
Figure 3-9: A schematic representation of the Piezo-electric setup.

3.2 Transducer

The choice of transducer is obviously dependent on the choice of read-out. To make the sensing device interesting for future commercialization, a handy and cheap production process is required and should consist of compounds which are sufficiently stable, readily processable and commercially available at low cost. One of the 'new materials', which are currently a hot topic in the world of novel displays, solar-cells, etc. are conjugated polymers. A. J. Heeger, A. G. MacDiarmid and H. Shirakawa found in 1977 that by oxidation with chlorine, bromine or iodine vapor, polymers films could be doped and thus could be made conductive [125]. This discovery led to their Noble price in chemistry in 2000. The semi-conducting polymers are typically conjugated π-electron systems

consisting of alternating single and double bonds between the carbon atoms in their main chains.

In this work OC_1C_{10}-PPV was used as the conjugated polymer. It is commonly known as MDMO-PPV and can also be used in polymer LEDs, solar cells, etc. The PPV derivative used for the sensor studies was synthesized via the sulphinyl precursor route [126]. This route gives conjugated polymers with an enhanced purity as compared to other preparation methods. All chemical and physical properties were in agreement with previously reported data. This polymer behaves as a p-type semiconductor with a bandgap of 2.1 eV. The molecular structure is shown in Figure 3-10.

monomer   polymer chain
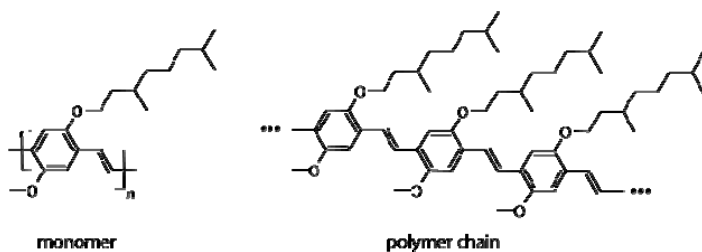
Figure 3-10: Molecular structure of OC_1C_{10}-PPV and
the polymer chain with alternative single and double bonds.

The semi-conducting properties of these materials make them ideal for the use as a transducer layer with an electronic readout, like impedance spectroscopy. The straightforward processing and application of these polymers make them also applicable for use in the transducer layer for piezo-electric read-out.

3.3 Immobilization

The choice of the above transducer layer is also dependent on the ability of immobilizing the receptors. In section 1.2.3 several immobilization techniques are mentioned. The main prerequisite is a reproducible method of immobilization with a sufficient coverage of the electrode. Directly spincoating of the solution of monomers, initiators and template, which is used to make the MIP, would prevent the formation of a network in which the target molecule can bind and is

therefore not possible. Hence, first a monolith is prepared and subsequently the MIP is mechanically grinded into microparticles.

These small microparticles, the receptors of the sensor, have to be firmly attached to the transducer layer. The first method is spincoating a mixture of the micro-particles and the conjugated polymer on top of the polymer film. Using these techniques the particles will be distributed over the whole thickness of the polymer film. Another technique to concentrate the particles only at the surface of the sensor, uses the low glass-transition temperature of about 80°C of the conjugated polymer. The idea now is to partially submerge the microparticles into the polymer film, creating an 'iceberg effect'. The analogy is demonstrated in Figure 3-11. This technique is a kind of a surface matrix entrapment.
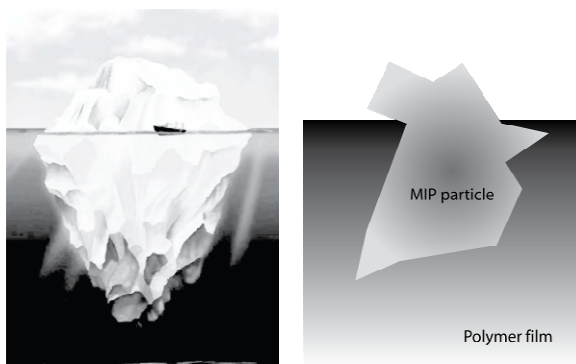
Figure 3-11: Iceberg analogy of the immobilization method.

In order to have a homogeneous and reproducible distribution of the particles at the surface, several methods can be utilized. The first and most straightforward method is placing a pile of powder on the film and heating the sample for several minutes above the glass transition temperature of the conjugated polymer. Another method is using a polydimethylsiloxane (PDMS) stamp. The stamp is covered with MIP particles and pressed with a few Newton onto the sensor surface before heating the sample. Both techniques are demonstrated in Figure 3-12. In theory the stamp method should produce a more uniform

distribute film of MIP particles. Both methods are compared in the characterization section of this thesis.
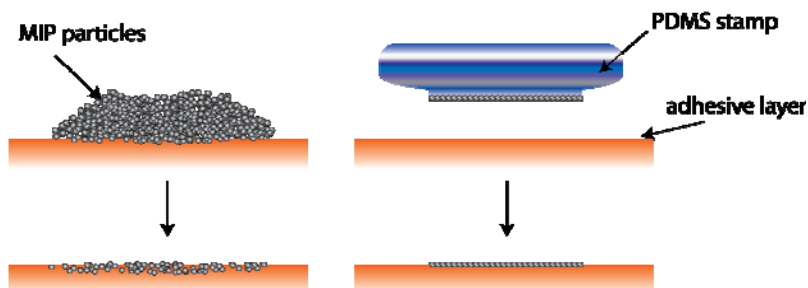
Figure 3-12: Immobilization methods, pile (left) and stamp method (right).

3.4 Electrodes

For the electronic read-out, different kinds of materials, such as Au, Ti, Pt, Al, can be used as an electrode. Au and Al electrodes can be obtained by physical vapor deposition (PVD), while Ti and Pt are deposited by DC-pulsed magnetron sputtering. The main prerequisite of the electrode material is that it should be inert and not interfere with the measurement technique. Different electrode configurations were used during this work, see Figure 3-13.
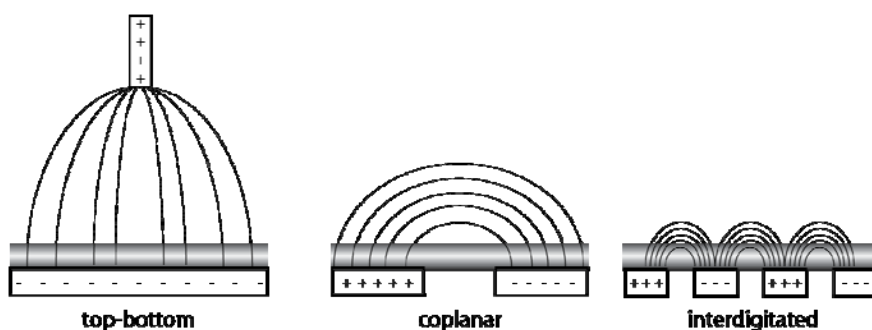
Figure 3-13: Electrode configurations.

The first method is the top-bottom configuration. One electrode is placed on the substrate on which the polymer was coated. The other electrode is placed in the

electrolyte. The field lines pass throughout the whole measurement cell. The top bare electrode is exposed to compounds introduced in the sensor cell, which can react or adsorb to its surface. This may interfere with the measurement.

Another technique to reduce the electrolyte influence and eliminate reactions of compounds with the counter electrode is the coplanar method. Both electrodes are covered with the polymer. They are not in contact with the electrolyte. In addition, the field lines pass twice through the polymer layer.

An improvement to the coplanar method is the use of interdigitated electrodes. These are fingerlike configured electrodes spaced at a micrometer range distance from each other. The field lines do not penetrate as deep in the electrolyte like the coplanar electrodes, reducing interfering effects by changes in the electrolyte.

3.5 The sensor setup

When all materials are chosen the sensing devices can be build. First, the impedance based sensor will be described. During this thesis several sensor devices were used. Since for future biosensors the use of a differential set-up is desirable, the sensor design allows for a comparison of the reference with the activated surface.

All sensor samples are prepared in a glovebox. This is a protected environment in which the concentrations of O_2 and H_2O are kept below 1 ppm to avoid degradation. First a glass substrate, 20 by 10 millimeter, is cut from a microscope slide. The substrates require an intensive cleaning procedure with subsequently

- o ultrasonic baths in a soap solution for 30 minutes,
- o ultrasonic baths in acetone for 10 minutes
- o immersing in hot isopropanol for 10 minutes.

Afterwards the samples are dry blown with an nitrogen gun (N_2).

Next, electrodes of about 70 nm are deposited on the substrate either by evaporation or sputtering using a mask or by etching techniques. In the beginning Au electrodes were used but the adhesion of Au on glass is not good. Next, Ti electrodes were sputtered. This adhesion was good but the Ti electrodes corroded when they were not directly protected with a polymer film. Next, platinum was being used. This is an inert electrode material widely used in electrochemical applications. The OC_1C_{10}-PPV is spincoated from a chlorobenzene (0.7 wt%) solution. The thickness of the polymer layer is determined by the speed and the duration. In this way layers of about 100 à 200 nm were obtained for the impedance based sensors. Subsequently, MIP or NIP is immobilized in the conjugated transducer film. The sample is then mounted in a sensor chip and the contacts are connected to the pads of the chip using wire-bonding. This chip could be plugged into a slot which was connected to the impedance analyzer. Finally, the measurement cell is closed using a Teflon® hood and a PDMS o-ring to make it watertight. The opening on top of the Teflon® cover created an addition setup and droplets of the target solution can be added to the background electrolyte using a syringe.

The desire for more advanced measurements lead to a device with four channels and a coplanar configuration of the electrodes as a more favorable alternative. The process from substrate to this sensing device is depicted in Figure 3-14. In this four-channel setup there is more room for additional reference channels and comparison between two identically prepared activated samples.
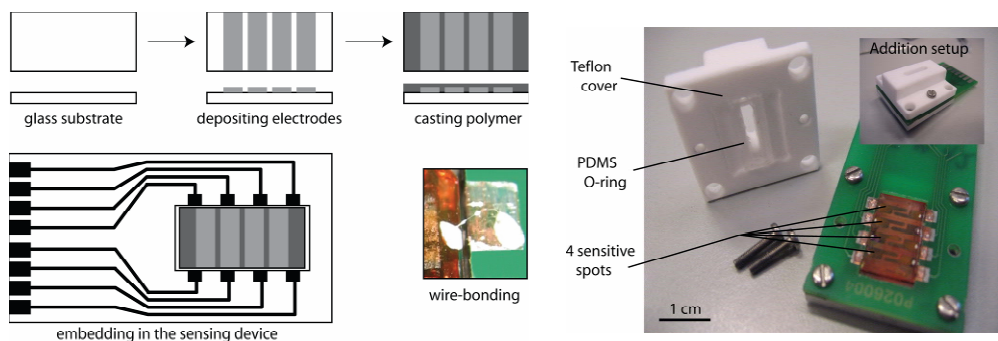
Figure 3-14: Sensing device for electronic read-out.

The piezo-electric sensing device is synthesized in the same way. Piezo-electric crystals were purchased from Maxtek, Inc., Cypress, USA. They were one-inch diameter crystals commonly available for liquid work with a resonant frequency of 5 MHz. These crystals were optimized for temperature around 25°C. This ensuring a minimal influence of temperature on the resonance frequency [127]. The electrode material was gold and the Q factor was about 120 000. The Q factor is used to compares the frequency at which a system oscillates to the rate at which it dissipates its energy. A higher Q indicates a lower rate of energy dissipation relative to the oscillation frequency, so the oscillations die out more slowly. The sensitivity factor of the crystal was 0.056 Hz/ng/cm² at 20°C. The crystals were cleaned using the above procedure. The micro MIP particles were immobilized in the same ways on the electrodes as done with the impedance devices. The crystal was mounted in a 100 microliter Teflon flow cell as shown in Figure 3-15.
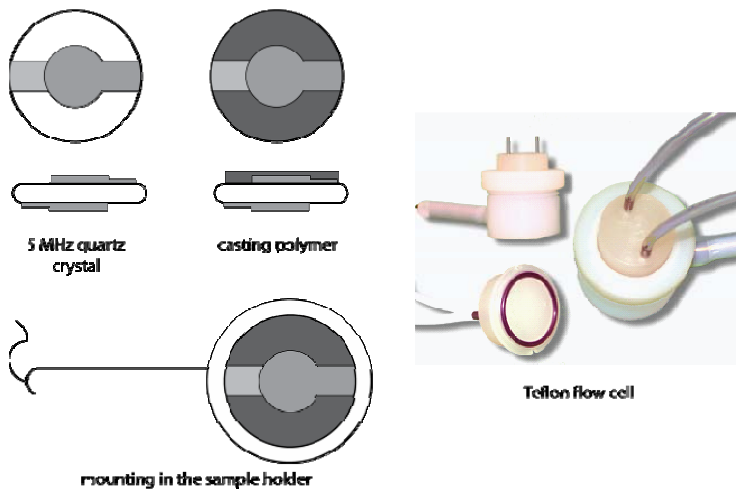
Figure 3-15: Piezo-electric sensor synthesis.

Chapter 4 - Characterization of the MIPs and the sensing devices

Before to being able to sense target molecules, the selected techniques and materials are characterized. UV/Vis absorption spectroscopy is used to get a better understanding of the specificity, selectivity and binding characteristics of the MIP particles. Common optical microscopy is employed to look at the macroscopic size of the MIP particles and to investigate the immobilization in the polymer film. Scanning electron microscopy, SEM, is utilized to look even closer at the particles and to give an idea about the microscopic distribution of the MIP on the sensor surface. Further, fluorescence techniques are used to look at the optic properties of the polymers during synthesis. Finally, contact angle measurements are performed to investigate the hydrophobicity of the surface.

4.1 UV/VIS spectroscopy

For a refined analysis of the binding mechanisms between MIPs/NIPs and nicotine/cotinine, batch rebinding experiments were performed using UV-Vis absorption spectroscopy by measuring the nicotine optical absorption at 260 nm. To test the specificity of the L-nicotine imprinted polymers, the MIP particles were also exposed to several concentrations of L-cotinine. The same experiments were performed with the NIP-particles. A fixed amount of MIP particles, 20 mg, was added to different concentrations of L-nicotine C_i from 0.2 to 1 mM. After stirring these solutions for one hour at room temperature, the concentration of target molecules remaining in solution (C_f) was measured.

Subsequently, the amount of target molecules bound to the MIP (S_b) and the amount of bound molecules per gram MIP were calculated. Binding isotherms for the imprinted and non-imprinted polymers are shown in Figure 4-1.
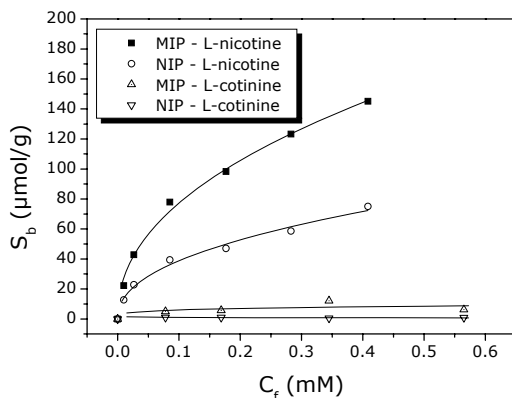
Figure 4-1: Graph of binding isotherms for imprinted and non-imprinted polymers exposed to L-nicotine and L-cotinine.

Due to the high affinity of the specific binding sites in the MIP, the amount of L-nicotine bound to the MIP is higher than in the NIP. The amounts of L-cotinine bound to MIP and NIP are equal and significantly lower compared to the L-nicotine binding characteristics. The binding of L-cotinine is non-specific and may involve the free acid groups of the functional monomer at the surface of the polymer.

To get a better understanding about the binding characteristics the binding isotherms can be further analyzed using various models. The simplest model is the Langmuir isotherm. [128] This isotherm is based on three assumptions:

- adsorption cannot proceed beyond monolayer coverage
- all surface binding sites are equivalent and can accommodate, at most, one adsorbed template
- the ability of a template to bind at a given sites does not depend on the neighboring sites.

Thus Langmuir describes a sorption which takes place at specific homogeneous sites. The Scatchard plot from this isotherm can be fitted with a straight line as seen in equation (4.1), where N is the total number of binding sites and K the affinity constant.

$$S_b = \frac{NKC_f}{1 + KC_f} \rightarrow \frac{S_b}{C_f} = -KS_b + NK \tag{4.1}$$

The Scatchard plots, Figure 4-2, indicate however the existence of a non-linear relationship, thus implying a heterogeneous distribution of the binding sites, each with different affinity.
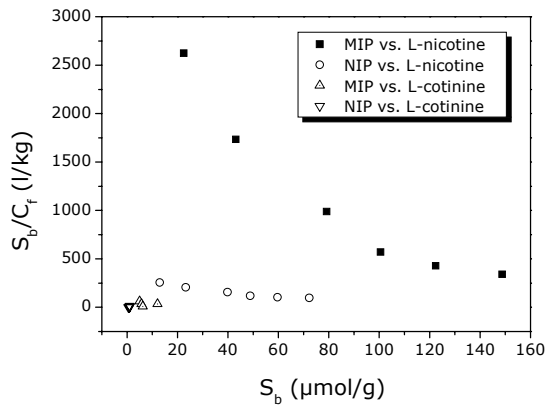
Figure 4-2: The Scatchard plot for imprinted and non-imprinted polymers exposed to L-nicotine and L-cotinine.

The binding sites in imprinted polymers have a large heterogeneous distribution due to different organization of the complementary functional groups and different shape-selective cavities [103, 104]. For this type of distribution the binding isotherm can be better analyzed using the Freundlich model [129], see equation (4.2). This model describes an adsorption system with emphasis on two factors, namely the lateral interaction between the adsorbed molecules and the energetic surface heterogeneity.

$$S_b = A \cdot C_f^{\nu} \tag{4.2}$$

Where S_b is the amount of target molecule bound per gram of MIP/NIP, A is the Freundlich constant and ν the Freundlich heterogeneity parameter. The binding isotherms in Figure 4-1 were fitted using equation (4.2).

The parameters are used to plot the affinity distribution according to equation (4.3), where N(K) is the amount of binding sites available for each association constant K. This can be seen in Figure 4-3. Typically the binding parameters were calculated from $K_{min}=1/C_f^{max}$ to $K_{max}=1/C_f^{min}$.

$$N(K_i) = A\frac{\sin(\pi\nu)}{\pi} K_i^{-\nu} \tag{4.3}$$
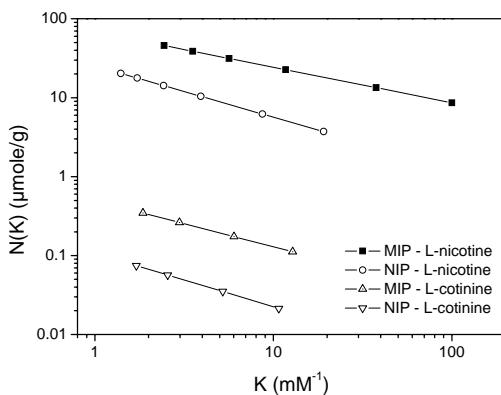
Figure 4-3: Graph of the affinity distribution based on the Freundlich model, for imprinted and non-imprinted polymers exposed to L-nicotine and L-cotinine.

The area under the graph of the affinity distribution gives the total number of binding sites per gram MIP. By integrating equation (4.3) a new function is obtained which represents the total number of binding sites for a specified range from $K_{min} - K_{max}$. The integral can be simplified as seen in equation (4.4).

$$N = \int_{K_{min}}^{K_{max}} N(K_i)d(K) = \frac{A\sin(\pi\nu)}{\pi}(K_{min}^{-\nu} - K_{max}^{-\nu}) \tag{4.4}$$

The total number of binding sites, N, within the range of binding constants from $1 - 100$ mM^{-1} are calculated and shown in Table 4-1 [103].

Table 4-1:The total number of binding sites within the range from 1-100 mM^{-1}.

		N_{tot} (µmol/g)
MIP	L-nicotine	59.8
	L-cotinine	0.46
NIP	L-nicotine	24.3
	L-cotinine	0.11

The results confirm the higher affinity of the MIP for L-nicotine than for L-cotinine. This indicates that the MIP particles have twice as many binding sites for L-nicotine as the NIP. In addition, it can be seen that for L-cotinine the amount of binding sites in this region is even lower for the MIP and the NIP. This may be a result of its different chemical structure. Notwithstanding, it can be concluded that the MIP recognizes the L-nicotine specifically.

To find the average binding constant of the MIP or NIP, the sum of all sites N_i multiplied by the corresponding affinity constant, K_i, is divided by the sum of N_i, which is the total number of sites N.

$$K_{av} = \frac{\sum N_i K_i}{\sum N_i} = \sum \frac{N_i K_i}{N} = \frac{\int_{K_{min}}^{K_{max}} N(K_i) K_i d(K)}{\int_{K_{min}}^{K_{max}} N(K_i) d(K)} = \frac{v}{1-v} \frac{(K_{max}^{1-v} - K_{min}^{1-v})}{(K_{min}^{-v} - K_{max}^{-v})} \qquad (4.5)$$

From the parameter from the Freundlich fit the average binding constant for the MIP and NIPs are calculated and displayed in Table 4-2.

Table 4-2: The average binding constant within the range from 1-100 mM^{-1}.

		K_{av} (M^{-1})
MIP	L-nicotine	11.21
	L-cotinine	4.77
NIP	L-nicotine	10.84
	L-cotinine	4.71

The results show the average binding constant of the MIP for L-nicotine is higher than for L-cotinine while the binding constant for L-cotinine are much lower.

4.2 Optical microscopy

Optical microscopy is used to investigate the size and shape of the MIP particles. The crushed micro particles are sieved and the particles smaller than 25 micrometer are immobilized on the sensor surface. In Figure 4-4 a picture is shown of the MIP particles. Subsequently, these particles have been immobilized on the sensor electrode, which is covered with the conjugated polymer OC_1C_{10}-PPV.
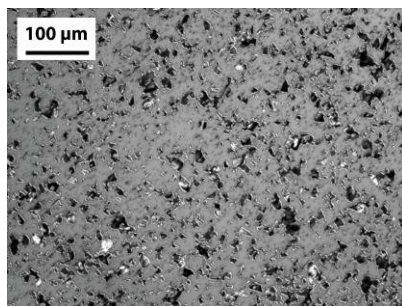
Figure 4-4: Optical image of the MIP particles.

Different methods are implemented trying to adhere the micro particles onto the electrodes. For the following samples, the heating time is ten minutes and the temperature is 100° C unless noted otherwise. The first method (method I) is dropping the samples in a powder pile before heating the sample, depicted in Figure 4-5b. The MIPs are in the picture darker compared to the transducer polymer. Other methods are covering the sample with a pile of MIPs (method II), Figure 4-5c, and spincoating the MIP particles mixed with the OC_1C_{10}-PPV (method III), Figure 4-5d.

The pile-drop method I causes a random distribution of the particles with a heterogeneous coverage and not all particles are firmly stuck in the transducer. The pile method II gives a good distribution and coverage. The spincoat method III introduces cluttering of the particles creating large clusters of particles. The major drawback of the methods mentioned above is that these methods are not appropriate to use for sensing devices consisting of different small scaled channels that need to be immobilized separately. Methods I and II have the risk

of contaminations of the other channels and it is difficult spincoating different channels separately using method III.
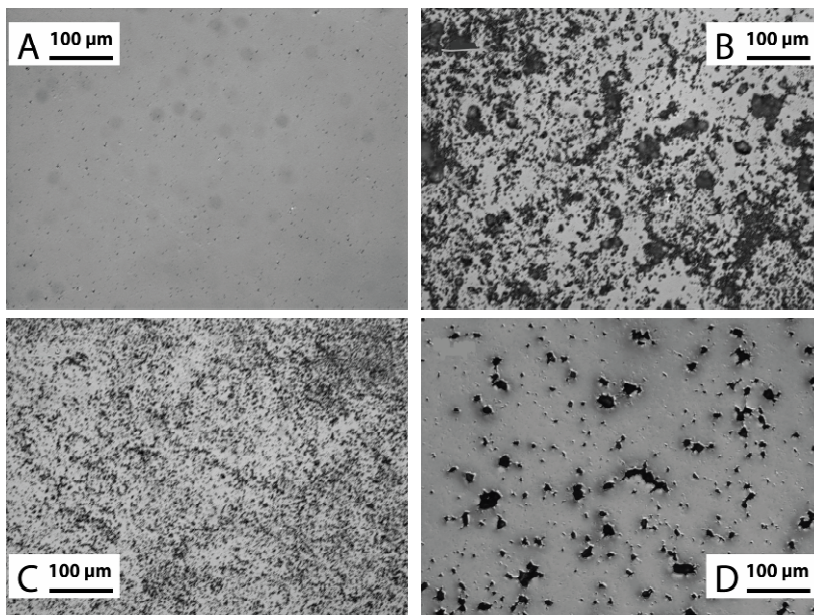
Figure 4-5: Different immobilization methods of MIP particles in the OC_1C_{10}-PPV film.
(a: blank polymer, b: pile-drop method, c: pile method, d: spincoat method)

Hence, a new method was developed. Key to this new method is the covering of the substrate with the MIP micro particles using a PDMS stamp. The obtained surface is shown in Figure 4-6. Using a small stamp, different channels can be loaded with MIP powder separately.
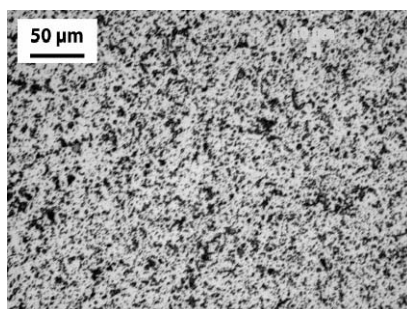
Figure 4-6: MIP particles immobilized on the OC_1C_{10}-PPV film using the stamping-method.

To investigate how firm the particles are attached to the transducer layer, the samples are rinsed with deionised water and iso-propanol. As can be seen in Figure 4-7, the particles remain on top of the surface, indicating that they are firmly attached to the sensor electrodes.
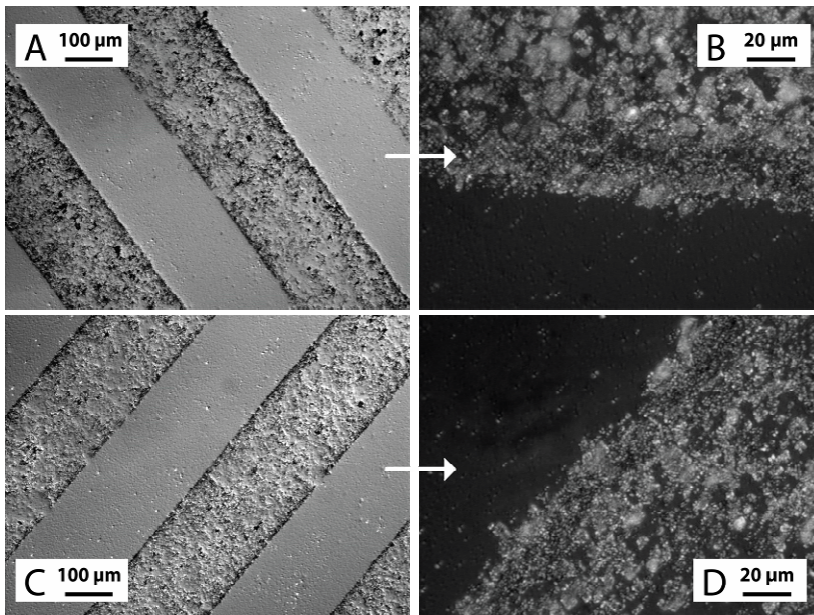
Figure 4-7: Rinsing of the sensor surface after immobilization, A,B thoroughly rinsed with deionised water and C,D thoroughly rinsed with iso-propanol.

Further, heating time and temperature are investigated in Figure 4-8. To investigate the temperature influence a heating time of 10 minutes was applied. The average particles/cluster size was calculated together with the percentage covered of the surface. Microscope images were processed using the image analysis program ImageJ 1.37v from the National Institute of Health, USA [130]. From these measurements, it can be seen that with increasing heating time the average cluster size increases together with the coverage. However the transducer layer is OC_1C_{10}-PPV, which can degrade when exposed to higher temperatures and oxygen. As a result, it may be more favorable to keep the heating time as short as possible.
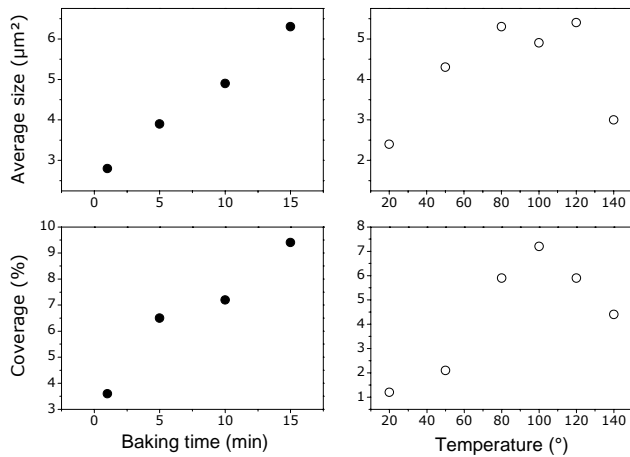
Figure 4-8: Influence of heating time (right) and temperature (left) during immobilization.

In Figure 4-8 a graph is shown of the heating temperature influence on the surface coverage and cluster size. As can be seen, temperatures below the glass transition temperature of the OC_1C_{10}-PPV give low coverage. At higher temperature the coverage significantly improves. However, above 130 degrees the transducer starts to become transparent which is a sign of degradation of the backbone of PPV. An optimal temperature is between 100 and 120 degrees Celsius with a heating time of about 10 minutes.

The thickness of the transducer film plays also an important role in the degree of adhesion of the MIP particles to the film. In Figure 4-9 a thin film of 50 nanometers and a thicker film of 120 nanometers, covered with MIPs using the stamp method, are shown. The coverage of the thick film is 25.2 percent with an average cluster size of 2.5 µm². The thin polymer film has a coverage of 20.4 percent and an average size of 1.9 µm². Only smaller and fewer particles remain adhered to the thinner conjugated polymer film. The larger MIPs are not embedded firmly enough and come off when rinsing the sample. The preference for a sensing device goes to a thicker transducer, which can immobilize larger and more particles and a thicker film is also mechanically stronger.
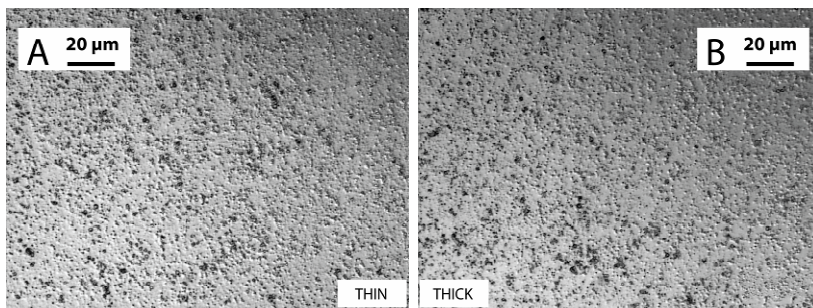
Figure 4-9: Influence of the thickness of the conjugated polymer during immobilization. (a: 50 nm; b: 120 nm)

4.3 Scanning Electron Microscopy

To study the coverage at the sub-micron scale, scanning electron microscopy (SEM) was used. The scanning electron microscope was a FEI Quanta 200 FEG-SEM. In between the large clusters seen with the optical microscope we can distinguish the separate MIP particles on top of the electrodes as shown in Figure 4-10. Here, an as prepared conjugated polymer film (a) is compared with a transducer layer covered with MIP particles using the stamp method (b) and the spincoat method (c). On this sub-micron scale the SEM images give the same conclusion as the optical microscope images.
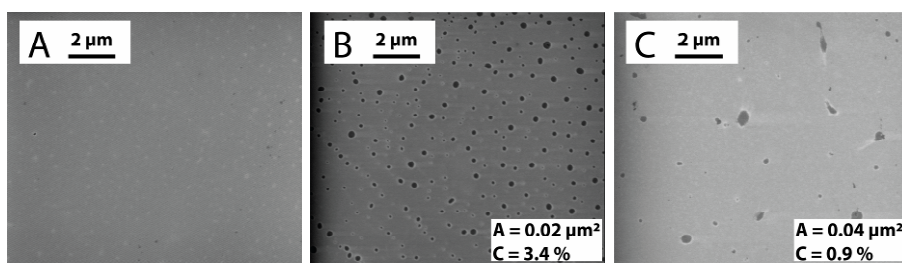
Figure 4-10: SEM image of an as prepared conjugated polymer film (a) and a polymer film with MIP particles immobilized with the stamp (b) and spincoat method (c) using an accelerating voltage of 15 keV and a large-field detector (LFD).

A low coverage and clustering of the particles is seen when the spincoating method is used. For this method the average particles size is 0.04 µm² with a poor coverage of 0.9%. The stamp method yields a particle size of 0.02 µm² and a coverage of 3.4%. This percent can be added to the coverage found with optical microscopy, while with SEM the small particles between the large clusters are visualized.

When looked closer at the small particles, the 'iceberg' effect can be seen. In Figure 4-11 the images of the MIP particles consist of a blurry part and a focused part. This visualizes the 'iceberg' with the blurry part being submerged in the polymer film while the part which sticks out of the film is in focus.
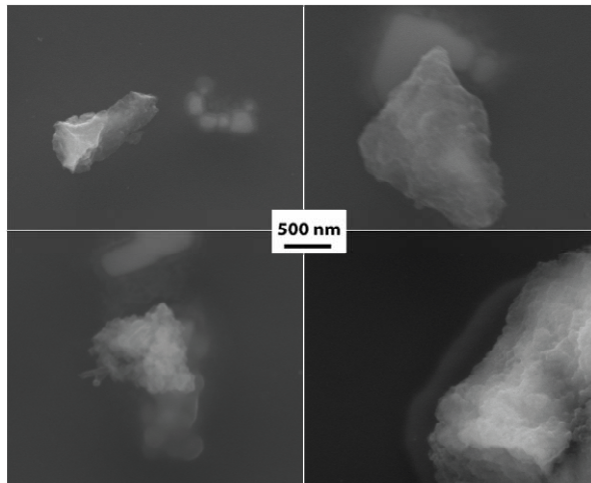
Figure 4-11: SEM image zoomed in on the MIP particles to visualize the iceberg effect using an accelerating voltage of 15 keV and an Everhart and Thornley detector (ETD).

Using the SEM also the surface of an individual MIP particle was studied. In Figure 4-12 the cloudy surface of the MIP can be seen. The sponge-like structure is due to the porogen, which introduces a 3D network on a nanometer scale. Further studies are in progress to investigate this surface more closely using transmission electron microscopy. (TEM)
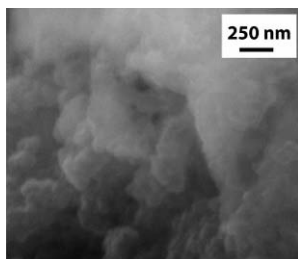
Figure 4-12: SEM images of the surface of a MIP particle
using an accelerating voltage of 15 keV and an ETD.

To investigate the sinking of the MIP particles into the polymer layer, a cross-section was taken of the same specimen. In Figure 4-13a the wide variety of shapes and sizes of the particles can be seen. Figure 4-13b is zoomed in on a sunken particle. In this figure the substrate (1), the transducer (2) and the MIP particles are clearly visible. The splinter (3) has a diameter of 300 nm sunken in a thin polymer layer of 200 nm.
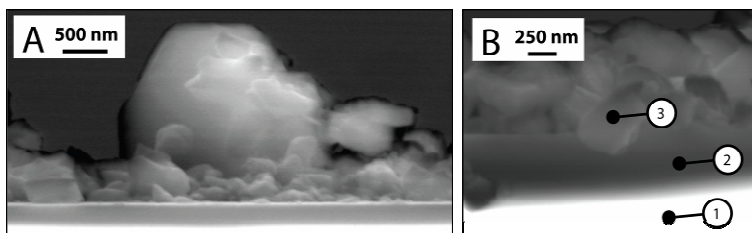
Figure 4-13: SEM images of a cross-section of the sensor surface
using an accelerating voltage of 15 keV and a large-field detector (LFD)
(1: glass substrate, 2: OC_1C_{10}-PPV film, 3: MIP particle).

The microscopy results show the successfully immobilization of the MIP particles on top of the electrode using a conjugated polymer as a semiconductive adhesive layer. However, an improvement of the distribution and uniformity of the MIP particles is desirable. A possible solution is the use of the suspension polymerized particles. A SEM images of such particles is shown in Figure 4-14.
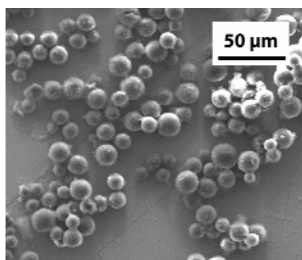
Figure 4-14: SEM images of suspension MIP particles
using an accelerating voltage of 15 keV and an ETD.

However, the suspension method produces beads, which are at least ten micrometer in diameter. Unfortunately this makes them not applicable for the previously discussed adhesion approach by partial submersion in a thin conjugated polymer film. Further work is needed to immobilize such particles firmly to the sensor surface.

Another method to increase the coverage of the MIP on the surface may be by direct spincoating of the MIP solution before UV curing. However this method would produce a dense PMAA film with low affinity for L-nicotine since the porogen would already evaporate during spincoating, and no network would be created in which the target molecule can bind.

4.4 Fluorescence

4.4.1 Theory

When molecules absorb and subsequently emit light, the process is called photoluminescence. Phosphorescence is when the emission continues for a few milliseconds just after the excitation energy is discontinued and fluorescence describes the light emission that continues just after the absorption of the excitation energy and usually occurs in the nano- or microsecond timescale.

The opto-electronic processes associated with fluorescence are schematically shown in Figure 4-15. Prior to the excitation, the molecule is in the electronic ground state S_0, when absorbing a photon of the excitation energy, electrons

may be raised to a higher energy and vibrationally excited state. This process usually takes only a few femtoseconds.
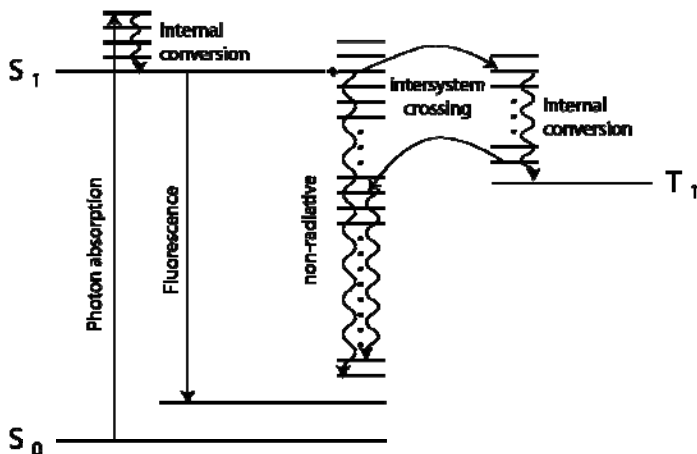
Figure 4-15: Jablonski energy diagram.

In fluorescence, the excited electrons may loose vibronic energy to the surrounding environment in the form of heat, and return to the lowest excited singlet state. From this state the electrons are able to 'relax' back to the ground state with simultaneous emission of fluorescent light. Because of this loss of energy the emission of fluorescence will have a longer wavelength than the excitation. This phenomenon is called the Stokes shift, see Figure 4-16.
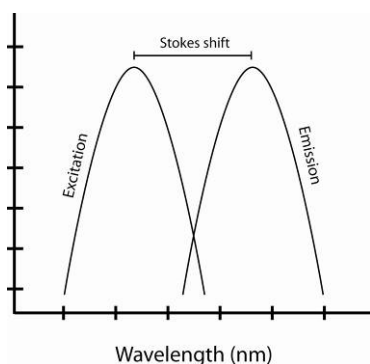
Figure 4-16: Schematic representation of the fluorescence adsorption and emission peaks.

Occasionally, the excited electrons make a forbidden transition to the excited triplet state instead of relaxing to the lowest singlet state through vibrational interaction. In this process, the emission of radiation may be considerably delayed. This is called phosphorescence. This phenomenon is not common because most of these triplet states will be absorbed by oxygen.

4.4.2 Experimental set up

The confocal microscope used in this work was the Zeiss LSM 510 META laser scanning microscope (LSCM) system with an Axiovert 200 motorized frame from Carl Zeiss, Jena, Germany. This confocal microscope is equipped with different light sources with wavelengths 365, 458, 488 and 514 nm. The LSM Meta software version 3.0 to control the Zeiss LSM 510 META was delivered by Zeiss. Using this apparatus images could be taken of the sample surfaces.

To obtain a fluorescence spectrum a QuantaMaster NIR fluorescence spectrophotometer, from Photon Technology International, Seefeld, Germany, was used. The excitation wavelength could be chosen using a monochromator from xenon light source. The spectrophotometer was setup in T-format, the excitation beam is perpendicular to the detector monochromator. The solutions are measured in PMMA cuvettes or quartz cuvettes. The solid films are measured using a substrate holder, placing the sample in front of the incident beam and rotating the sample 30 degrees. The setups is depicted in Figure 4-17.
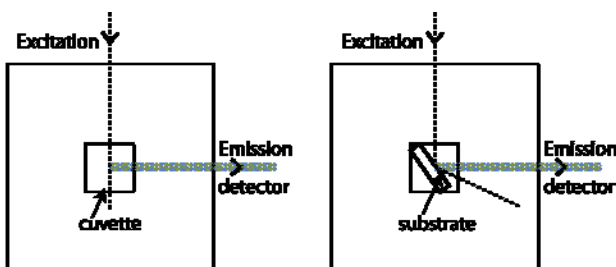
Figure 4-17: Measurement format used to measure fluorescence spectra, left: cuvettes and right: thin films.

4.4.3 Results and Discussion

A fluorescent transducer

Fluorescence spectroscopy was used to investigate the influence of the immobilization step towards the characteristics of the transducer layer. OC_1C_{10}-PPV is a highly fluorescent material. The emission spectrum of the polymer film when excited with 480nm wavelength is shown in Figure 4-18. The extra peak at higher wavelengths are due to aggregation phenomena of two or more polymer chains which interact with each other.
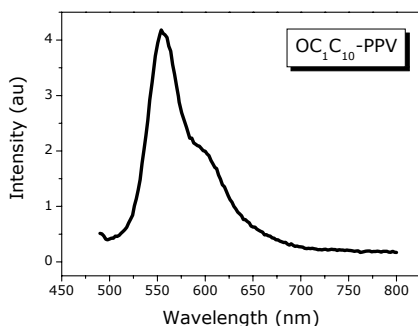
Figure 4-18: Emission spectrum of the transducer layer, OC_1C_{10}-PPV.

Using the confocal microscope, Zeiss LSM 510 Meta, images of the surface were taken to compare the fluorescence properties of the polymer before and after melting the MIP particles. In Figure 4-19 a blank polymer film without and with MIPs immobilized are compared.
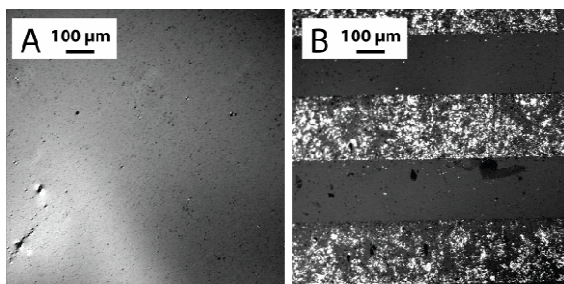
Figure 4-19: Fluorescence image of a blank polymer film (a) and stamped MIP polymer film (b). (excitation 488nm)

It can be clearly seen that the polymer film become less fluorescent when heated above the glass-transition temperature, indicating that the onset of degradation may have occurred. The polymer around the particles is strongly concentrated due to the melting causing bright spots around the particles. The degradation of the polymer film is due to the creation of defects in the conjugated backbone of the polymer. An indication of this degradation is the discoloring of the film. This effect is more evident when the film is exposed to oxygen and UV-light. The energy of the UV-light makes the conjugated polymers more reactive towards oxidation. This oxidation progresses faster at the elevated temperatures used when the MIP particles are immobilized by heating the sample. In Figure 4-20 it is seen how the samples are exposed to UV-light during 15, 30, 60, 120, and 180 minutes at room temperature. This experiment is performed in an oxygen rich environment, *i.e.* air, and a 99.9% nitrogen atmosphere.
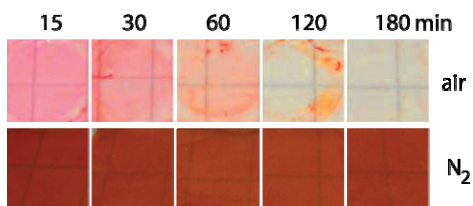
Figure 4-20: Degradation of the OC_1C_{10}-PPV exposed to UV-light.

It can be seen that the series, exposed to oxygen, looses its color rapidly, while the set of samples in the nitrogen atmosphere do not degrade. From all samples also a fluorescence spectrum is taken, which can be seen in Figure 4-21.
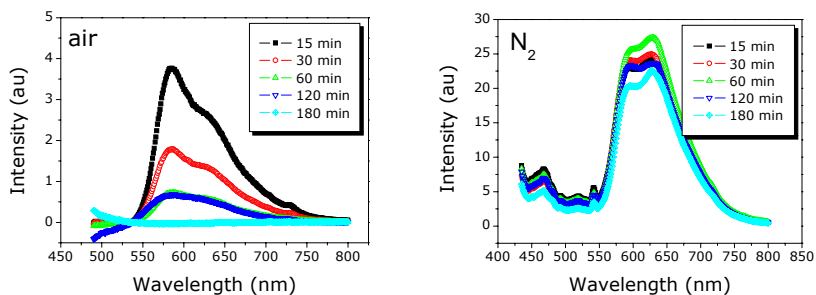
Figure 4-21: Fluorescence spectra, visualizing the degradation of the OC_1C_{10}-PPV.

From these spectra also the conclusion can be drawn that the samples exposed to air degrade fast, while the other set remains intact. This is the reason why the heating time should be taken as short as possible to eliminate degradation of the transducer. The option of immobilizing the powder in a glovebox in nitrogen atmosphere was not possible due to the possibility of contamination with small particles in the glovebox where other sensitive device preparations were performed.

Fluorescence detection read-out

The use of fluorescence for the detection using incorporated MIPs is described in the literature [131-134]. In these articles the authors make use of either fluorescent MIPs from which the fluorescence in quenched upon addition of the target molecule or sometimes the target molecule fluorescence, which causes an increase of the fluorescence upon binding of the analyte [135].

The MAA MIP used in this work does not exhibit fluorescence. In contrast, the conjugated polymer OC_1C_{10}-PPV used in this work, does exhibit notable fluorescence.

While the MAA particles from the MIP are sunken into the conjugated polymer matrix, the distance for influencing the fluorescence of the transducer when L-nicotine is bound in the MIP unfortunately is too large. The quenching typically occurs in close vicinity, *i.e.* about ten nanometers. A solution for this can be the polymerization of the MAA mixed with OC_1C_{10}-PPV and a conjugated polymer containing MIP is obtained (MIP-PPV). When done in an inert atmosphere the

physical properties do not change, as seen in Figure 4-21 and the conjugated polymer apparently remains intact.

Before starting to measure the influence upon binding of the target molecule, first, the influence of the target molecule added to a solution of PPV is investigated. In order to be able to use fluorescence as a detection method the quenching capabilities of L-nicotine and L-cotinine are investigated.

L-nicotine was added in a variety of concentrations to a 0.04 weight% OC_1C_{10}-PPV solution in dichloromethane. After the addition, seen in Figure 4-22, the intensity seems to drop when nicotine is introduced in the solution. The fluorescence intensity peak drops upon addition of 2.5 nM L-nicotine about 20%, and further decreases 20% when the concentration is increased to 6.3 nM.
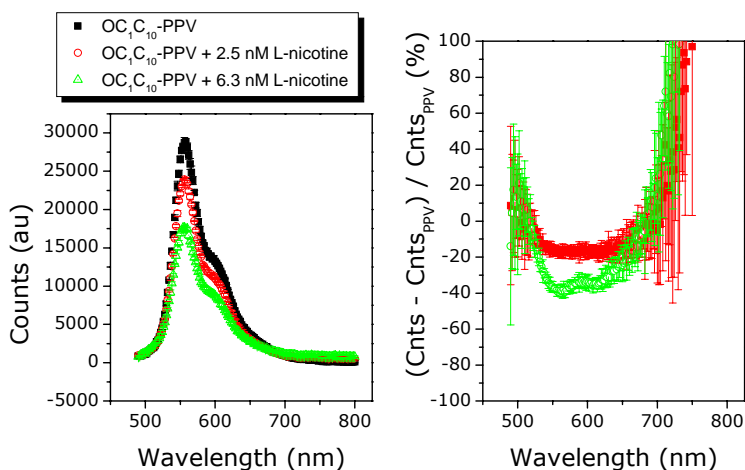
Figure 4-22: Fluorescence signal of OC_1C_{10}-PPV upon addition of L-nicotine.

In Figure 4-23, the same protocol was applied, but now L-cotinine was introduced instead of L-nicotine. Again, the intensity peak of the fluorescence of PPV decreased.
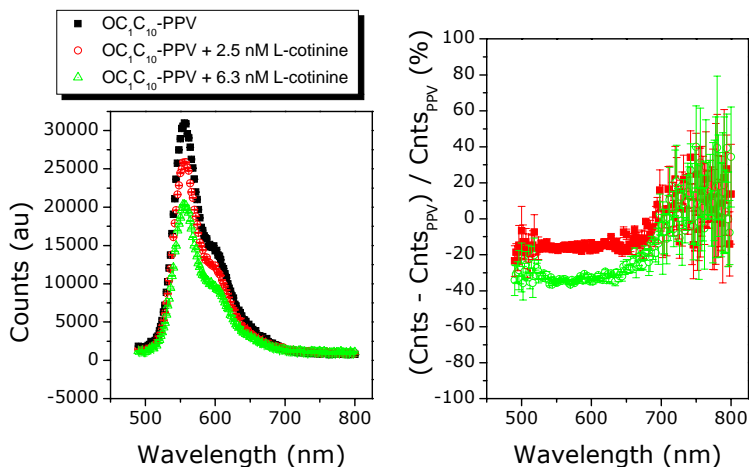
Figure 4-23: Fluorescence signal of OC_1C_{10}-PPV upon addition of L-cotinine.

When 2.5 nM L-cotinine was introduced the fluorescence dropped with 20% and when the concentration was increased the intensity decreased further to 60% of the initial intensity.

Both molecules cause an intensity decrease. In order to be able to use fluorescence as detection method both target molecule and reference molecule have to have the same quenching abilities. In this way the specificity of the binding with the MIP can be investigated. Before assuming the actual presence of a viable quenching effect it is important to verify whether the observed intensity decreases are not due to the dilution of the polymer solution when a certain concentration of L-nicotine or L-cotinine are introduced. The added volumes the L-nicotine and L-cotinine solutions were 300 µL and 900 µL.

As can be seen in Figure 4-24 the fluorescence also decreases when 300 µL and 900µL are introduced without any L-nicotine or L-cotinine present. This indicates a dilution of the conjugated polymer solution. However, the decrease is slightly smaller when compared to the decreases caused by L-nicotine and L-cotinine. This may show a small influence of the target molecules on the opto-electronic properties of the conjugated polymer.
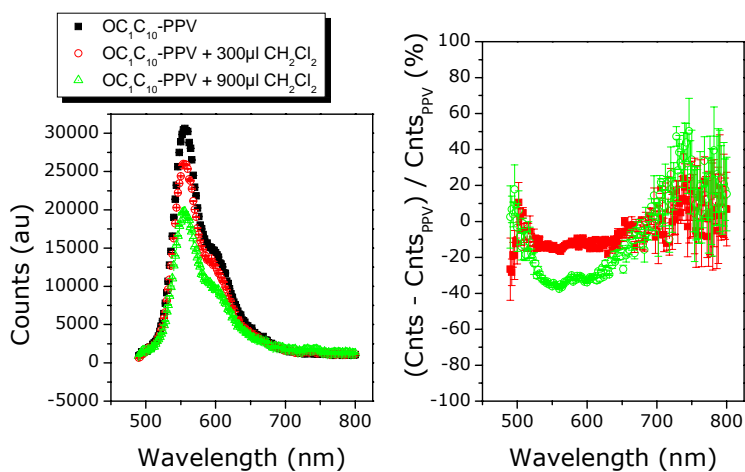
Figure 4-24: Fluorescence signal of OC_1C_{10}-PPV upon addition of dichloromethane.

This influence is better visualized when the curves for L-nicotine and L-cotinine are corrected for the dilution. In Figure 4-25 it is shown that there is a small quenching effect of both molecules, even though it is not evident that this effect is significant. Although the above discussion suggests that the combination OC_1C_{10}-PPV and L-nicotine is not suitable for sensing based on a quenching mechanism, a final experiment was performed with the actual MIP-PPV.
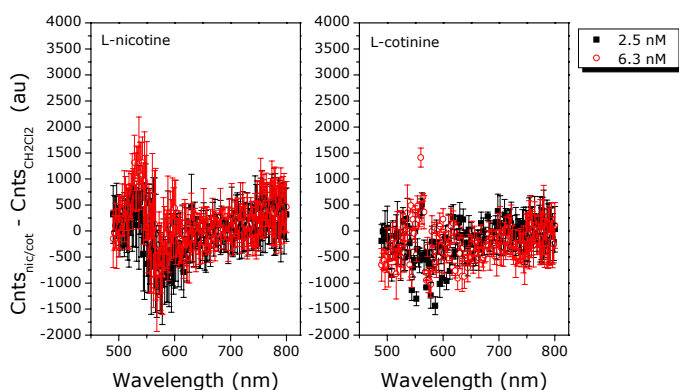
Figure 4-25: Corrected Fluorescence signal of OC_1C_{10}-PPV
upon addition of L-nicotine and L-cotinine.

As mentioned above these detection measurements are performed with conjugated polymer containing MIP particles submerged in concentration of L-nicotine and L-cotinine dissolved in distilled water. These MIP-PPV particles are immobilized on a glass substrate using PDMS, which does not fluorescence in the same spectral region as OC_1C_{10}-PPV.

In Figure 4-26 a MIP-PPV sample is exposed to a concentration of 600 nM and 100 µM L-nicotine. The fluorescence intensity is dropped with respectively 5% and 7.5%.
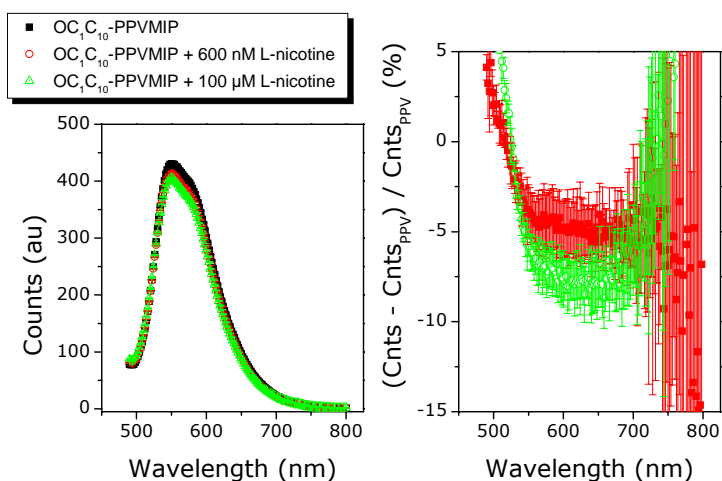
Figure 4-26: Fluorescence signal of OC_1C_{10}-PPVMIP upon addition of L-nicotine.

When a similar sample is exposed to L-cotinine in Figure 4-28, the intensity decreases also upon addition of the molecule. The decrease is in the same order as the decrease upon adding L-nicotine.
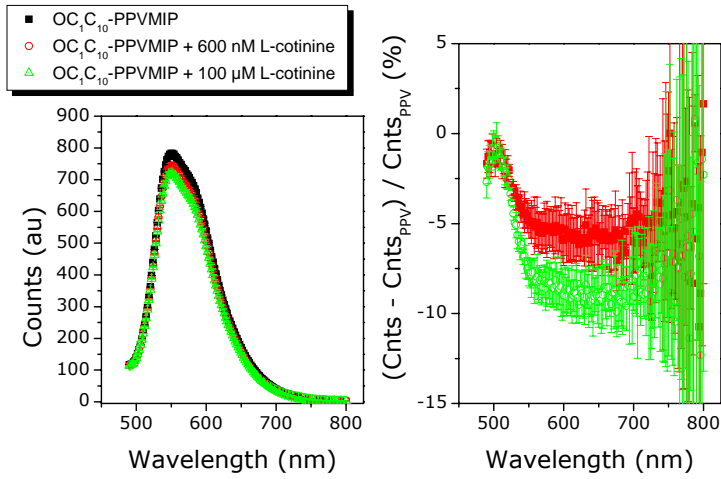
Figure 4-27: Fluorescence signal of OC_1C_{10}-PPVMIP upon addition of L-cotinine.

Both measurements further indicate that these OC_1C_{10}-PPV-MIPs are unsuitable for sensing purposes of L-nicotine, since the decrease can not be assigned to the quenching effect of the molecules, but can also be caused by drift of the signal,.
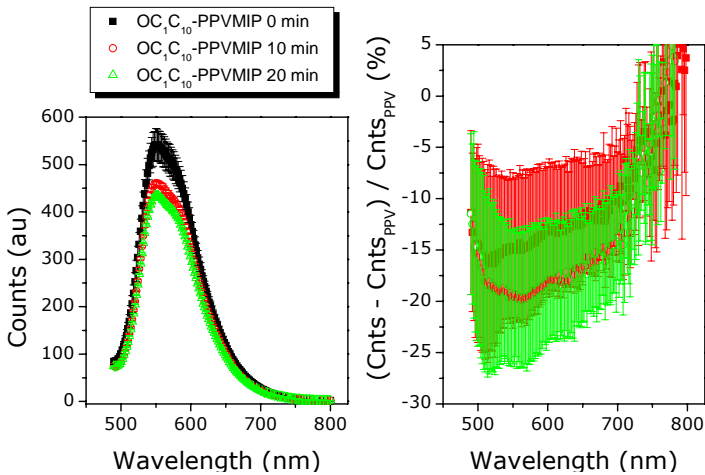
Figure 4-28: Time dependence of the Fluorescence signal of OC_1C_{10}-PPVMIP.

As can be seen in Figure 4-28, an unstable fluorescence signal is observed when these PPV-MIP particles are submerged in an aqueous solution.

4.5 Contact angle studies

4.5.1 Theory

Contact angle measurement is a technique to determine the hydrophilicity of a surface. A droplet of distilled water is dropped onto the sample and the angle the drop makes with the surface is measured. The volume of the droplet is independent of the contact angle. An increasing angle means the surface is more hydrophobic while a decrease in contact angle means it is more hydrophilic, see Figure 4-29. The hydrophilicity is determined by roughness and polarity of the surface.

$\theta > 90°$ $\theta = 90°$ $\theta < 90°$ $\theta = 0°$

repelling   spreading   wetting

more hydrophilic
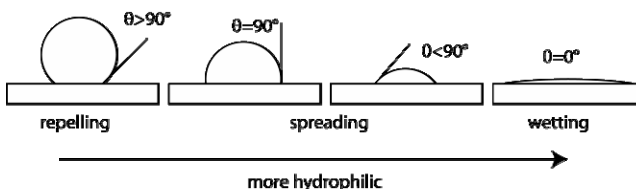
Figure 4-29: Contact angle principle

4.5.2 Experimental results

The contact angle measurements were performed using an OCA 15 plus, video based optical angle measuring device from Dataphysics Instruments GmbH, Filderstadt, Germany. A droplet of distilled water of 1 µl is deposited on the surface and the contact angle is measured by fitting the droplet image of the camera.

The contact angle measurements in Figure 4-30 show a distinct difference between OC_1C_{10}-PPV, OC_1C_{10}-PPV with MIPs and MIPs spincoated together with OC_1C_{10}-PPV . Pure OC_1C_{10}-PPV is strongly hydrophobic, characterized by its large contact angle.
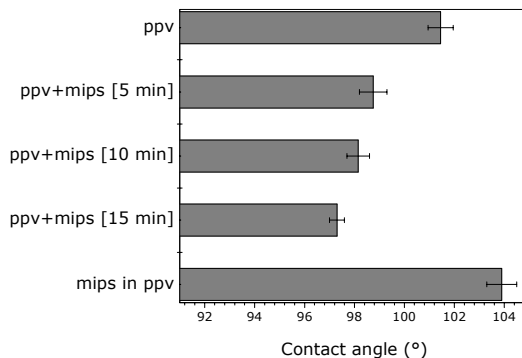
Figure 4-30: Wettability of the sensor surface.

The roughness of a surface improves the wettability for hydrophilic surfaces (< 90°). The drop will seem to sink into the hydrophilic surface. The wettability decreases for hydrophobic surfaces ($\theta > 90°$). It gets energetically too unfavorable to wet a rough hydrophobic surface. The result is an increased water-repellency. As can be seen from the decreasing contact angles, the OC_1C_{10}-PPV becomes somewhat less hydrophobic upon introduction of the MIP particles to its surface. However, when the particles are spincoated together with the conjugated polymer, which is hydrophobic, a hydrophobic rough surface is obtained, increasing the contact angle. This wettability effect can be important since the sensor will operate in a liquid environment.

4.6 Discussion

UV-Vis spectroscopy has been used to characterize the MIPs before implementing them in the sensing device. Binding properties have been investigated using the Freundlich model, which indicates the occurrence of specific recognition of L-nicotine and insensitivity towards L-cotinine. The measured values of the binding parameters are comparable to literature values [136].

The microscopy results show a good immobilization of the powdered MIP to the OC_1C_{10}-PPV covered electrode surface using the PDMS stamping technique. With

the SEM smaller particles between the large clusters could be noticed. Although only about 24 percent of the surface was covered with MIP particles, this may be improved in the future by growing thin films of MIP directly onto the conjugated polymer covered electrode surface.

The influence of the heating of the MIPs to the physical properties of the transducer was investigated using fluorescence spectroscopy. The measurements reveal that it is favorable to keep the heating time a as short as possible to prevent degradation of the transducer. An optimum was found between good coverage and minimal destruction of the backbone of the OC_1C_{10}-PPV polymer, by heating the polymer with the stamped MIPs for 10 minutes at 100 degrees Celsius.

The fluorescence data showed no clear evidence of a quenching effect of L-nicotine towards the conjugated polymer OC_1C_{10}-PPV. For the development of a optical sensing device based on the quenching effect the lowest unoccupied molecular orbital (LUMO) level of the target molecule should be sufficiently low as compared to the conjugated polymer. This is apparently not the case for L-nicotine. However for some molecule which can effect the fluorescence of the polymer, fluorescence spectroscopy could a useful reference technique.

Using the contact angle measurement an insight is be obtained on the wettability of the surface when the substrate is exposed to liquid. This property is very important for the understanding whether dissolved target molecules have good access to the porous MIP structure.

Chapter 5 - Impedimetric detection of nicotine and histamine

The electronic detection of the target molecules is performed using electrochemical impedance spectroscopy. This technique is a very sensitive technique, which is very popular in literature for use as a detection method [17, 34, 121, 137-140]. First, the proof of principle using this technique is combination with MIPs will be shown. The target molecule L-nicotine is used for this. Next, a medical more relevant target molecule is chosen, *i.e.* histamine.

5.1 Materials and Methods

During this work two different impedance analyzers were used. The first apparatus was the 'HP4194A impedance/gain-phase analyzer', from Hewlett-Packard, USA. The successor apparatus to be used for the electronic sensing is 'IVIUMstat electrochemical interface' from Ivium Technologies, the Netherlands. Both analyzers are shown in Figure 5-1.

Figure 5-1: A) 'HP4194A impedance/gain-phase analyzer', from Hewlett-Packard, USA B) 'IVIUMstat' electrochemical interface, from Ivium Technologies, the Netherlands.

The HP4194A has a frequency range from 100 Hz to 40 MHz, capable of measuring 10mΩ to 100MΩ impedance values. Because for the sensing measurements it is important to have sufficient sensitivity in the lower frequency range, a successor, *i.e.* the IVIUMstat, was chosen, which is capable of measuring with a frequency range from 10μHz to 1MHz with impedance values of 1 Ω to 100 GΩ. The electrochemical impedance experiments were done using a homemade electrochemical impedance cells. The different channels were measurement subsequently using a multiplexer.

For the first step towards a handheld device a home made impedance analyzer was build. This device was capable of measuring the impedance at a fixed frequency between 0.1 and 1000 Hz within the range of 50 kΩ and 100 mΩ. The main advantage of this system is the low influence of cable interference because the closed system. This enables the device of measuring currents in the nano ampere range with almost no noise as a result of interference.

The data collection protocol consisted of measuring both Z and the phase shift as function of frequency. This was done time resolved mostly monitoring at a fixed frequency in the lower range (100 Hz – 1 kHz) and monitoring the change when a certain concentration of target molecules was added. Data collection software was a self-developed Labview program (National Instruments). After stabilization, the entire spectrum was used to fit according to an equivalent electrical circuit. ZSimpWIN from Princeton Applied Research, USA, was used to fit the data.

In this project different kinds of measurement configurations were used. They are all visualized in Figure 5-2. In the following description of the measurements, the cell code letter will be used to indicate which configuration is utilized.
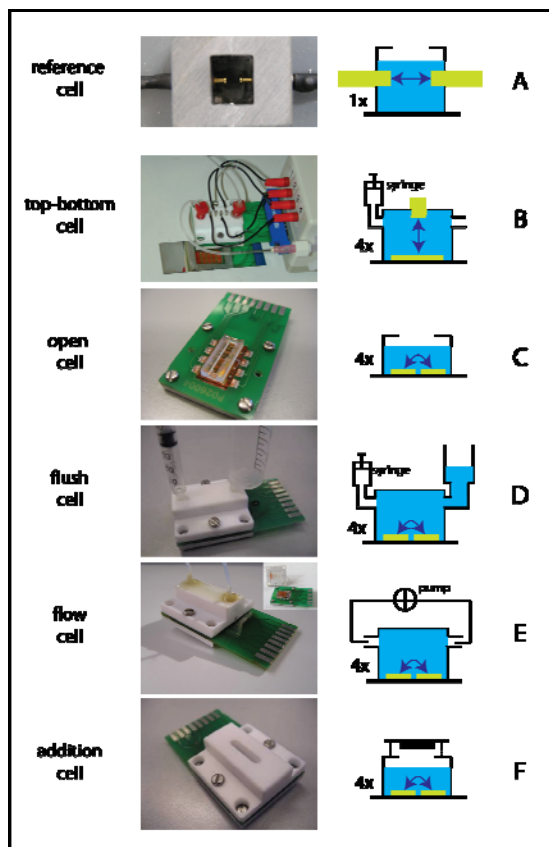
Figure 5-2: Different types of configurations used in this work shown with picture, schematic cross-section and sensor code, see text for explanation in detail.

5.2 L-Nicotine detection

As a proof of principle, the early tests were performed with MIPs for L-nicotine. This MIP is already described in the literature and fine tuned for our goals. First, influences of electrolyte, temperature, light, pH etc. need to be considered before going to actual detection tests. The electrolyte is of significant influence on the measurement. To get a better understanding, first distilled water was used to dissolve L-nicotine. Because the goal was making a sensor for medical

or environmental purposes, the sensor should after all be able operate in aqueous solutions.

5.2.1 L-nicotine in distilled water

In Figure 5-3 the different impedance spectra are shown of the test solutions. The impedance of the solutions was measured using two gold electrodes opposite to each other. The cell constant is 6.3 cm^{-1}. Distilled water, dH$_2$O, is compared with L-nicotine and L-cotinine dissolved in distilled water.
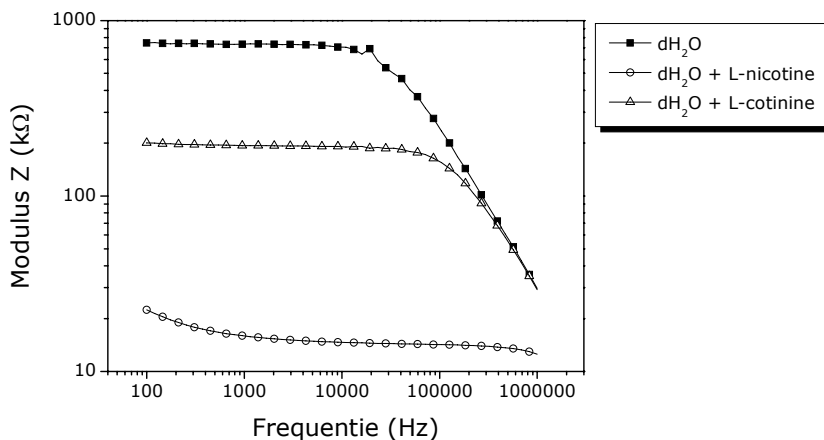
Figure 5-3: Impedance spectra of distilled water, 1 mM L-Nicotine in distilled water, and 1 mM L-cotinine in distilled water (cell A).

Distilled water has a poor conductivity, being at the lower frequency range about 1.3 µS/cm. L-nicotine increases the conductivity more in comparison with L-cotinine in distilled water. This indicates that the target molecule plays an important role in the impedance change. Therefore when detection measurements are performed a reference channel should be taken into account to eliminate this influence.

Table 5-1 shows the parameters from the equivalent electrical circuit from the data in Figure 5-3. As equivalent circuit the Randles cell is used. For the distilled water measurement, an evaluation of the solution resistance shows the L-nicotine decreases the resistance more than L-cotinine. Apparently, L-nicotine acts in water as a better charge carrier than L-cotinine. When the solution is

more conductive the double layer at the electrode interface will be thinner. This results in a higher double layer capacitance. This thinner double layer makes it also easier to exchange charge at the interface, which relates to the charge transfer resistance.

Table 5-1: Parameters of the equivalent circuit fitted from Figure 5-3.

	$R_{solution}$ (Ω)	$C_{double\ layer}$ (pF)	$R_{charge\ transfer}$ $(k\Omega)$
dH_2O	4369 ± 655	5.86 ± 0.05	727 ± 7
dH_2O + L-nicotine	2391 ± 356	8.23 ± 0.07	10 ± 0
dH_2O + L-cotinine	3158 ± 473	5.68 ± 0.06	190 ± 1.9
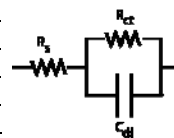
The next measurements are performed in sensor device B. The change in the Nyquist plots when one electrode is covered with the conjugated polymer and MIPs is shown in Figure 5-4. The first semi-circle which is also present for the Au-Au electrodes returns for the Au-Au/PPV/MIPs electrodes. However, in addition at the lower frequency range another semi-circle starts to form for the PPV/MIPs coated sample.
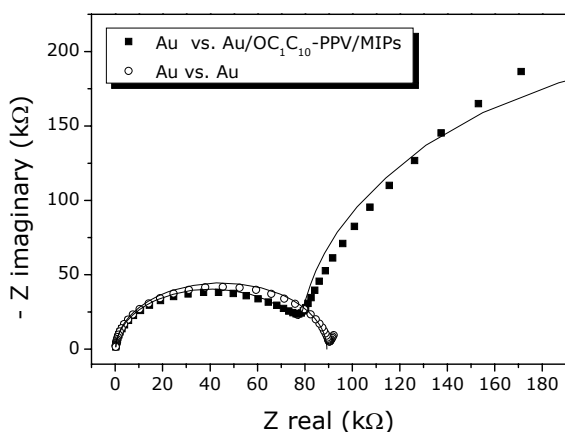
Figure 5-4: Nyquist plots of Au-Au and Au-Au/PPV/MIPs in distilled water (cell B).

In Table 5-2 the parameters of the spectra are shown. The Au-Au cell can still be fitted using the Randles circuit, while the Au-Au/PPV/MIPs cell is now fitted with the Randles circuit in series with a parallel circuit of a resistor and a capacitor. The fitted curves are indicated by the solid line in the figure.

Table 5-2: Parameters of the equivalent circuit fitted from Figure 5-4.

	Au – Au/OC$_1$C$_{10}$-PPV/MIPs	Au-Au
R$_{solution}$ (Ω)	227 $\pm$ 36	235 $\pm$ 35
C$_{double\ layer}$ (pF)	108 $\pm$ 1	104 $\pm$ 1
R$_{charge\ transfer}$ (kΩ)	78 $\pm$ 1	89 $\pm$ 1
C$_{coating}$ (nF)	6.1 $\pm$ 0.1	/
R$_{coating}$ (kΩ)	403 $\pm$ 20	/
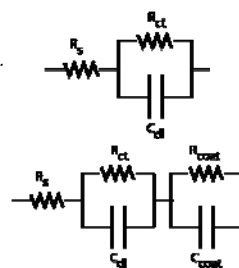
The value from the first semi-circle in Table 5-2 differ somewhat in comparison to the values of the semi-circle obtained for distilled water in Table 5-1. This is due to the change of measurement cell dimensions, thus a change of cell constant. The capacitance of the coating is about 6.1 nF from which the thickness of this capacitor can be calculated using equation (5.1) where ε_r is the relative dielectric constant of the polymer being about 3.01 [141], ε_0 the permittivity of free space (8.854.10^{-12} F/m), A the area and d the distance between the 'plates' of the capacitor.

$$C = \varepsilon_r \varepsilon_0 \frac{A}{d} \qquad (5.1)$$

From the above equation the distance between the capacitor plates is about 176±7 nm. This value is close to the thickness of the conjugated polymer in which the MIP particles are submerged.

The first measurements using device B are performed in distilled water and the impedance at the lower frequencies is tracked in time. In Figure 5-5 the reference channels are depicted, and in Figure 5-6 the MIP coated electrodes are shown. The addition of the target molecule is indicated with an arrow. In general the lower frequencies represent interactions, which take place at the interface of the electrodes. These effects are important to investigate the binding of the target molecule with the MIPs. The start volume in the cell was 200 μl. To this background solution 50 μl of a certain concentration is added, resulting in the total concentration mentioned in the graph. After optimization, a frequency of 213 Hz was chosen.
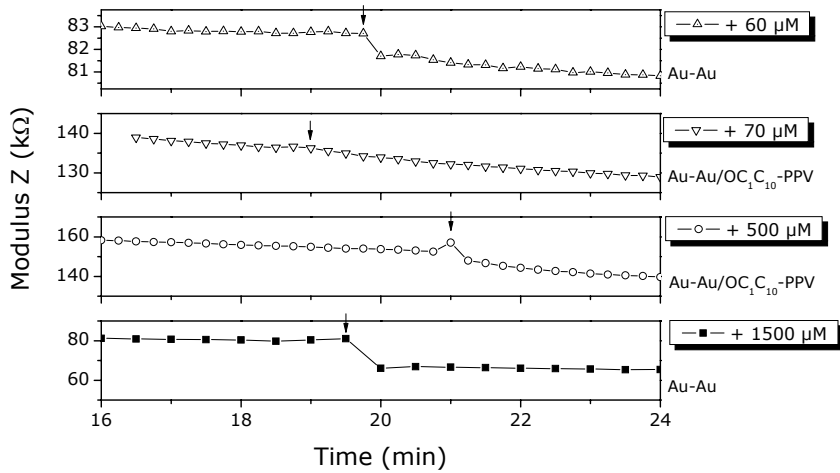
Figure 5-5: Time-resolved impedance signal of the reference channels
upon addition of L-nicotine in distilled water, measured at 213 Hz. (cell B)
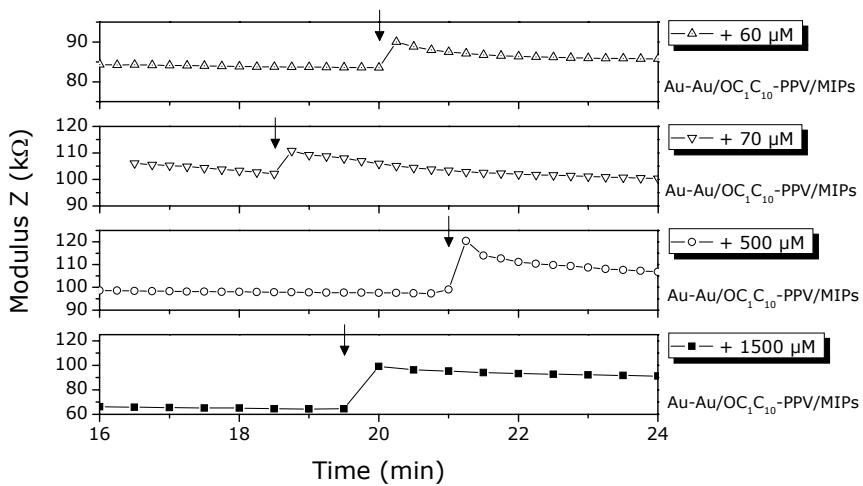
Figure 5-6: Time-resolved impedance of the MIP coated electrodes
upon addition of L-nicotine in distilled water, measured at 213 Hz. (cell B)

All measurements were performed at a constant temperature of 37.5°C to mimic the body temperature for medical relevant measurements. The graphs show, for the reference channels, a decrease of the impedance signals when L-nicotine is introduced into the measurement cell. This is probably due to the introduction of

L-nicotine as a charge carrier in the solution. The impedance signal of the MIP on the other hand increases upon addition of L-nicotine in the cell. The explanation of this increase can be found in L-nicotine replacing the water, which is present in the MIP structures. The dielectric constant of L-nicotine, 8.9 is much lower than the one from water ~80. [142, 143] The dielectric constant is proportional to the capacitance while the capacitance is inversely proportional to the impedance. This explains the increase of the impedance when L-nicotine is introduced.

Further developments lead to a switch from sensor B to sensor C. This device allows simultaneous detection of four different channels and all electrodes are covered with the transducer. Whereas, this increases the resistance and thus the noise, the influence of undesired changes at the counter electrode are eliminated. The Au electrode is replaced by a Ti electrode. Ti adheres better to the glass substrate resulting in a more stable electrode. Sensor C also allows for the measurement with an 'addition' or a 'flow' design by changing the cap of the measurement cell. The extra channels allow the monitoring of the behavior of a non-imprinted polymer, NIP, which is measured as an extra reference. Figure 5-7 shows the changes to the impedance signal upon addition of L-nicotine using sensor B with the addition design. Also for this cell, an increase of the modulus is seen for the MIP.
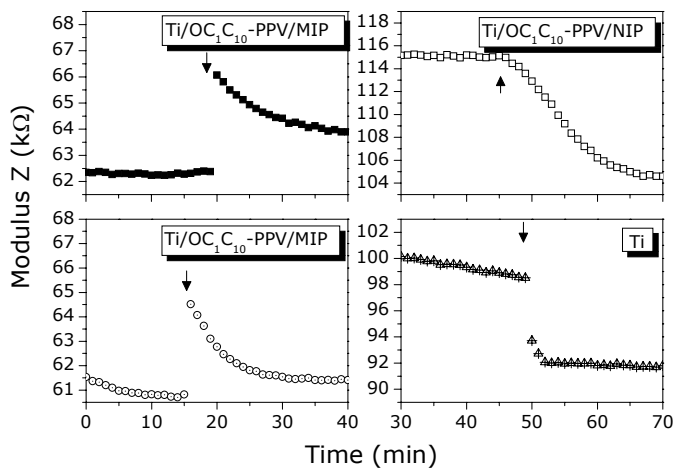
Figure 5-7: Time-resolved impedance of the MIP coated electrodes
upon addition of 500 µM L-nicotine in distilled water measured at 213 Hz. (cell C),

A repetitive addition of L-nicotine in the sensor device is depicted in Figure 5-8. A NIP covered electrode and a blank Ti electrode serve as references and are compared with the MIP.
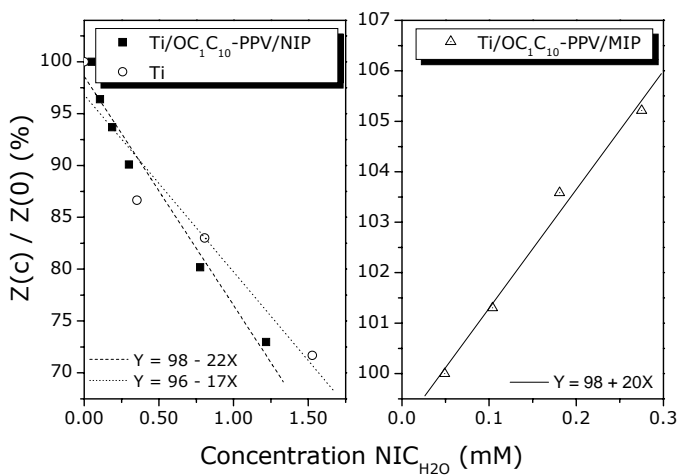
Figure 5-8: Dose-response curve of the reference electrodes and
the MIP coated electrodes, measured at 213 Hz. (cell C)

The impedance change is plotted against the concentration, which is introduced. The linear fits are presented in the graph. The dose-response curve indicates specific response of the sensor with a sensitivity of 20% increase of impedance per millimolar. The fits from these measurements are shown in Figure 5-9 and the parameters from respectively the equivalent circuit can be found in Table 5-3 for a variety of L-nicotine concentrations. From the parameters it can be seen that the impedance in at the lower frequency range (212 Hz) can be sued as a measure for the charge transfer resistance.

Table 5-3: Parameters from the R(CR)(CR) circuit fitted from Figure 5-9.

	Ti/OC_1C_{10}-PPV/MIP				Ti/OC_1C_{10}-PPV/NIP			
conc. (µM)	0	48	104	184	0	48	56	200
$R_{solution}$ (Ω)	140±21	138±20	134±20	126±18	166±24	165±23	151±24	114±17
$C_{double\ layer}$ (pF)	144±1	145±1	146±1	148±0	82±1	82±1	83±0	84±1
R_{ct} (kΩ)	62±1	64±0	66±0	75±0	1002±1	926±0	745±0	423±0
$C_{coating}$ (nF)	8.6±0.7	8.6±0.6	8.2±0.5	7.4±0.8	5.9±0.7	6.6±0.5	7.6±0.4	12.5±0.2
$R_{coating}$ (MΩ)	3.5±0.5	3.3±0.4	3.2±0.6	3.9±0.7	2.1±0.4	2.4±0.6	2.0±0.4	7.3±2
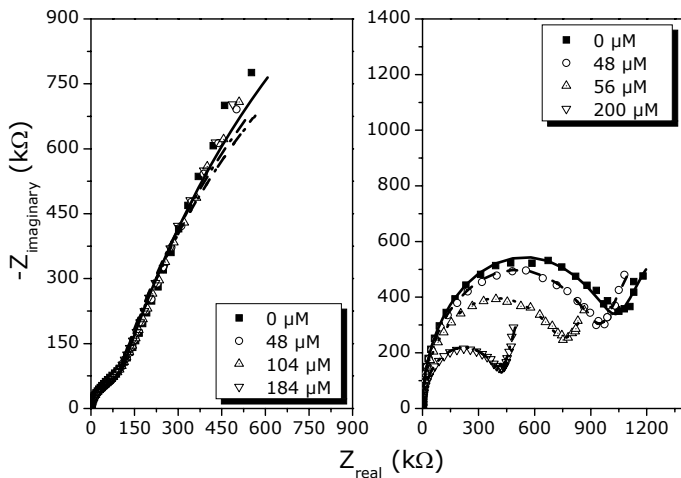
Figure 5-9: Nyquist plots of Ti/OC_1C_{10}-PPV/MIP and Ti/OC_1C_{10}-PPV/NIP in distilled water (cell C).

There are also some trends discernable for the other fitting parameters associated with the electrode coating, but they are less trustworthy because

when these parameters are used to simulate the complete Nyquist plot, it can be seen that to be sure whether or not these values are correct a complete spectrum has to be recorded from 1 MHz until 0.1 Hz, which is not possible with the HP4194A. Please not that the IVIUMstat was not yet available at that moment.
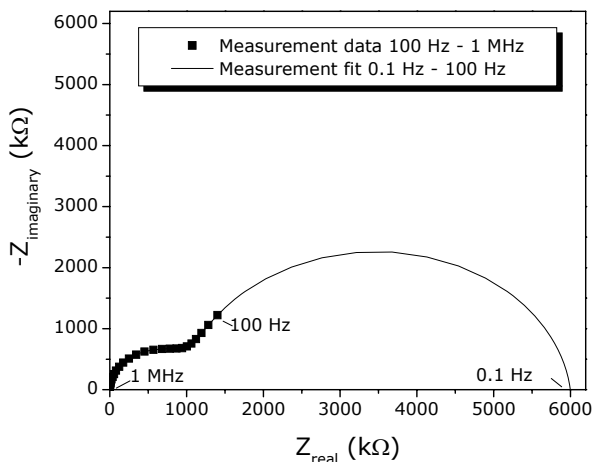
Figure 5-10: Simulated Nyquist plot using the parameters from Table 5-3.

In Figure 5-10, the simulated curve is plotted for the Ti/PPV/MIP channel where 184 µM L-nicotine is added. The resistance of the coating of 3.9 MΩ, which was obtained at the very low frequency of 0.1 Hz.

Introducing L-nicotine decreases the resistance of Ti, the Ti/PPV and the Ti/PPV/NIP channels. This fact applies for all the measurements. When the Ti/PPV/MIP channels are exposed to L-nicotine mostly the impedance increases, but in some cases the impedance does not change or decreases. One such measurement is shown in Figure 5-11.
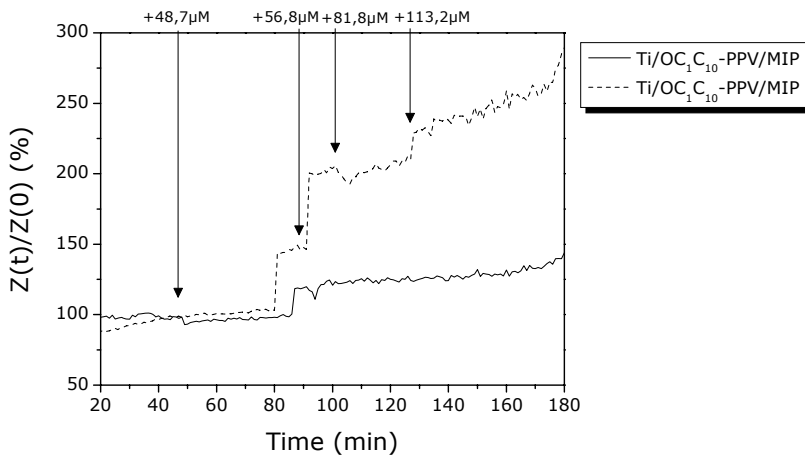
Figure 5-11: Time resolved impedance of two Ti/OC$_1$C$_{10}$-PPV/MIP channels upon addition of L-nicotine in distilled water (cell C)

Here upon addition of the target molecule the impedance does not react as expected. A variety of reasons can be identified which might explain the mixed results of the sensor. For example, there could be too few MIPs immobilized on the surface, MIPs coming off the transducer or the occurrence of degradation of the polymer film. Other explanations could be due to uncontrollable parameters such pH and ionic strength of the solution when using distilled water as solvent.

5.2.2 L-nicotine dissolved in acetonitrile

Trying to solve the reproducibility problems several ideas were brought up. First, L-nicotine can be measured in acetonitrile CH$_3$CN, ACN, instead of water, which is the same solvent as used with the UV/Vis measurements. This should decrease influences of other molecules in the solution and, enhance the MIP selectivity.
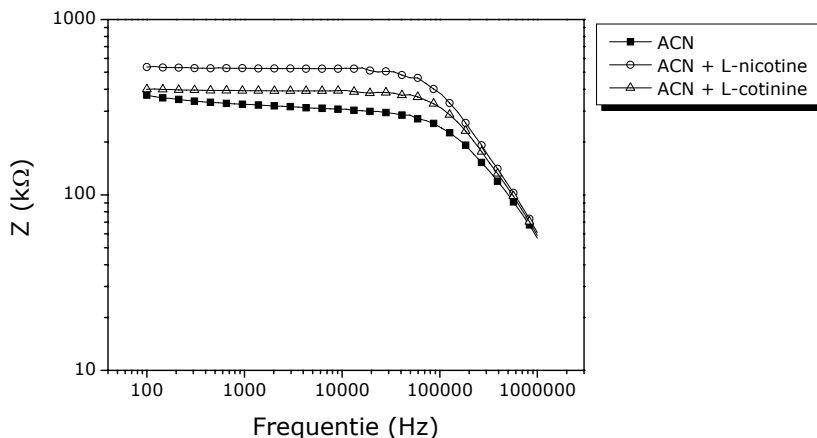
Table 5-4: Parameters of the equivalent circuit fitted from Figure 5-12.

	$R_{solution}$ (Ω)	$C_{double\ layer}$ (pF)	$R_{charge\ transfer}$ (kΩ)
ACN	10310 ± 1340	2.79 ± 0.03	1008 ± 12
ACN + L-nicotine	10360 ± 1346	2.87 ± 0.05	683 ± 5
ACN + L-cotinine	10600 ± 1399	2.82 ± 0.06	1883 ± 18
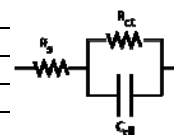
Although the target molecules would not be dissolved in ACN in typical biological samples, which is the main drawback of using ACN as an analyte solution, ACN would be a good reference to be able to compare the UV-Vis measurements with the impedance spectroscopy. In Figure 5-12 and Table 5-4 the impedance spectra and fit parameters are shown for the different solutions of ACN. These indicate that L-nicotine decreases the charge transfer resistivity while L-cotinine increases the resistivity. Using this electrolyte an addition measurement is performed using ACN, shown in Figure 5-13. Here the MIP and NIP particles were stamped on top of the PPV coated electrodes.
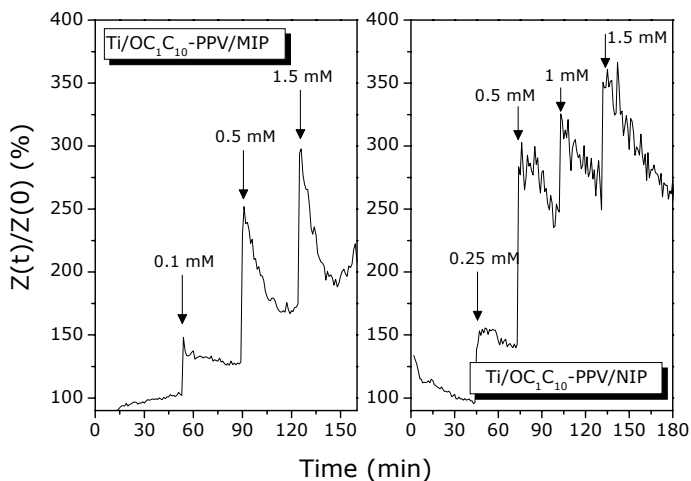
Figure 5-13: Time resolved impedance of a Ti//OC$_1$C$_{10}$-PPV/MIP and Ti//OC$_1$C$_{10}$-PPV/NIP channel upon addition of L-nicotine in ACN (cell F).

The impedance change of the MIP channel is smaller in comparison to the NIP channel. In this measurement it is not clear which effect is seen, while the signal change is not related consistently with the addition of the target molecule. Probably, these effects are related to the impedance change of the solution resistance, which was also seen in Figure 5-12.

Using ACN, also an alternative type of activated electrodes was tried out in which the electrodes were covered with the synthetic receptors by spincoating the MIP and NIP before UV-hardening. The graphs are shown in Figure 5-14. This measurement was performed with a syringe system to be able to flush the cell after introducing the target-molecule. The cell was first filled with can. After this a solution of L-nicotine in ACN is used to fill the cell. Subsequently, after the cell is again flushed with ACN, a solution of L-cotinine is introduced. Finally, the cell is again flushed with ACN. The impedance from the MIP channel drops 70% when 1 mM of L-nicotine is introduced and drops 60% when L-cotinine is introduced. For the NIP channel the impedance drops 20% upon addition of L-nicotine and 30% upon addition of L-cotinine.
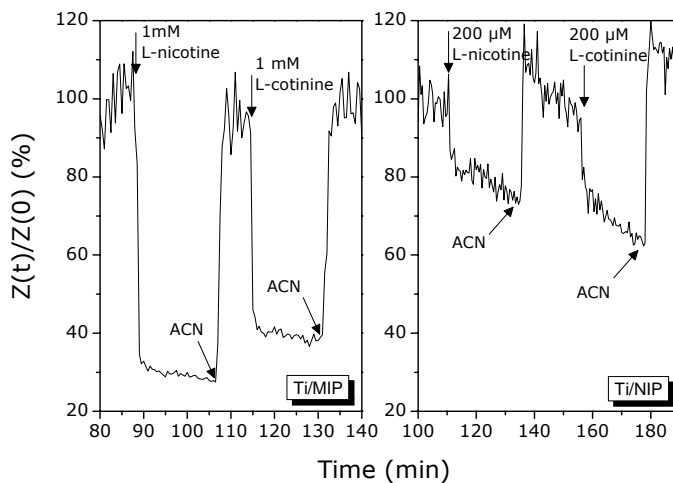
Figure 5-14: Time resolved impedance of two Ti/MIP and Ti/NIP channel upon addition of L-nicotine and L-cotinine in ACN (cell D).

The spincoated MIP and NIP samples initially have a high resistance. From the reaction of the MIP and NIP channels no consistency can be found between the samples. The spincoating of the solution of the MIP and NIP probably affects the working principle of the MIP. The porogen, which is present in the solution evaporates during spincoating before the samples are UV hardened. This will limit the porosity and thus the specific binding sites will be blocked. The ACN also causes some other problems, like dissolving the glue from the Teflon cover. Hence, the use of this solvent was not deemed viable. Notwithstanding, the impedimetric method of measuring MIPs in organic solvents may be applicable providing further optimizations.

5.2.3 Saline solution as electrolyte

In the following measurements, an attempt is made to limit the influence of L-nicotine or L-cotinine as a charge carrier by making the solution highly conductive. In this way, adding the target molecule will have only a minimal influence on the conductivity of the solution.

In Figure 5-15 the Nyquist plots are shown of adding salt, NaCl, to distilled water. This is measured between two gold electrodes. The lower concentration

range has little effect on the conduction mechanism inside the measurement cell. The Nyquist plots can still be considered as semi-circles. However, at the higher concentration range other effects come into play while the Nyquist plots are no longer just semi-circles. For good conducting electrolytes the simple Randles circuit does not apply any more, but other processes like diffusion, electrode roughness, etc. have a significant influence.
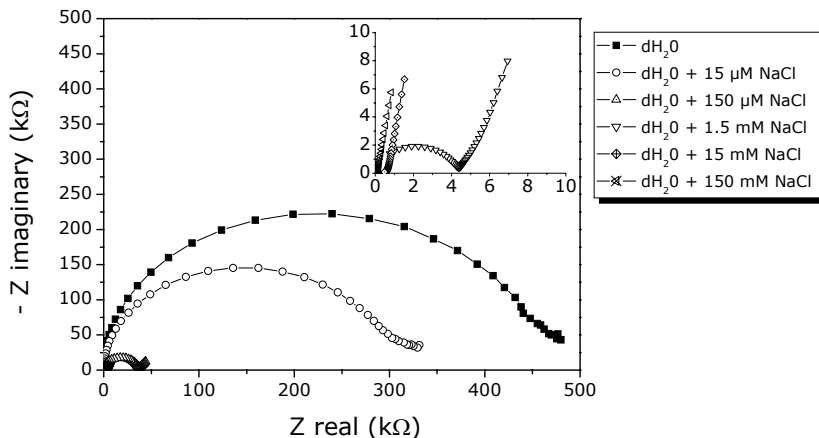
Figure 5-15: Nyquist plot of NaCl concentrations dissolved in distilled water, the inset shows a closer view of the higher NaCl concentration. (cell A)

In Figure 5-16 the bode plots are shown of 0.9 w% NaCl concentration to which 200 µM L-nicotine and L-cotinine are added. As indicated above another equivalent electrical circuit was used to obtain the fitting parameters. The values are fitted using an electrolyte resistance in series with a leaking capacitance, which is represented by a constant phase element, CPE. The parameters can be found in Table 5-5.
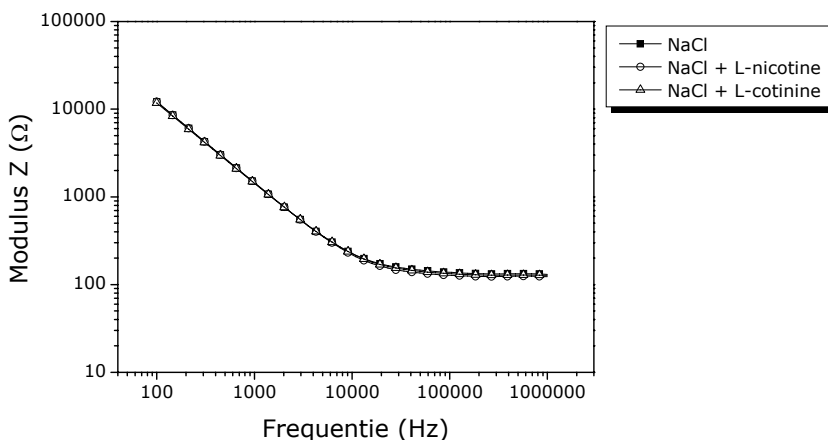
Figure 5-16: Impedance spectra of 0.9 w% NaCl solution, 200 µM L-nicotine in 0.9 w% NaCl solution, and 200 µM L-cotinine in 0.9 w% NaCl solution (cell A).

Table 5-5: Parameters of the equivalent circuit fitted from Figure 5-16.

	$R_{solution}$ (Ω)	$CPE_{double\ layer}$ (nF)	n	
NaCl	134 ± 20	211.5 ± 0.3	0.92 ± 0.00	
NaCl + L-nicotine	128 ± 19	212.6 ± 0.1	0.92 ± 0.00	
NaCl + L-cotinine	132 ± 20	227.1 ± 0.5	0.92 ± 0.00	
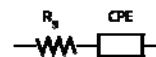
Both, graph and table, show that the effect of the L-nicotine and L-cotinine on the conductance of the solution is minimized. Svob Troje described also three forms in which L-nicotine can be present [144] in aqueous saline solutions. The transition from the protonated form (at low pH) to the unprotonated form of L-nicotine is visualized in Figure 5-17. The protonated form is the most soluble in aqueous solutions but the additional protons can potentially impede the correct fitting of the L-nicotine molecule in the nanocavity of the MIP. Literature studies therefore indicate that a stable pH is required [145].
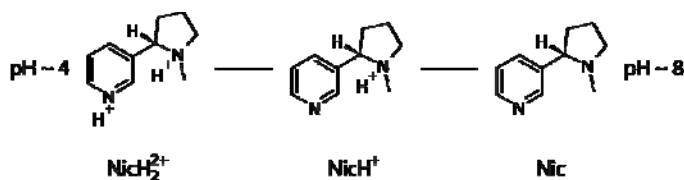
Figure 5-17: Different forms of the L-nicotine molecule, depending on the acidity of the solution.

Keeping the pH constant would also eliminate the charge transfer decrease, which is caused when L-nicotine is introduced in the measurement cell, as previously seen in the reference measurements. The fact that dependent on the pH, nicotine may be positively charged indicates that also the bias of the measurement can be a variable of interest. This bias was previously kept at 0 mV can influence the measurement positively. In Figure 5-18 measurements are performed in saline solutions at pH 4 and 8 at zero bias. The measurement at pH 4 exhibits the largest change in impedance, whereas the measurement performed at pH 8 is more sensitive and starts to detect L-nicotine at lower concentrations. This indicates that at pH 8 the unprotonated form can bind specifically at lower concentrations. At pH 4 the protonated form of L-nicotine starts to bind notably at higher concentration, which may be the result of non-specific binding.
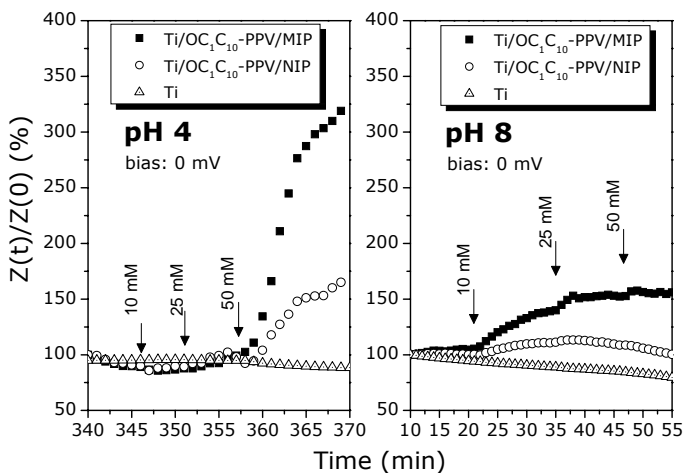
Figure 5-18: Influence of impedance of Ti//OC$_1$C$_{10}$-PPV/MIP, Ti//OC$_1$C$_{10}$-PPV/NIP and Ti channel upon addition of L-nicotine at pH 4 and 8.(cell F)

Investigating the bias dependence, the measurements at pH 4 showed, as expected, a stronger impedance change at negative bias. At this lower pH the positively charged L-nicotine is more attracted to the negative electrodes. This can also be seen in Figure 5-19. At zero and positive bias the sensor only reacts to the higher concentrations.
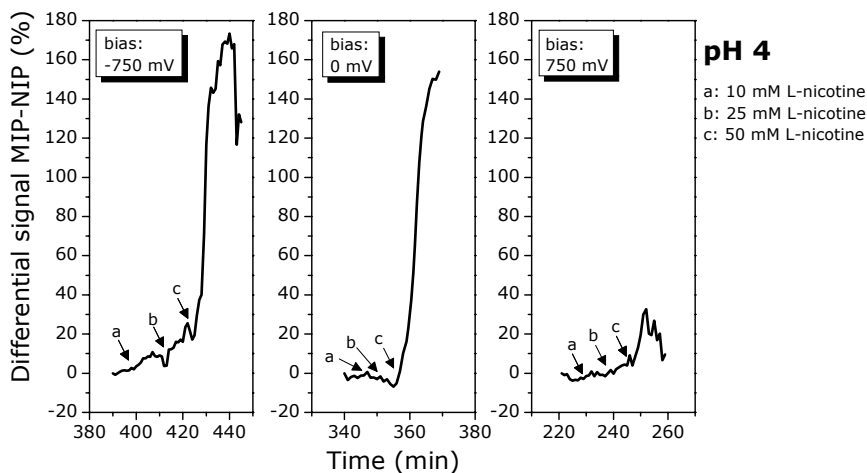
Figure 5-19: Bias dependent differential signal, NIP subtracted from MIP channel, of the normalized modulus of the impedance upon addition of L-nicotine at pH 4. (cell F)

At a higher pH, the response is much less pronounced, see Figure 5-20. However, at negative and zero bias, the device can detect the target molecules in the lower concentration range. At positive bias the binding of the L-nicotine causes an impedance decrease of the MIP and NIP channel. At this pH 8 the sample did not react anymore to the lower concentration range. At pH 8, were L-nicotine is unprotonated, the best results are obtained at zero bias voltage.

From these measurements it can be concluded that the best solvent conditions to measure the target molecule, L-nicotine, should be at a stable pH, preferable around pH 8 and the solvent should have a high conductivity. The proposed solution is therefore a phosphate buffered saline solution (PBS), mimicking the ionic strength and the pH of 7.4 of the human blood.
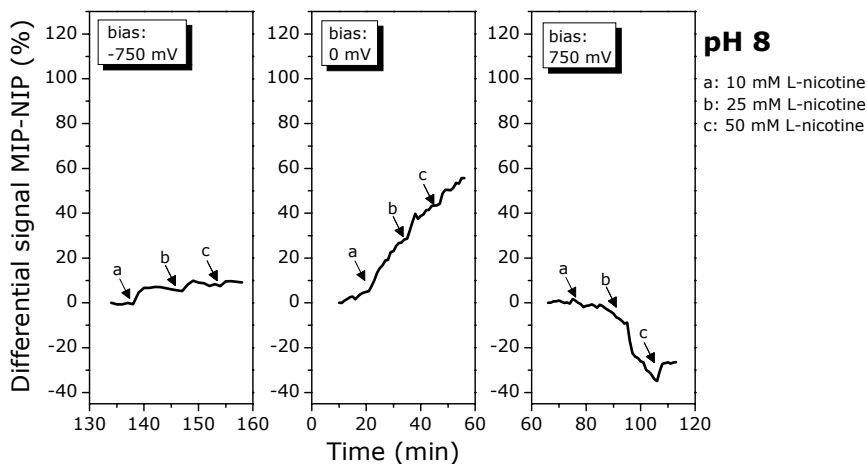
Figure 5-20: Bias dependent differential signal, NIP subtracted from MIP channel, of the normalized modulus of the impedance upon addition of L-nicotine at pH 8. (cell F)

5.2.4 Phosphate buffered saline solution as electrolyte

In the remainder of this chapter, all impedimetric measurements on L-nicotine are performed in PBS. A further improvement is the use of a flow setup instead of an addition design. The measurement device can be connected to a pump, which constantly flows liquid through the cell at a rate of 50 µL/min. In contrast, the steady liquid system offers the possibility of adding a desired concentration of the target molecule in the cell without a constant flow by using a syringe.

In Figure 5-21 a measurement is depicted were a constant flow runs through the cell and the concentration of L-nicotine is introduced by the pump. After introducing the L-nicotine the cell is flushed with a blank PBS solution and afterwards a concentration of L-cotinine is added. The MIP channel reacts stronger to the addition in comparison to the NIP. When adding 1 mM L-nicotine to the cell an increase of 20% of the impedance is obtained, while the NIP channels only changes by 16.5%. The reaction to L-cotinine is much lower and in the range of only 5%.
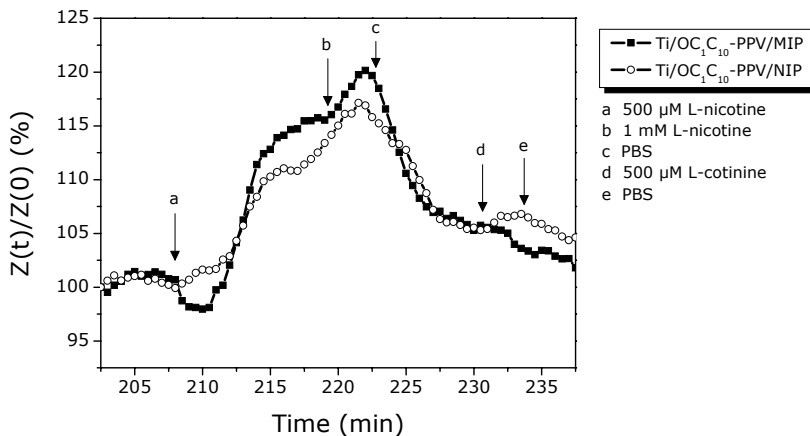
Figure 5-21: Time resolved impedance of Ti/ OC_1C_{10}-PPV/MIP and Ti/ OC_1C_{10}-PPV/NIP channels upon addition of L-nicotine in PBS (cell E).

The measurement also shows that regeneration of the cell is possible by flushing the measurement device with the blank PBS solution. The PBS buffer, being an aqueous solution, apparently is able to break up the hydrogen bonds by which the target molecule rebinds to the MIP.

In Figure 5-22 the steady liquid measurements are shown. In these measurements, the desired amounts of L-nicotine are introduced by a syringe, leaving the liquid in the cell motionless except for the possibility of convection. For the MIP channel an increase of about 17% in the impedance is found when 1 mM L-nicotine is introduced. The NIP channel reacts less, only 5%. When both measurements are performed using the flow system, comparable results are found compared to those of the syringe-based system. However, it is noteworthy that the reaction of one sample is not always the same in comparison to a sample prepared earlier.
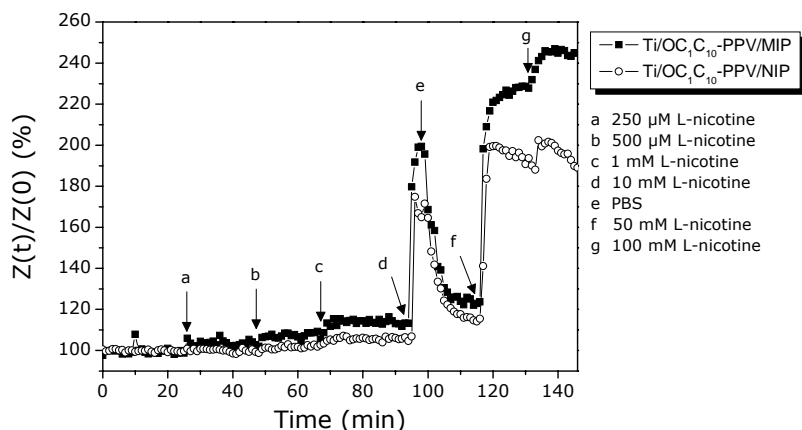
Figure 5-22: Time resolved impedance of Ti/ OC$_1$C$_{10}$-PPV/MIP and Ti/ OC$_1$C$_{10}$-PPV/NIP channels upon addition of L-nicotine in PBS (cell D).

This problem of reproducibility is shown in Figure 5-23. Here the sample was prepared in the same manner as the previous samples. However, the response of the sample upon exposure to 10 nM L-nicotine gave a impedance change of about 2%. This response is much stronger than found in the previous measurements. This significantly lowered detection limit apparently is is associated with a small detection range. After introducing 1 µM L-nicotine the MIP sensor appears to be saturated and further addition does not increase the impedance signal. This may be due to when the liquid is changes inside the cell with the syringe, L-nicotine is flushed out of the MIP structure. The force of the rinsing fluid breaks the weak hydrogen bonds.
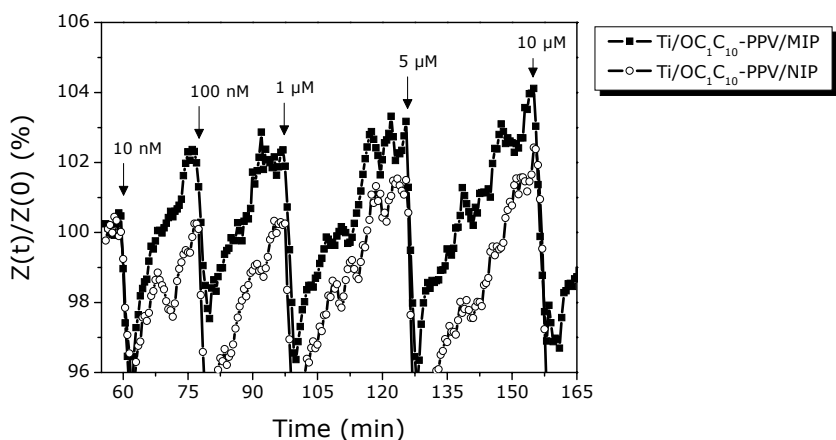
Figure 5-23: Time resolved impedance of Ti/ OC₁C₁₀-PPV/MIP and Ti/ OC₁C₁₀-PPV/NIP channels upon addition of L-nicotine in PBS (cell D).

This observation of the above effects lead to a further development of the design of the sensing device. Instead of measuring with the a flow or syringe based system, an addition design is used. The Teflon hood is open on top to be able to add the desired amount of target molecules to the background solution. Now, the home-made equipment is used to track one selected frequency in time. This system allows more accurate measurements with a better signal to noise ratio and is able to measure quicker, to investigate shorter variations of the signal in time. In Figure 5-24 the time resolved signal is shown of four different channels measured at 212 Hz. The MIP channel increases more than the NIP and conjugated polymer background channels. The Ti channel does not react to the addition of L-nicotine. The particular sample shown has an impedance increase of about 17% upon addition of 600 nM L-nicotine.
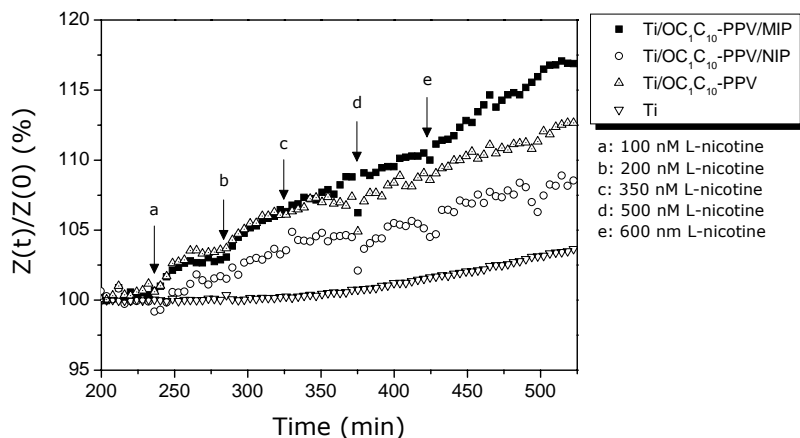
Figure 5-24: Time resolved impedance of Ti/ OC_1C_{10}-PPV/MIP, Ti/ OC_1C_{10}-PPV/NIP, Ti/ OC_1C_{10}-PPV, and Ti channels upon addition of L-nicotine in PBS (cell F).

This step-like increase of the impedance upon addition of the target molecules can be visualized in a dose-response curve. The reaction change in impedance is plotted against the concentration. This dose-response curve can be considered as a variation of a binding isotherm, similar to those found in the batch-rebinding experiments. For this representation it is assumed that the free concentration of the target molecule is much higher than the bound concentration. In this way the free concentration can be estimated as equal to the initial concentration of the target molecule. ($C_i=C_f$) When considering this curve as a binding isotherm the same calculations can be made to obtain an impedance-affinity distribution. For this equation the impedance change is assumed to be directly proportional to the amount of target molecules bound to the MIP (S_b). Otherwise, the same equations are applied and both binding isotherm and impedance affinity distribution are depicted in Figure 5-25. Please note that the units of the vertical axis in the affinity distributions are undefined, since no true S_b (with proper units) is available.

From the impedance affinity distribution it is clear that the MIP has a higher affinity compared to the bare OC_1C_{10}-PPV and NIP covered electrodes. The blank metal has an even lower affinity for L-nicotine.
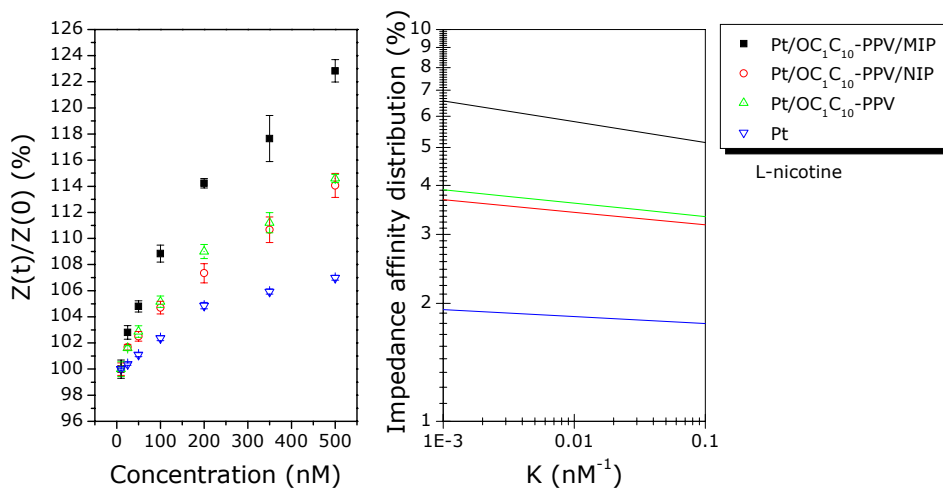
Figure 5-25: Binding isotherm (left) and impedance affinity distribution (right) of Pt/ OC$_1$C$_{10}$-PPV/MIP, Pt/ OC$_1$C$_{10}$-PPV/NIP, Pt/ OC$_1$C$_{10}$-PV, and Pt channels upon addition of L-nicotine in PBS (cell F).

The fact that bare OC$_1$C$_{10}$-PPV and NIP covered electrodes exhibit an impedance change upon addition of L-nicotine is probably due to non-specific adsorption. For both cases a similar affinity distribution is found, suggesting that the majority of the non-specific binding in both cases has the same origin, *i.e.* non-specific binding at OC$_1$C$_{10}$-PPV. In the case of OC$_1$C$_{10}$-PPV this may be the result of π–π interactions. It can be expected that also some non-specific adsorption occurs at the NIP involving the free acid-groups. Therefore, when differential measurements are performed, the NIP channel can be subtracted from the MIP channel to eliminate the influence of the non-specific binding of the target molecules.

The graph is shown in Figure 5-26. Here the first part of the curve is linear with a detection of 0.036 % per nM within a range of 10 to 200 nM. At the higher concentrations the sensor appears to reach saturation since no further reaction is observed upon addition of L-nicotine.
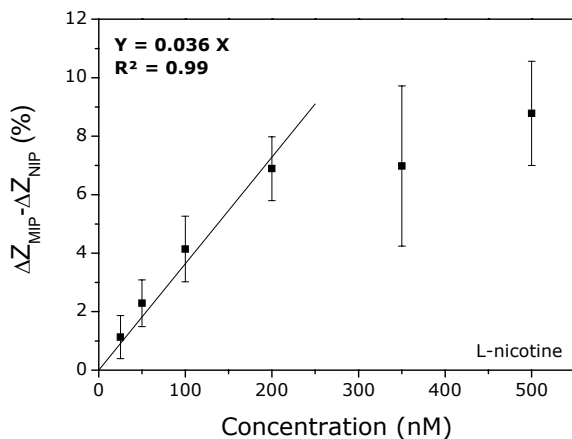
Figure 5-26: Specific impedance change of the sensor upon addition of L-nicotine (cell F).

Trying to lower the detection limit, another sample is measured and shown in Figure 5-27. Here the real part of the modulus gave a larger difference between the MIP and NIP channel. This improved the signal to noise ratio. Also, a second reference measurement is performed by exposure to L-cotinine.
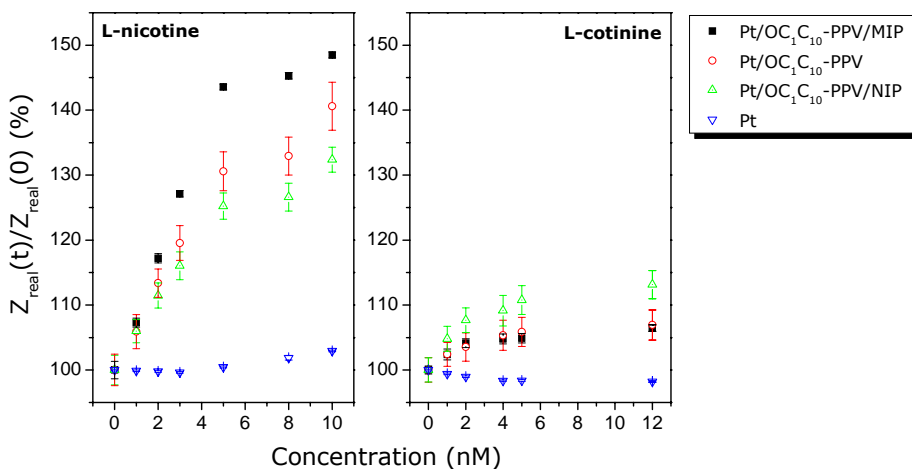
Figure 5-27: Binding isotherm of Pt/ OC_1C_{10}-PPV/MIP, Pt/ OC_1C_{10}-PPV/NIP, Pt/ OC_1C_{10}-PPV, and Pt channels upon addition of L-nicotine (left) and L-cotinine (right) in PBS (cell F).

The binding isotherm shows a higher affinity of the MIP channel while, the NIP and PPV channels cause a somewhat lower response. The sample shows also a much lower affinity to the similar molecule L-cotinine. All channels react very similar upon addition to L-cotinine, indicating the occurrence of non-specific adsorption of L-cotinine to the surface. From these binding isotherms again an impedance-affinity distribution can be calculated using the Freundlich model, see Figure 5-28. Likewise, it can be seen that the MIP shows the highest affinity to L-nicotine in comparison to the other channels. L-cotinine has a much lower and non-specific affinity.
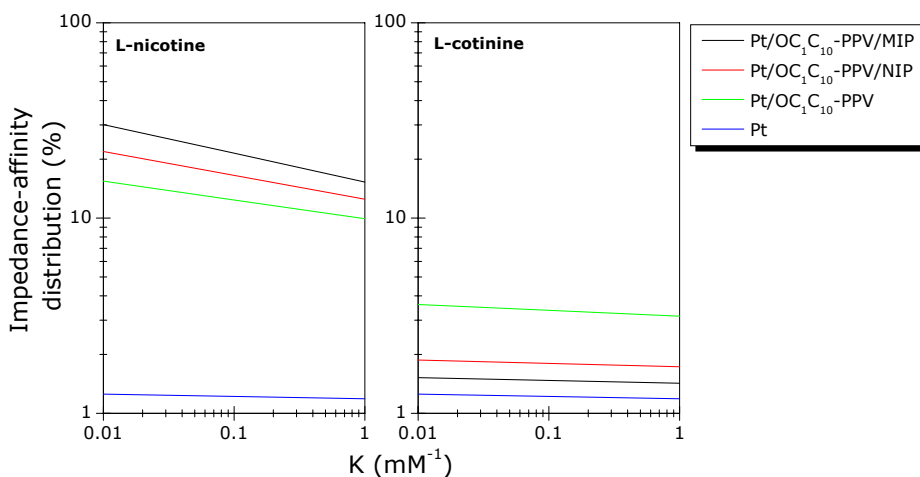
Figure 5-28: Impedance affinity distribution of Pt/ OC₁C₁₀-PPV/MIP, Pt/ OC₁C₁₀-PPV/NIP, Pt/ OC₁C₁₀-PPV, and Pt channels upon addition of L-nicotine (left) and L-cotinine (right) in PBS (cell F).

As mentioned above, the non-specific binding of the target molecule is eliminated from the signal by subtracting the MIP from the NIP channel. In Figure 5-29 the specific reaction to L-nicotine is clearly visualized while the reaction to L-cotinine is clearly non-specific.

This sample has a much lower detection limit compared to Figure 5-26, which is about 2 nM. The sensitivity is much higher, while the linear range, from 2 to 5 nM, indicates a response of 4.3 % per nM.
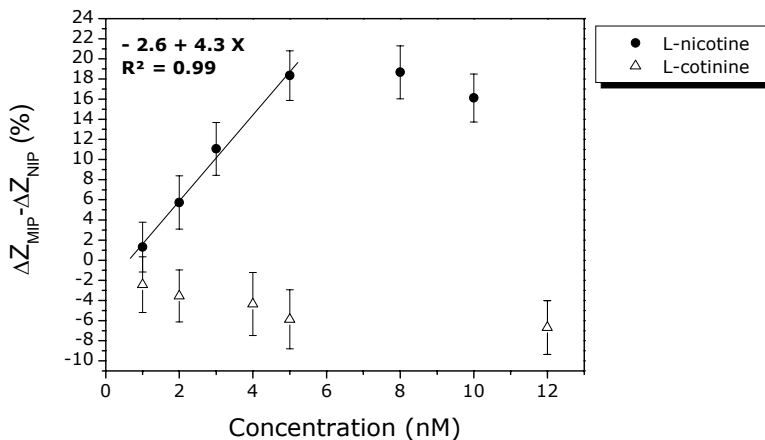
Figure 5-29: Specific impedance change of the sensor upon addition of L-nicotine and L-cotinine (cell F).

The main problem associated with the stamping method is the irreproducibility of the sample. While some samples have a small sensitivity region, other have a larger region but with a higher detection limit. In Figure 5-30 a sample achieved with a linear detection range from 25-175 µM. The sensitivity was 0.02 % per µM, which smaller compared with the sample with a small detection range. Apparently the detection range is related to the sensitivity.
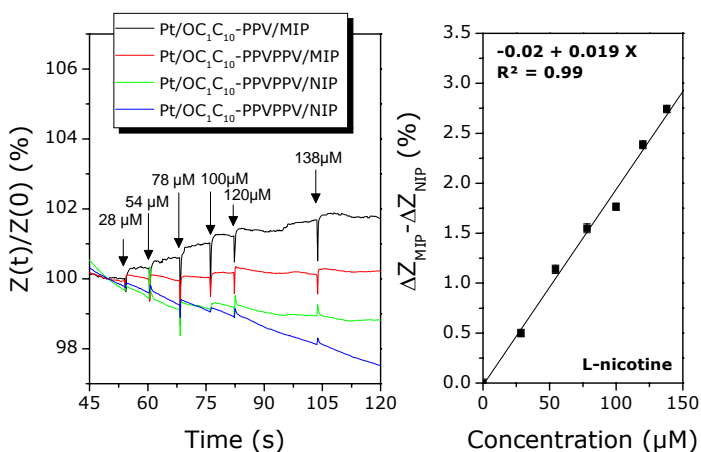
Figure 5-30: Specific impedance change of the sensor upon addition of L-nicotine and L-cotinine (cell F).

The response time of the sensor is related to the concentration as seen in Figure 5-31. Here a addition of 2.5 nM L-nicotine in PBS reaches a stabilization of the impedance change after 60 minutes, while when adding a higher concentration in the micro molar range as seen in Figure 5-30 the signal response after a few minutes. The time constant of for this low concentration is 46 minutes while the time constant from the previous measurement when the sensor was exposed to 28 µM was 0.8 minutes.
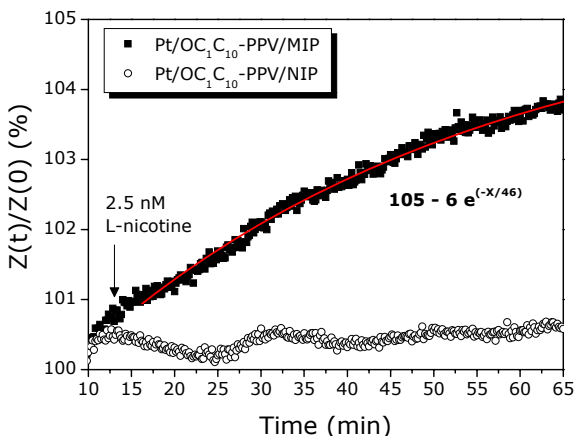
Figure 5-31: Time resolved impedance of Pt/ OC_1C_{10}-PPV/MIP and a Pt/ OC_1C_{10}-PPV/NIP channels upon addition of 2.5 nM L-nicotine in PBS (cell F)

5.3 Discussion

The reported data demonstrate that by using impedimetric detection, molecularly imprinted polymers, which are immobilized onto a conjugated polymer thin film, can be utilized for the recognition of low-MW molecules, such as L-nicotine. The conjugated polymer allows for the detection of capacitive changes. However, a significant amount of non-specific adsorption occurs at the OC_1C_{10}-PPV film. Hence, the development of a novel conjugated polymer with lower non-specific sorption would be desirable.

The impedimetric detection technique offers the possibility to detect 10nM with a response increase of 45% at a frequency of 213 Hz, which is below the relevant

medical concentrations. The reference measurement with L-cotinine, which only differs by one oxygen atom from L-nicotine, indicates a high specificity. The response time varied according to the concentration which was introduced. This is expected for this binding principle. For concentration in the micromolar range the sensor responded within 1 minutes while adding concentrations in the low nanomolar range the response time increased to about 45 minutes. The difference in response between different sample can be contributed to the difference in coverage. A lower coverage means a higher non-specific reaction at conjugated polymer surface, this translate in a smaller difference between the MIP and the NIP channels. These measurements indicate that the MIP-based impedimetric sensor is a fast, easy-to-use sensor with electronic readout.

There are however several drawbacks, which have to be overcome prior to application. The main bottleneck is the reproducibility of the sensor. The stamping method is a straightforward technique of immobilizing MIP particles onto the sensor, but the coverage and the reproducibility of this coverage remain poor. A potential solution could be the use of MIP beads. These beads, when stamped, could spread more uniformly and thus reproducibly in combination with a higher coverage. There are several literature reports about these beads but mostly they concern beads with a diameter of several micrometers [94, 146, 147]. These large beads do not stick when sunken into a 100 nm thin film of polymer. In order to use these large beads, other transducers should be found, which can be casted in thicker films, while still having a good conductivity in order to be able to obtain an electrical signal using impedance spectroscopy. Alternatively, smaller MIP beads should be developed.

Another solution is trying to grow the MIP directly on top of the electrodes. This would require the presence of an initiator or polymerizable group attached to the electrodes or the conjugated polymer film covering the electrodes. It is expected that in this way a thin film of a few nanometers can be grown. Potentially the transducer and receptor layer can even be combined in a single layer, which makes the production process of the sensing even more straightforward. Currently efforts are underway to develop such a method.

Fixing the problem of reproducibility will give the impedimetric method of sensing small molecules a bright future for applications in the pharmaceutical, environmental, diagnostic and biotechnological sector.

Chapter 6 - Piëzo-electric detection of nicotine and histamine

Piëzo-electricity is a principle lying at the basis of various applications such as production and detection of sounds, ultra fine focusing of optical assemblies and in a number of scientific techniques with atomic resolution like scanning probe microscopy. One application, which is of interest for detection purposes, is the use as microbalance for low masses. This principle is useful as an additional reference technique, from which an electronic signal is produced. In this chapter the first measurements are shown, trying to validate the use of this technique for sensing purposes involving MIPs.

6.1 Materials and Methods

To perform these measurements first the resonance peak was tracked by scanning the spectrum around the 5 MHz resonance peak. These spectra were recorded using the HP4194A analyzer, from Hewlett-Packard, USA. Afterwards a Maxtek PLO-10i phase lock oscillator was obtained from Inficon, USA. The equipment is shown in Figure 6-1.

The HP4194A was the same apparatus as used for the impedance measurements. Here the phase signal was used to search for the resonant peak found at the frequency were the phase shift is zero degrees. The calculations from the spectra to the resonant peak were performed with a self-made Labview program. For the phase lock oscillator (PLO), the resonance frequency was found

by the hardware. The PLO utilizes a internal oscillator to drive the crystal. The crystal current is than monitored and the frequency of the oscillator is adjusted until there is zero phase between the crystal voltage and current. The standard quartz crystals used were AT-cut, with a resonant frequency of 5 MHz.

Figure 6-1: A) 'HP4194A impedance/gain-phase analyzer', from Hewlett-Packard, USA
B) Maxtek 'PLO-10i' phase-lock oscillator, from Inficon, USA.

In Figure 6-2 the sensor setup is depicted. Here a flow cell is connected to a gradient pump. The volume inside the flow cell is approximately 100 µl. The quartz crystal is coated with the conjugated polymer OC_1C_{10}-PPV and the MIP particles are immobilized in the same manner as was done for the impedance measurements, *i.e.* using the stamping method.
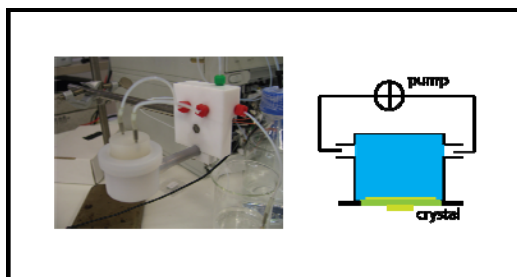
Figure 6-2: The sensor setup used for the gravimetric method and a
schematic cross-section of the QCM flow cell.

6.2 Detection of L-nicotine

The first test was performed by submerging the crystals coated with MIP and NIP particles using OC_1C_{10}-PPV as an adhesive layer into acetonitrile. After stabilization a concentration of the target molecule was added to the solution.

In Figure 6-3 a MIP and NIP sample were exposed to 400 µM of L-nicotine. The resonant peak shifted for the NIP sample with 66 Hz to the right while the MIP sample peak shifted to the left with 200 Hz.
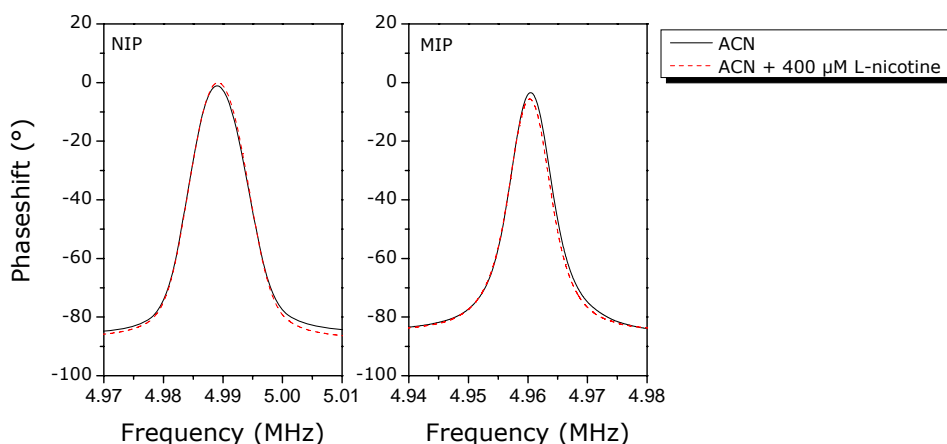
Figure 6-3: Resonance spectrum of a MIP and NIP coated quartz using a OC_1C_{10}-PPV adhesive layer upon addition of 400 µM L-nicotine.

The actual resolution of this technique is the amount of points measured divided by the frequency range. For this measurement the range was 40 kHz and 600 points were measured over this range. This resulted in a resolution of about 66 Hz.

To obtain a better resolution the position of the peak has to be investigated more closely. The software was adapted and the software automatically detects the peak and the scans were recorded with a resolution of 0.5 Hz. In Figure 6-4 the quartz crystal was exposed to 150 mM L-nicotine. To achieve maximum resolution, these graphs show only the top of the resonance peak. It can be seen that that the frequency decreases 992.5 Hz. This frequency change

corresponds to a mass change of about 26.99 µg according to the Sauerbrey equation. The amount of L-nicotine present in the ACN solution was 1.5 mmol or 243 mg. Apparently, the fraction bound to the sensor is only 0.01%.
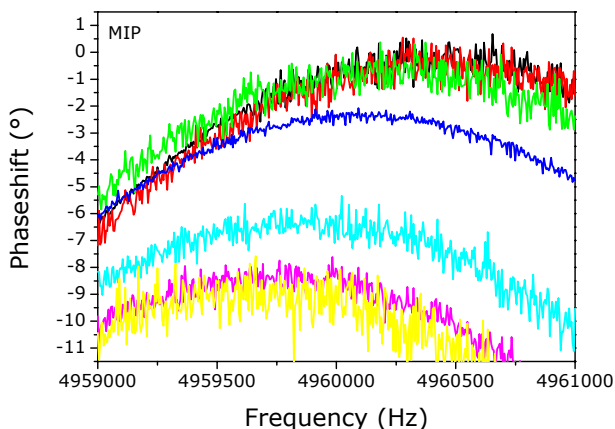
Figure 6-4: Resonance spectrum of a MIP coated quartz using a OC$_1$C$_{10}$-PPV adhesive layer upon addition of 150 mM L-nicotine in ACN.

In Figure 6-5 the frequency change is tracked in time for a MIP and NIP sample upon addition of, respectively, 150 mM and 330 mM L-nicotine in ACN. The MIP channel has a stronger affinity for the addition of L-nicotine compared to the NIP channel. The MIP channels exhibits a mass change of 19 µg, whereas the NIP only binds 3.9 µg. The fraction bound in the MIP is 0.008% and for the NIP 0.0007%. In view of these low bound fractions, probably the used concentrations were too high and saturation took place.
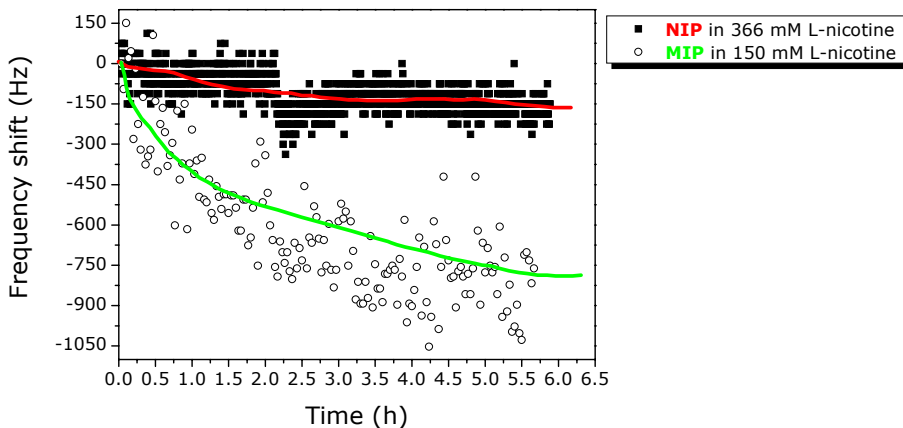
*Figure 6-5: Time resolved frequency shift from a MIP and NIP sample
respectively exposed to 150 and 366 mM L-nicotine in ACN.*

In Figure 6-6 MIP and NIP samples are measured in distilled H_2O instead of ACN. They are exposed to a concentration of 1 mM L-nicotine. When decreasing the noise with a moving average filter, *i.e.* solid line in the graph, the frequency drop of the two samples could be estimated at 50 Hz for the NIP and 150 Hz for the MIP. The corresponding mass changes were 1.3 µg for the NIP and 4.9 µg for the MIP. The bound L-nicotine fractions of these measurements are 0.03 % for the MIP and 0.008% for the NIP.
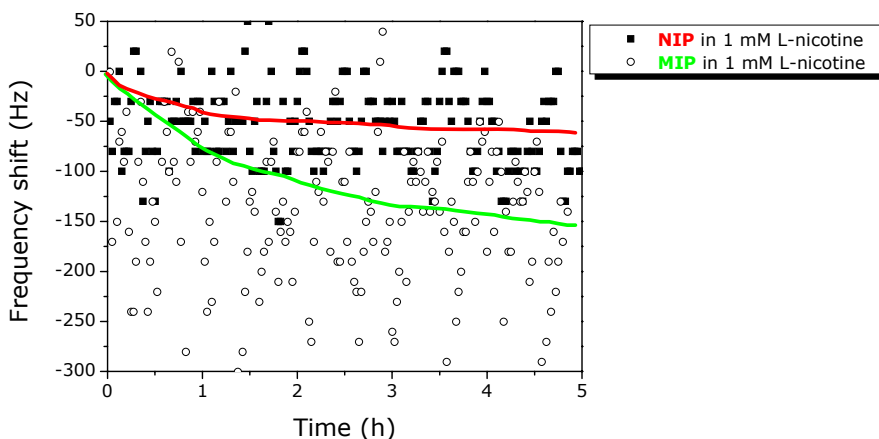
*Figure 6-6: Time resolved frequency shift from a MIP and NIP sample exposed to 1 mM
L-nicotine in distilled H_2O. (solid line produced by a moving average filter)*

In order to decrease the significant noise, which is clearly visible in Figure 6-6, the measurement cell was changes and a flow cell was used instead of the previously discussed method based on submerging the crystal holder in the solution. The advantage of using this flow cell is the possibility of rinsing the cell after introduction of the target molecule.

In Figure 6-7 the flow cell with a MIP coated crystal was filled with a solution of 600 mM L-nicotine using a syringe. After 10 minutes at steady state (no flow) the cell is again rinsed with distilled water and the same protocol is repeated. The measurements indicate that, when by rinsing the MIP with distilled water, it is possible to regenerate them. The MIP sample incorporated in the flow cell measured a mass change of 20.4 μg while the cell was filled with 50 mg of L-nicotine. The fraction bound is 0.04%.
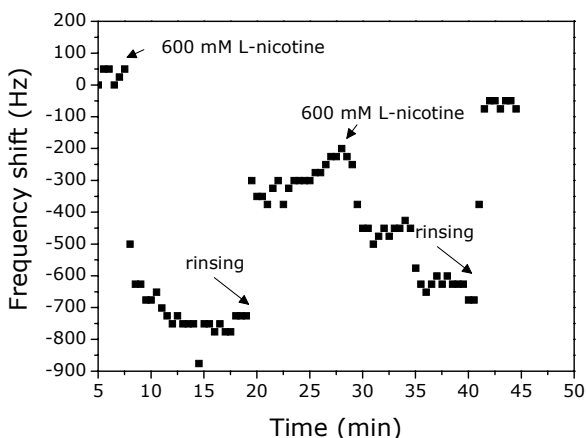
Figure 6-7: Time resolved frequency shift of a MIP sample
exposed to 600 mM L-nicotine in dH$_2$O.

Apparently, the fraction of target molecule bound to the MIP remains in the same order of magnitude for the different above mentioned concentrations. This indicates that the measurements are likely performed in a concentration range were the MIP particles are fully occupied, *i.e.* at saturation. Hence, for further measurements the concentrations added will be decreased, while using continuous flow. Concomitantly the crystal used will be changes. Instead of

using the 5 MHz vacuum crystal with an unpolished silver electrode, further work is performed using 5 MHz quartz crystals with a gold polished electrode.

Figure 6-8 shows a MIP coated quartz crystal, which is exposed to a 0.5 ml/min flow of ACN. After stabilization, two concentrations of L-nicotine, *viz.* 100 µM and 500 µM, are added to the background solution. The frequency shift indicated mass changes of 367 ng and 1.01 µg. The mass which has passed the sensor is 48.6 µg and 243 µg. In this case a percentage of 0.76 % and 0.42 % is achieved respectively.
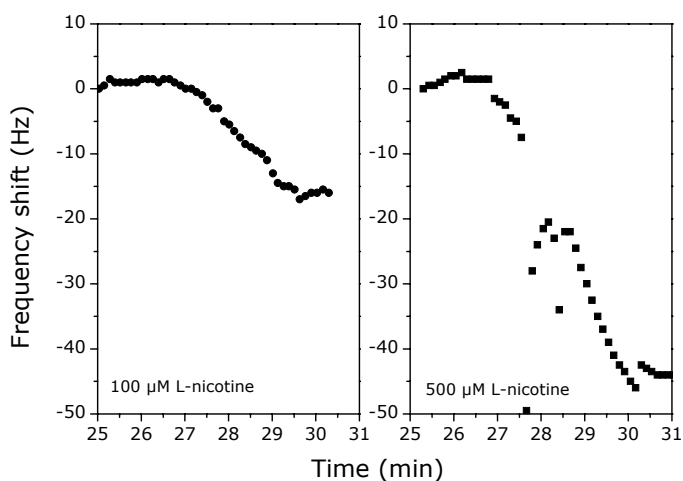
Figure 6-8: Time resolved frequency shift of a MIP sample
exposed to 500 and 100 µM L-nicotine in ACN flowing at 0.5 ml/min.

For the following measurement, shown in Figure *6-9*, another sample could bind 3.3% of the 25 µM and 2.9% of the 29 µM L-nicotine concentration which has passed through the flow cell.
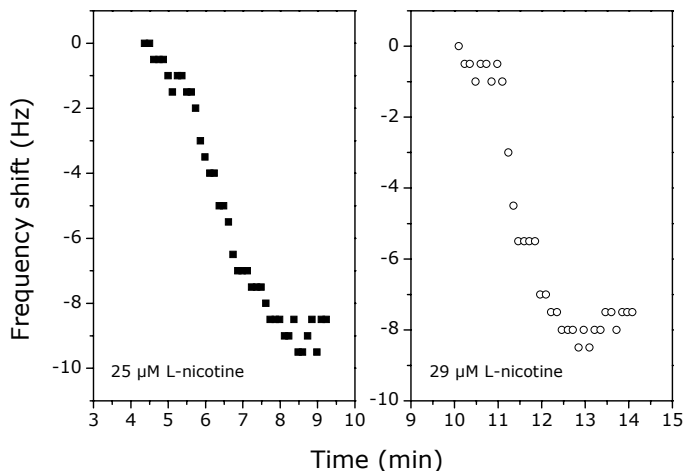
Figure 6-9: Time resolved frequency shift of a MIP sample
exposed to 25 and 29 μM L-nicotine in ACN flowing at 0.5 ml/min.

The response time of these flow measurements was 3 minutes, which is longer than the previous measurements using steady state conditions. This is probably due to the binding characteristics of the MIP. Equilibrium or even saturation, will be faster achieved when exposing the MIPs to higher concentrations.

The flow system is also tested using an aqueous solvent for the target molecule. The flow rate is also decreased in an attempt to try to further increase the fraction of L-nicotine bound. Although a fast detection is favorable, it can be anticipated that at low flow rates it will take somewhat longer to reach equilibrium. Hence, an optimum between response time and flow rate has to be achieved. In Figure 6-10, a MIP coated quartz crystal is exposed to 1 mM L-nicotine concentration in distilled water flowing at a rate of 0.05 ml/min through the sensor.

The measurement shows for the first 1.6 % and the second MIP sample 7.3% of the target molecule is bound in the MIP. These measurements highlight the problem of reproducibility between two different samples prepared in the same way. However, the 7.3 % sample demonstrates the potential of using these type of samples for sensing purposes. The large variation in the bound percentage of L-nicotine in these measurements originates from the occurrence of significant

differences in the amount of available binding sites between individual sensors. This can be a result of variations in the amount of immobilized MIPs or variations in the accessibility of the binding sites.
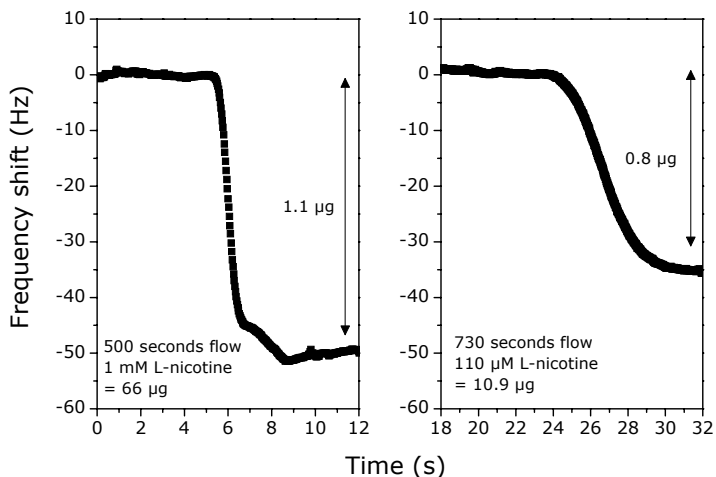
Figure 6-10: Time resolved frequency shift of two MIP samples
exposed to 1 mM and 110 µM L-nicotine in distilled H_2O flowing at 0.05 ml/min.

The utilized pump system allows for the possibility to change the eluents passing through the flow cell. In Figure 6-11 a MIP coated sample was exposed 3 times for 30 minutes to 0.5 mM L-nicotine and after rinsing with distilled H_2O for one hour to 0.5 mM L-cotinine.
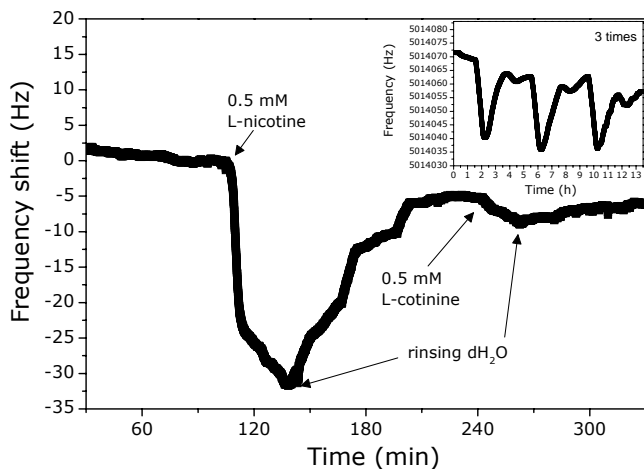
*Figure 6-11: Time resolved frequency shift from a MIP sample exposed 3 times
to 0.5 mM L-nicotine and L-cotinine in distilled H_2O flowing at 0.05 ml/min.*

It can be seen that flushing the cell with dH_2O causes the hydrogen bound to
break and the analyte is extracted from the MIP. The fraction of L-nicotine which
could be bound in this way was 0.56 %. This value is quite low, however
consistent during the whole measurement. The fraction of L-cotinine which
binded non-specifically was only 0.09%.

The sensitivity of the sensing device is different for each sample. The previous
measurement is repeated for a different MIP sample with the same
concentration of L-nicotine exposing the sample for 30 minutes at a flow rate of
50 µl/min, see Figure 6-12. The fraction of L-nicotine in this case was 3%, which
is much higher compared with the previous measurement. This highlights once
again the reproducibility problem.
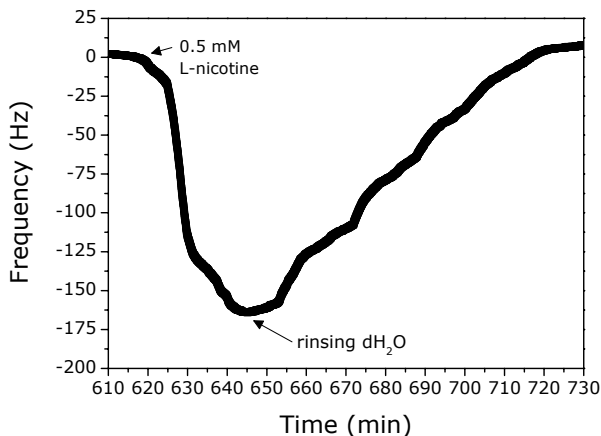
Figure 6-12: Time resolved frequency shift from a MIP sample exposed to 0.5 mM L-nicotine in distilled H$_2$O flowing at 0.05 ml/min.

In Figure 6-13 a MIP and NIP sample were exposed to an increasing concentration of L-nicotine and after rinsing the MIP sample was again exposed to an increasing concentration of L-cotinine. The concentrations used were ranging from 50 µM to 300 µM. As can be seen in the graph the MIP sample binds the highest amount of target molecules which passes through the flow cell. This graph can be converted to a binding isotherm when the amount of MIP on top of the electrode is known, see Figure 6-14.
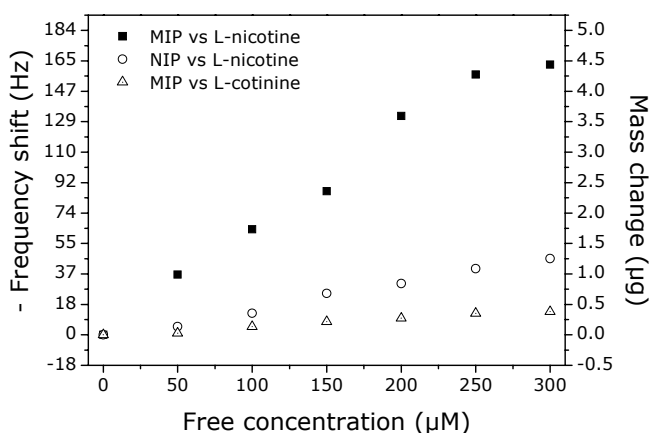
Figure 6-13: Frequency and mass response of a MIP and NIP sensor exposed to an increasing concentration of L-nicotine and L-cotinine in dH$_2$O flowing at 0.05 ml/min.

115

To obtain an estimate for the amount of MIP immobilized on top of the conjugated polymer film, a large substrate of five by five centimeters is spincoated and covered with MIP particles using the stamp method. Using a micro scale the weight difference before and after applying the particles is measured. In this way the coverage was calculated, being 0.16 µg per square millimeter. When this value is extrapolated to the area of the quartz crystal the weight of the MIP on top of this crystal can be estimated at about 21 µg.
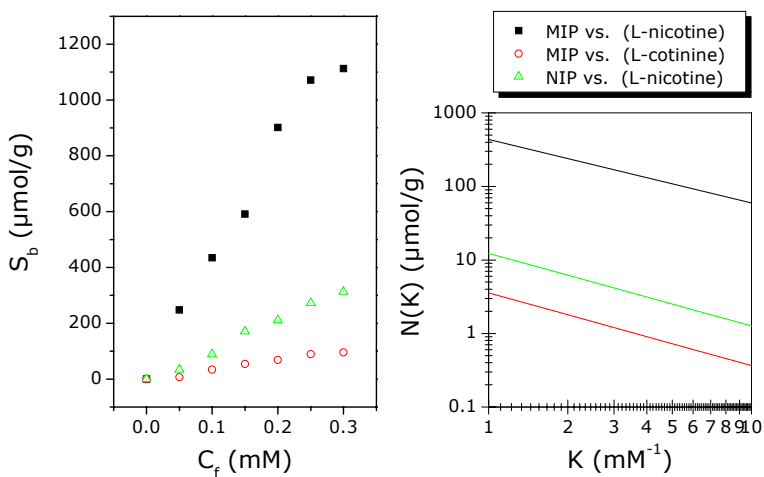
Figure 6-14: Graph of the binding isotherm and the affinity distribution, for imprinted and non-imprinted polymers exposed to L-nicotine and L-cotinine.

The affinity distribution is obtained by fitting the binding isotherm with the Freundlich model in the same way as the UV-Vis rebind experiments. The range, 50µM until 300µM, is much lower compared to those results, where the free concentration is varied from 0.2 µM to 1 mM. The total number of binding sites can be calculated using the Freundlich model. The values are shown in Table 6-1. It is clear that MIP sensor possesses a considerable affinity for L-nicotine and a low affinity for L-cotinine. The NIP sensor also has a low affinity for L-nicotine.

Table 6-1: The average binding constant within the range from 1-100 mM^{-1}.

		N_{tot} (µmol/g)	K_{av} (M^{-1})
MIP	L-nicotine	391	2.7
	L-cotinine	3	2.5
NIP	L-nicotine	21	2.5

When the data from UV-vis spectroscopy are compared with those from QCM measurements, the number of available binding sites with a specific binding constant found with UV-Vis spectroscopy appears to be considerably lower, cfr. Table 4-1. The may be due to the fact that when performing the optical technique the MIP particles are dissolved in the solution are therefore more accessible then when the MIP particles are partly submerged on a flat surface. This is analog with a 3 dimensional approach for the UV-Vis and a 2 dimensional accessibility for the QCM. This differs about a hundred times.

In order to increase the reproducibility of the measurements, other types MIP particles have been proposed in previous chapters. To obtain particles, which are more reproducible in shape and sensitivity, suspension polymerization has been utilized. This method can be viewed as a bulk polymerization in micro containers. Using this controlled synthesis technique no grinding is required and uniform round particles are obtained. The only drawback for sensor purposes is the size. The diameter of the particles is currently still several micrometers, which makes it impossible to immobilize these particles in a thin film of about 100 nanometers. Therefore other transducer materials have to be found, which are able to produce a thicker uniform intermediate layer to adhere and partially submerge these particles in a similar way as previously described. Since for the gravimetric sensor the electronic properties are not important, a non-conjugated polymer, *i.e.* polystyrene, has been chosen.

In Figure 6-15 the first results are depicted. A quartz crystal coated with a polystyrene layer in which micro beads of MIP are embedded. The sensor is exposed during the measurement to 6 nmol of L-nicotine. The frequency shift of 180 Hz related to a mass change of 4 µg. This device was able to detect 0.42 % of the L-nicotine. This confirms the viability of MIP based gravimetric sensors.
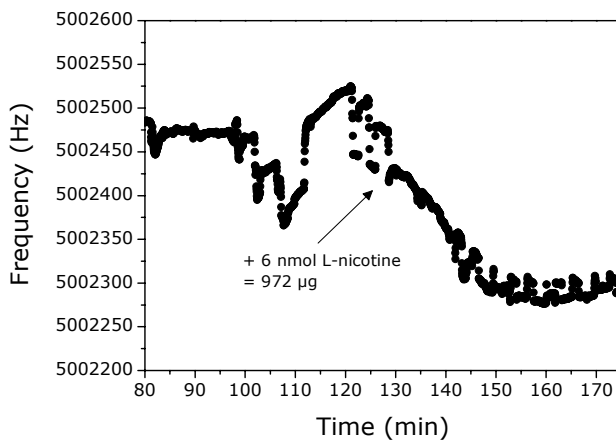
*Figure 6-15: Time resolved frequency shift from a polystyrene MIP sample
exposed to 6 nmol of L-nicotine in distilled H_2O in a flow of 0.05 ml/min.*

6.3 Detection of histamine

The following step in the development of the sensing devices is the changeover
to a more medically relevant molecule, *i.e.* histamine. The same measurement
protocol is used. In Figure 6-16 a crystal coated with histamine MIPs is exposed
to increasing concentration of histamine from 10 µM to 60 µM. After the
introduction of the highest concentration the cell is again rinsed with the
background solution, distilled water.
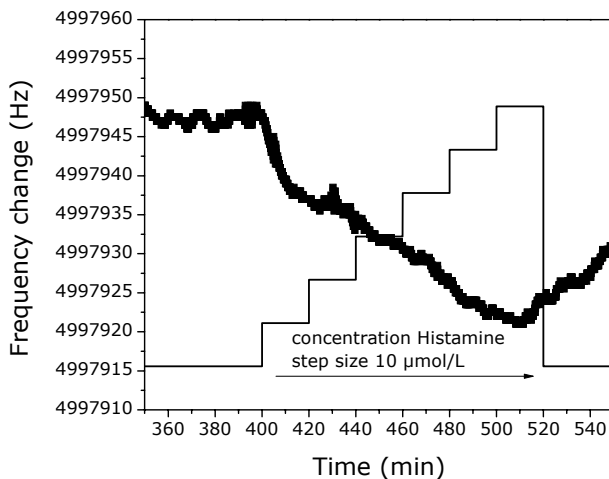
Figure 6-16: Time resolved frequency shift from a MIP sample exposed to
an increasing concentration of histamine in distilled H_2O in a flow of 0.05 ml/min.

Similarly to the previous measurements, a binding isotherm and an affinity
distribution can be plotted. The total number of binding sites can be calculated
again using the Freundlich model. For this case the total number of binding sites
for histamine equals 396 µmol/g for the MIP while the average binding constant
is 8.6 M^{-1}.
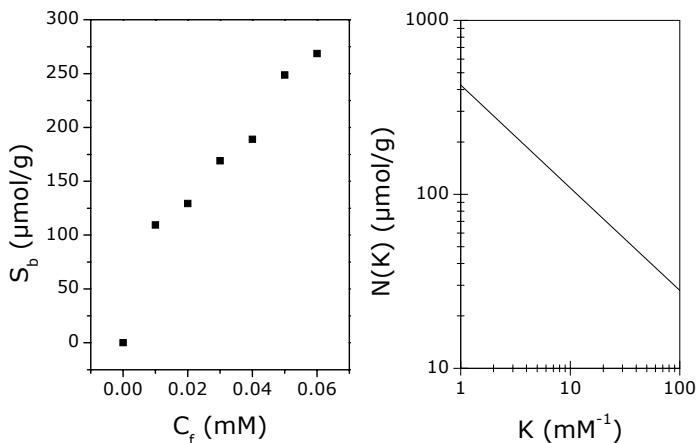
Figure 6-17: Graph of the binding isotherm and the affinity distribution,
for imprinted and non-imprinted polymers exposed to histamine.

6.4 Discussion

The microgravimetric method proves to be good reference technique to test the sensor setup. The same materials and immobilization techniques can be used and compared with the results from the impedance measurement and the optical batch-rebinding experiments.

The QCM shows that the MIP coated sensor can detect L-nicotine with a detection limit of 50 µM within 10 minutes. Under the used experimental conditions, only a low percentage of the target molecules, which pass through the flow cell, bind to the synthetic receptors. The MIP sensor does not significantly react to the addition of L-cotinine. The results can also be analyzed using the Freundlich isotherm. From the results of this analysis it can be seen that these measurements are performed under different conditions as compared to the batch-rebinding experiments.

It can also be seen that the sensor can be regenerated by flushing the cell with distilled water. This breaks the hydrogen bonds between the MIP and the target molecules. The rate at which the MIP responds to target molecules and subsequently can be regenerated depends on the flow rate.

The first tests were performed for detecting a medically relevant molecule, *i.e.* histamine. This sensor had a detection limit of 10 µM with a response time below 10 minutes. The MIP based histamine sensor exhibits even a higher affinity as compared to the L-nicotine sensor. Further measurements have to be carried out in order to lower the detection limit to reach the relevant medical concentrations of histamine, being in the picomolar range.

Chapter 7 - Conclusions and outlook

The goal of the research described in this thesis was the development of a MIP-based sensor with an electronic read-out to detect low molecular weight molecules. With a straightforward protocol a very sensitive and specific synthetic receptor was obtained. The target molecules were mixed with the polymer and after polymerization the template was removed, leaving a nano-cavity behind, which could rebind the analyte.

The binding characteristics of the MIPs particles were analyzed using UV/Vis spectroscopy before implementing them in the sensing device. Binding properties have been investigated and a heterogenous distribution of the binding sites was found. The Freundlich model could be used to describe the binding properties. The analysis confirmed the occurrence of specific recognition of the MIP for L-nicotine and insensitivity towards L-cotinine, the resembling molecule which differs only one oxygen.

The microscopy results showed a good immobilization of the powdered MIP to the OC_1C_{10}-PPV covered electrode surface using the PDMS stamping technique. With SEM, smaller particles between the large clusters could be noticed, although only about 20 percent of the surface was covered with MIP particles. A suggestion to improve the coverage is to develop a method to grow thin films of MIP directly onto the sensor surface. To achieve this, a tailor-made conjugated polymer is needed with reactive functional groups. These functional groups can act as initiators or further participate in the polymerization when the film is exposed to the mixture of MAA, EGDM and the template. Afterwards the template is removed from the thin grown film and one can imagine that a highly

selective receptor film is formed. Another way to improve the coverage is using nano-beads. The nano-beads MIPs could already be synthesized using a suspension polymerization, a polymerization process in which the monomer, or mixture of monomers, is dispersed by mechanical agitation in a liquid phase. In this phase the monomer droplets are directly polymerized, giving polymer beads with a defined size and shape. However, this technique produces particles in the micro-meter range. These are to large to embed into a 100 nm thin conjugated polymer film.

The use of fluorescence spectroscopy was attempted as a reference technique. When binding sites are close to an OC_1C_{10}-PPV chain the binding of L-nicotine possibly would quench the fluorescence. The measurements showed however no indication of L-nicotine or L-cotinine quenching the fluorescence of the conjugated polymer. To be able to use fluorescence quenching as a reference technique, the target molecule should be able to act as an electron acceptor. In the literature an example can be found based on TNT which quenched the fluorescence of a conjugated polymer (MEH-PPV) [135].

In the main part of this work it is demonstrated that by using impedimetric detection, it is possible to detect low-MW molecules using molecularly imprinted polymers, which are immobilized onto a conjugated polymer thin film. This technique offers the possibility to detect 10 nM with a response increase of 45 percent, which is significantly below relevant medical concentrations. The reference measurement with L-cotinine, which only differs one oxygen atom from L-nicotine, indicates a high specificity. Non-specific adsorption was visible at the NIP and bare conjugated polymer film. The response of each channel was similar, which indicates that the major part of the non-specific adsorption takes place at the conjugated polymer film. This can be expected since OC_1C_{10}-PPV is hydrophobic. A suggestion for the continuation of this project would be to try to make to surface of the sensor more hydrophilic to reduce non-specific adsorption. In this way, the difference between the MIP and reference channels would be larger.

The gravimetric method proved to be good reference technique to test the sensor setup. The same protocol as the impedance measurement could be used.

With this technique L-nicotine could be readily detected. Also the specificity could be evaluated by measuring L-cotinine. The concentrations which could be measured were higher compared to the impedance setup. However the difference originates from the detection limit of the 5 MHz quartz crystal. The protocol can easily be transferred to a more sensitive 9 MHz crystal. Otherwise, the gravimetric results were comparable to the results from the impedance measurement as well as the optical batch-rebinding experiments. The only difference is that currently the measurements were performed in a flow setup, whereas the batch rebinding experiments were performed in steady state. In this way the QCM method tests the MIP sensor in equilibrium with a constant concentration. For the optical method the concentration in which the MIPs are exposed decrease upon binding of the target in the MIP. An advantage of the flow setup is the fact that it is possible to flush the MIP sensor, making it reusable. First tests were carried out for detecting a more medically relevant molecule, histamine, with the gravimetric method. The histamine MIPs showed a higher affinity as compared to the L-nicotine MIPs. Further measurements have to be carried out in order to lower the detection limit to reach the relevant medical concentrations of histamine, being in the picomolar range. The QCM proved to be a good reference technique to investigate the binding more in the MIP as a result of the fact that the frequency change is directly related to the mass loading. However, the QCM measurements require optimal measuring circumstances, concerning temperature, pressure, etc, in making them less favorable for sensor applications.

With this thesis a first step is made to investigate and develop synthetic sensors, which are tailor-made and show high affinity and specificity. Such sensors potentially can be used under a wide range of circumstances, while produceing a fast and straightforward electronic read-out. However, there remain several drawbacks, which will have to be overcome in order to make the step towards a usable device. Notwithstanding, it is certainly shown that a MIP, Molecularly Imprinted Polymer, based impedimetric sensor for the detection of small MW molecules has a bright future in the pharmaceutical, environmental, diagnostic and biotechnological sector.

References

1. Mohanty, S. and E. Kougianos, *Biosensors: A tutorial review.* IEEE Potentials, 2006. **25**(2): p. 35-40.
2. in *The American Heritage® Dictionary of the English Language.* , J.P. Pickett, Editor. 2000, Houghton Mifflin Company: Boston. p. 2074.
3. Malhotra, B.D. and A. Chaubey, *Biosensors for clinical diagnostics industry.* Sensors and Actuators B: Chemical, 2003. **91**(1-3): p. 117-127.
4. Eggins, B., *Biosensors An Introduction*. 1996, West Sussex: Wiley.
5. Haber, F. and Z. Clemensiewitz, *Über elektrische Phasengrenzkräfte.* Z. Phys. Chem., 1909. **67**.
6. Clark, L.C., Jr., et al., *Continuous recording of blood oxygen tensions by polarography.* J Appl Physiol, 1953. **6**(3): p. 189-93.
7. Clark, L.C., Jr. and C. Lyons, *Electrode systems for continuous monitoring in cardiovascular surgery.* Ann N Y Acad Sci, 1962. **102**: p. 29-45.
8. Bergveld, P., *Development, operation, and application of ion-sensitive field-effect transistor as a tool for electrophysiology.* IEEE Transactions on Biomedical Engineering, 1972. **19**(5).
9. Schultz, J.S., S. Mansouri, and I.J. Goldstein, *Affinity sensor: a new technique for developing implantable sensors for glucose and other metabolites.* Diabetes Care, 1982. **5**(3): p. 245-53.
10. Cass, A.E., et al., *Ferrocene-mediated enzyme electrode for amperometric determination of glucose.* Anal Chem, 1984. **56**(4): p. 667-71.
11. Maines, A., et al., *Use of surfactant-modified cellulose acetate for a high-linearity and pH-resistant glucose electrode.* Analytical Communications, 1996. **33**(1): p. 27-30.
12. Marquette, C.A. and L.J. Blum, *Electro-chemiluminescent biosensing.* Analytical and Bioanalytical Chemistry, 2008. **390**(1): p. 155-168.
13. Prodromidis, M.I. and M.I. Karayannis, *Enzyme based amperometric Biosensors for food analysis.* Electroanalysis, 2002. **14**(4): p. 241-261.
14. Wang, J., *Glucose biosensors: 40 years of advances and challenges.* Electroanalysis, 2001. **13**(12): p. 983-988.
15. Bonroy, K., et al., *Comparison of random and oriented immobilisation of antibody fragments on mixed self-assembled monolayers.* Journal of Immunological Methods, 2006. **312**(1-2): p. 167-181.

16.   Frederix, F., et al., *Enhanced performance of an affinity biosensor interface based on mixed self-assembled monolayers of thiols on gold.* Langmuir, 2003. **19**(10): p. 4351-4357.

17.   Cooreman, P., et al., *Impedimetric immunosensors based on the conjugated polymer PPV: Selected Papers from the Eighth World Congress on Biosensors, Part II.* Biosensors and Bioelectronics, 2005. **20**(10): p. 2151-2156.

18.   Vermeeren, V., et al., *Towards a real-time, label-free, diamond-based DNA sensor.* Langmuir, 2007. **23**(26): p. 13193-13202.

19.   Wenmackers, S., et al., *Head-on immobilization of DNA fragments on CVD-diamond layers.* Functionally Graded Materials VIII, 2005. **492-493**: p. 267-272.

20.   Schöning, M.J. and A. Poghossian, *Bio FEDs (Field-Effect devices): state-of-the-art and new directions.* Electroanalysis, 2006. **18**(19-20): p. 1893-1900.

21.   Piletsky, S.A., S. Alcock, and A.P.F. Turner, *Molecular imprinting: at the edge of the third millennium.* Trends in Biotechnology, 2001. **19**(1): p. 9-12.

22.   Piletsky, S.A., et al., *Substitution of antibodies and receptors with molecularly imprinted polymers in enzyme-linked and fluorescent assays.* Biosensors & Bioelectronics, 2001. **16**(9-12): p. 701-707.

23.   Piletsky, S.A., et al., *A biomimetic receptor system for sialic acid based on molecular imprinting.* Analytical Letters, 1996. **29**(2): p. 157-170.

24.   Thoelen, R., et al., *A MIP-based impedimetric sensor for the detection of low-MW molecules.* Biosensors & Bioelectronics, 2008. **23**(6): p. 913-918.

25.   Ansell, R.J., O. Ramstrøm, and K. Mosbach, *Towards artificial antibodies prepared by molecular imprinting.* Clinical Chemistry, 1996. **42**(9): p. 1506-1512.

26.   Cormack, P.A.G. and K. Mosbach, *Molecular imprinting: recent developments and the road ahead.* Reactive & Functional Polymers, 1999. **41**(1-3): p. 115-124.

27.   Haupt, K. and K. Mosbach, *Plastic antibodies: developments and applications.* Trends in Biotechnology, 1998. **16**(11): p. 468-475.

28.   Mosbach, K., *The technique of molecular imprinting in the formation of antibody mimics, and their applications to the analysis of pesticides.* Abstracts of Papers of the American Chemical Society, 1994. **207**: p. 149-AGRO.

29.   De Palma, R., et al., *Magnetic bead sensing platform for the detection of proteins.* Analytical Chemistry, 2007. **79**(22): p. 8669-8677.

30.   Marx, K.A., *Quartz crystal microbalance: A useful tool for studying thin polymer films and complex biomolecular systems at the solution-surface interface.* Biomacromolecules, 2003. **4**(5): p. 1099-1120.

31.   Emr, S.A. and A.M. Yacynych, *Use of polymer-films in amperometric biosensors.* Electroanalysis, 1995. **7**(10): p. 913-923.

32.   Van Severen, I., et al., *Application of functional PPV-derivatives prepared via the sulfinyl precursor route as transducers in impedimetric biosensors.* Abstracts of Papers of the American Chemical Society, 2006. **231**: p. 478-479.

33. Frederix, F., et al., *Biosensing based on light absorption of nanoscaled gold and silver particles.* Analytical Chemistry, 2003. **75**(24): p. 6894-6900.

34. Berggren, C., B. Bjarnason, and G. Johansson, *Capacitive biosensors.* Electroanalysis, 2001. **13**(3): p. 173-180.

35. Chaki, N.K. and K. Vijayamohanan, *Self-assembled monolayers as a tunable platform for biosensor applications.* Biosensors & Bioelectronics, 2002. **17**(1-2): p. 1-12.

36. Gao, Z.Q., et al., *Silicon nanowire arrays for label-free detection of DNA.* Analytical Chemistry, 2007. **79**(9): p. 3291-3297.

37. Letant, S.E., et al., *Integration of porous silicon chips in an electronic artificial nose.* Sensors and Actuators B-Chemical, 2000. **69**(1-2): p. 193-198.

38. Prieto, F., et al., *An integrated optical interferometric nanodevice based on silicon technology for biosensor applications.* Nanotechnology, 2003. **14**(8): p. 907-912.

39. Libertino, S., et al., *Layer uniformity in glucose oxidase immobilization on SiO_2 surfaces.* Applied Surface Science, 2007. **253**(23): p. 9116-9123.

40. Wang, J. and J.A. Carlisle, *Covalent immobilization of glucose oxidase on conducting ultrananocrystalline diamond thin films.* Diamond and Related Materials, 2006. **15**(2-3): p. 279-284.

41. Garrido, J.A., et al., *pH sensors based on hydrogenated diamond surfaces.* Applied Physics Letters, 2005. **86**(7).

42. Hartl, A., et al., *Protein-modified nanocrystalline diamond thin films for biosensor applications.* Nature Materials, 2004. **3**(10): p. 736-742.

43. Christiaens, P., et al., *EDC-mediated DNA attachment to nanocrystalline CVD diamond films.* Biosensors & Bioelectronics, 2006. **22**(2): p. 170-177.

44. Wenmackers, S., et al., *Covalent immobilization of DNA on CVD diamond films.* Physica Status Solidi a-Applied Research, 2003. **199**(1): p. 44-48.

45. Marrazza, G., I. Chianella, and M. Mascini, *Disposable DNA electrochemical biosensors for environmental monitoring.* Analytica Chimica Acta, 1999. **387**(3): p. 297-307.

46. Marrazza, G., I. Chianella, and M. Mascini, *Disposable DNA electrochemical sensor for hybridization detection.* Biosensors & Bioelectronics, 1999. **14**(1): p. 43-51.

47. Hrapovic, S., et al., *Electrochemical biosensing platforms using platinum nanoparticles and carbon nanotubes.* Analytical Chemistry, 2004. **76**(4): p. 1083-1088.

48. Millan, K.M., A. Saraullo, and S.R. Mikkelsen, *Voltammetric DNA biosensor for cystic-fibrosis based on a modified carbon-paste electrode.* Analytical Chemistry, 1994. **66**(18): p. 2943-2948.

49. Dumont, V., et al., *A surface plasmon resonance biosensor assay for the simultaneous determination of thiamphenicol, florefenicol, florefenicol amine and chloramphenicol residues in shrimps.* Analytica Chimica Acta, 2006. **567**(2): p. 179-183.

50. Marchesini, G.R., et al., *Dual biosensor immunoassay-directed identification of fluoroquinolones in chicken muscle by liquid*

chromatography electrospray time-of-flight mass spectrometry. Analytica Chimica Acta, 2007. **586**(1-2): p. 259-268.

51. Saerens, D., et al., *Engineering camel single-domain antibodies and immobilization chemistry for human prostate-specific antigen sensing.* Analytical Chemistry, 2005. **77**(23): p. 7547-7555.

52. Urban, G., et al., *The construction of microcalorimetric biosensors by use of high-resolution thin-film thermistors.* Biosensors & Bioelectronics, 1991. **6**(3): p. 275-280.

53. Xie, B. and B. Danielsson, *An integrated thermal biosensor array for multianalyte determination demonstrated with glucose, urea and penicillin.* Analytical Letters, 1996. **29**(11): p. 1921-1932.

54. Xie, B., et al., *Hybrid biosensor for simultaneous electrochemical and thermometric detection.* Analytical Letters, 1997. **30**(12): p. 2141-2158.

55. Cosnier, S., H. Perrot, and R. Wessel, *Biotinylated polypyrrole modified quartz crystal microbalance for the fast and reagentless determination of avidin concentration.* Electroanalysis, 2001. **13**(11): p. 971-974.

56. In'acio, P., J.N. Marat-Mendes, and C.J. Dias, *Development of a biosensor based on a piezoelectric film.* Ferroelectrics, 2003. **293**: p. 351-356.

57. Lucklum, R. and P. Hauptmann, *Acoustic microsensors-the challenge behind microgravimetry.* Analytical and Bioanalytical Chemistry, 2006. **384**(3): p. 667-682.

58. Jimenez, J., et al., *Magneto-induced self-assembling of conductive nanowires for biosensor applications.* Journal of Physical Chemistry C, 2008. **112**(19): p. 7337-7344.

59. Zhou, Y.C., *Discrete contact continuous film magnetoresistive biosensor.* Journal of Applied Physics, 2008. **103**(7): p. -.

60. Piletsky, S.A., N.W. Turner, and P. Laitenberger, *Molecularly imprinted polymers in clinical diagnostics - future potential and existing problems: developments in biosensors: new structural designs for functional interfaces.* Medical Engineering & Physics, 2006. **28**(10): p. 971-977.

61. Dickert, F.L., *Molecularly imprinted polymers for mass sensitive devices*, in *Molecular Imprinting of Polymers*, A.T. Sergey Piletsky, Editor. 2006, Eurekah.com Landes Bioscience: Texas.

62. Polyakov, M.V., *Adsorption properties and structure of silica gel.* Zhur. Fiz. Khim., 1931. **2**.

63. Dickey, F.H., *The preparation of specific adsorbents.* Proc. Natl. Acas. Sci., 1949. **35**(5): p. 227-229.

64. Takagish.T and I.M. Klotz, *Macromolecule-small molecule interactions - introduction of additional binding-sites in polyethyleneimine by disulfide crosslinkages.* Biopolymers, 1972. **11**(2): p. 483-&.

65. Wulff, G., *The role of binding-site interactions in the molecular imprinting of polymers.* Trends in Biotechnology, 1993. **11**(3): p. 85-87.

66. Wulff, G., et al., *Enzyme-analogue built polymers, .4. synthesis of polymers containing chiral cavities and their use for resolution of racemates.* Makromolekulare Chemie-Macromolecular Chemistry and Physics, 1977. **178**(10): p. 2799-2816.

67. Mosbach, K., *Molecular Imprinting.* Trends in Biochemical Sciences, 1994. **19**(1): p. 9-14.

68. Arshady, R. and K. Mosbach, *Synthesis of substrate-selective polymers by host-guest polymerization.* Macromolecular Chemistry and Physics-Makromolekulare Chemie, 1981. **182**(2): p. 687-692.

69. Vlatakis, G., et al., *Drug assay using antibody mimics made by molecular imprinting.* Nature, 1993. **361**(6413): p. 645-647.

70. Makoto Komiyama, T.T., Takashi Mukawa, and Hiroyuki Asanuma, *Molecular imprinting from fundamentals to applications.* 2003, Weinheim: Wiley.

71. Atkins, P.W., *Physical chemistry.* 1996, Weinheim: VCH.

72. Atwood, J.W.S.J.L., *Supramolecular chemistry.* 2000, England: Wiley.

73. Langone, J.J., J. Franke, and H. Van Vanakis, *Nicotine and its metabolites. Radioimmunoassay for gamma-(3-pyridyl)-gamma-oxo-N-methylbutyramide.* Arch Biochem Biophys, 1974. **164**(2): p. 536-43.

74. Legros, J.J., *The radioimmunoassay of human neurophysins: contribution to the understanding of the physiopathology of neurohypophyseal function.* Ann N Y Acad Sci, 1975. **248**: p. 281-303.

75. Robinson, A.G., *Radioimmunoassay of neurophysin proteins: utilization of specific neurophysin assays to demonstrate independent secretion of different neurophysins in vivo.* Ann N Y Acad Sci, 1975. **248**: p. 246-56.

76. Bush, L.P., *Quantitative analysis of tobacco alkaloids by gas chromatography.* J Chromatogr, 1972. **73**(1): p. 243-7.

77. Cano, J.P., et al., *Determination of nicotine by gas chromatography. I. Material and method.* Ann Pharm Fr, 1970. **28**(9): p. 581-8.

78. Jacin, H., J.M. Slanski, and R.J. Moshy, *The determination of nicotine in tobacco and in particulate matter of smoke by gas chromatography.* Anal Chim Acta, 1968. **41**(2): p. 347-53.

79. Blache, D., et al., *A sensitive method for the routine determination of plasma nicotine by flame ionization gas-liquid chromatography.* Anal Biochem, 1984. **143**(2): p. 316-9.

80. Pendergrass, S.M., A.M. Krake, and L.B. Jaycox, *Development of a versatile method for the detection of nicotine in air.* AIHAJ, 2000. **61**(4): p. 469-72.

81. Medina, V.A., et al., *Mechanisms underlying the radioprotective effect of histamine on small intestine.* Int J Radiat Biol, 2007. **83**(10): p. 653-63.

82. Yamauchi, K., et al., *Progress in allergy signal research on mast cells: the role of histamine in goblet cell hyperplasia in allergic airway inflammation - a study using the Hdc knockout mouse.* J Pharmacol Sci, 2008. **106**(3): p. 354-60.

83. Ito, Y., T. Noguchi, and H. Naito, *Fluorometric-determination of gizzerosine, a histamine H2-receptor agonist discovered in feedstuffs, employing high-performance liquid-chromatography.* Analytical Biochemistry, 1985. **151**(1): p. 28-31.

84. Mell, L.D., R.N. Hawkins, and R.S. Thompson, *Fluorometric-determination of histamine in biological-fluids and tissue by high-performance liquid-chromatography.* Journal of Liquid Chromatography, 1979. **2**(9): p. 1393-1406.

85. Walters, M.J., *Determination of Histamine in Fish by Liquid-Chromatography with Post-Column Reaction and Fluorometric Detection.*

Journal of the Association of Official Analytical Chemists, 1984. **67**(6): p. 1040-1043.

86.   Bauza, T., et al., *Determination of biogenic-amines and their precursor amino-acids in wines of the vallee du Rhone by high-performance liquid-chromatography with precolumn derivatization and fluorometric detection.* Journal of Chromatography A, 1995. **707**(2): p. 373-379.

87.   Busto, O., et al., *Determination of biogenic amines in wines by high-performance liquid chromatography with on-column fluorescence derivatization.* Journal of Chromatography A, 1997. **757**(1-2): p. 311-318.

88.   Tan, C.J. and Y.W. Tong, *Molecularly imprinted beads by surface imprinting.* Analytical and Bioanalytical Chemistry, 2007. **389**(2): p. 369-376.

89.   Sellergren, B., *Imprinted dispersion polymers - a new class of easily accessible affinity stationary phases.* Journal of Chromatography A, 1994. **673**(1): p. 133-141.

90.   Sambe, H., et al., *Uniformly-sized, molecularly imprinted polymers for nicotine by precipitation polymerization.* Journal of Chromatography A, 2006. **1134**(1-2): p. 88-94.

91.   Sulitzky, C., et al., *Grafting of molecularly imprinted polymer films on silica supports containing surface-bound free radical initiators (vol 35, pg 79, 2002).* Macromolecules, 2002. **35**(8): p. 3314-3314.

92.   Haginaka, J., et al., *Uniform-sized molecularly imprinted polymer for (S)-naproxen selectively modified with hydrophilic external layer.* Journal of Chromatography A, 1999. **849**(2): p. 331-339.

93.   Zander, A., et al., *Analysis of nicotine and its oxidation products in nicotine chewing gum by a molecularly imprinted solid phase extraction.* Analytical Chemistry, 1998. **70**(15): p. 3304-3314.

94.   Ansell, R.J. and K. Mosbach, *Molecularly imprinted polymers by suspension polymerisation in perfluorocarbon liquids, with emphasis on the influence of the porogenic solvent.* Journal of Chromatography A, 1997. **787**(1-2): p. 55-66.

95.   Blahova, E. and J. Lehotay, *Sample preparation and HPLC determination of catechins in green tea.* Chemia Analityczna, 2006. **51**(5): p. 795-807.

96.   Piletsky, S.A., H.S. Andersson, and I.A. Nicholls, *Combined hydrophobic and electrostatic interaction-based recognition in molecularly imprinted polymers.* Macromolecules, 1999. **32**(3): p. 633-636.

97.   Toth, B., et al., *Which molecularly imprinted polymer is better?* Analytica Chimica Acta, 2007. **591**(1): p. 17-21.

98.   Turiel, E., et al., *HPLC imprinted-stationary phase prepared by precipitation polymerisation for the determination of thiabendazole in fruit.* Analyst, 2005. **130**(12): p. 1601-1607.

99.   Andersson, H.S., et al., *Study of the nature of recognition in molecularly imprinted polymers, II [1] - influence of monomer-template ratio and sample load on retention and selectivity.* Journal of Chromatography A, 1999. **848**(1-2): p. 39-49.

100.   Dirion, B., et al., *Water-compatible molecularly imprinted polymers obtained via high-throughput synthesis and experimental design.* Journal of the American Chemical Society, 2003. **125**(49): p. 15101-15109.

101. Lanza, F. and B. Sellergren, *Method for synthesis and screening of large groups of molecularly imprinted polymers.* Analytical Chemistry, 1999. **71**(11): p. 2092-2096.
102. Cheong, S.H., et al., *Synthesis and binding properties of a noncovalent molecularly imprinted testosterone-specific polymer.* Journal of Polymer Science Part a-Polymer Chemistry, 1998. **36**(11): p. 1725-1732.
103. Spivak, D.A., *Optimization, evaluation, and characterization of molecularly imprinted polymers.* Advanced Drug Delivery Reviews, 2005. **57**(12): p. 1779-1794.
104. Umpleby, R.J., M. Bode, and K.D. Shimizu, *Measurement of the continuous distribution of binding sites in molecularly imprinted polymers.* Analyst, 2000. **125**(7): p. 1261-1265.
105. Jenkins, A.L., O.M. Uy, and G.M. Murray, *Polymer-based lanthanide luminescent sensor for detection of the hydrolysis product of the nerve agent Soman in water.* Analytical Chemistry, 1999. **71**(2): p. 373-378.
106. Percival, C.J., et al., *Molecular imprinted polymer coated QCM for the detection of nandrolone.* Analyst, 2002. **127**(8): p. 1024-1026.
107. Dickert, F.L., et al., *Bioimprinted QCM sensors for virus detection - screening of plant sap.* Analytical and Bioanalytical Chemistry, 2004. **378**(8): p. 1929-1934.
108. Matsui, J., et al., *SPR sensor chip for detection of small molecules using molecularly imprinted polymer with embedded gold nanoparticles.* Analytical Chemistry, 2005. **77**(13): p. 4282-4285.
109. Rao, T.P., et al., *Biomimetic sensors for toxic pesticides and inorganics based on optoelectronic/electrochemical transducers - an overview.* Critical Reviews in Analytical Chemistry, 2007. **37**(3): p. 191-210.
110. Dickert, F.L., et al., *Synthetic receptors for chemical sensors - subnano- and micrometre patterning by imprinting techniques.* Biosensors & Bioelectronics, 2004. **20**(6): p. 1040-1044.
111. Sellergren, B., *Imprinted chiral stationary phases in high-performance liquid chromatography.* Journal of Chromatography A, 2001. **906**(1-2): p. 227-252.
112. Kempe, M., *Antibody-mimicking polymers as chiral stationary phases in HPLC.* Analytical Chemistry, 1996. **68**(11): p. 1948-1953.
113. Yin, J.F., G.L. Yang, and Y. Chen, *Rapid and efficient chiral separation of nateglinide and its L-enantiomer on monolithic molecularly imprinted polymers.* Journal of Chromatography A, 2005. **1090**(1-2): p. 68-75.
114. Wulff, G., *Enzyme-like catalysis by molecularly imprinted polymers.* Chemical Reviews, 2002. **102**(1): p. 1-27.
115. Strikovsky, A., J. Hradil, and G. Wulff, *Catalytically active, molecularly imprinted polymers in bead form.* Reactive & Functional Polymers, 2003. **54**(1-3): p. 49-61.
116. Yamazaki, T., et al., *Towards the use of molecularly imprinted polymers containing imidazoles and bivalent metal complexes for the detection and degradation of organophosphotriester pesticides.* Analytica Chimica Acta, 2001. **435**(1): p. 209-214.
117. Blackwell, A. and S.D. Minteer, *Molecularly imprinted poly(methylene green) as a drug release system.* Abstracts of Papers of the American Chemical Society, 2006. **231**: p. 1-12.

118.   Puoci, F., et al., *Molecularly imprinted polymers for alpha-tocopherol delivery.* Drug Delivery, 2008. **15**(4): p. 253-258.

119.   Schillemans, J.P. and C.F. van Nostrum, *Molecularly imprinted polymer particles: synthetic receptors for future medicine.* Nanomedicine, 2006. **1**(4): p. 437-447.

120.   N. Bonanos, B.C.H.S.E.P.B., *Impedance Spectroscopy: Applications of Impedance Spectroscopy.* 2 ed: John Wiley & Sons.

121.   Grimmes, S. and O.G. Martinsen, *Bioimpedance and bioelectricity basics.* 2000, London: Academic Press.

122.   Sauerbrey, G., *Verwendung von Schwingquarzen zur Wägung dünner Schichten und zur Mikrowägung.* Zeitschrift für Physik A Hadrons and Nuclei, 1959. **155**(2): p. 206-222.

123.   O'Sullivan, C.K. and G.G. Guilbault, *Commercial quartz crystal microbalances - theory and applications.* Biosensors and Bioelectronics, 1999. **14**(8-9): p. 663-670.

124.   O'Sullivan, C.K., R. Vaughan, and G.G. Guilbault, *Piezoelectric immunosensors - theory and applications.* Analytical Letters, 1999. **32**(12): p. 2353-2377.

125.   Shirakawa, H., et al., *Synthesis of electrically conducting organic polymers: halogen derivatives of polyacetylene, (CH)x.* J. Chem. Soc., Chem. Commun, 1977: p. 578-580.

126.   Louwet, F., D. Vanderzande, and J. Gelan, *A general synthetic route to high molecular weight poly(p-xylylene)-derivatives: a new route to poly(p-phenylene vinylene): Proceedings of the International Conference on Science and Technology of Synthetic Metals.* Synthetic Metals, 1995. **69**(1-3): p. 509-510.

127.   *Operation and service manual: PLO-10 series phase lock oscillator.* 2007, Cypress: Maxtek, Inc.

128.   Langmuir, I., *The adsorption of gases on plane surfaces of glass, mica and platinum.* Journal of the American Chemical Society, 1918. **40**(9): p. 1361-1403.

129.   Freundlich, H., *Colloid and capillary chemistry.* 1926, London: Methuen.

130.   Rasband, W.S., *ImageJ, U.S. National Institutes of Health, Bethesda, MD, USA* 2007.

131.   Cywinski, P., et al., *Fluorescent, molecularly imprinted thin-layer films based on a common polymer.* Journal of Applied Polymer Science, 2007. **105**(1): p. 229-235.

132.   Li, Z.M., et al., *Preparation for nitrocellulose membrane-poly(vinyl alcohol)-ionic imprinting and its application to determine trace copper by room temperature phosphorimetry.* Analytica Chimica Acta, 2007. **589**(1): p. 44-50.

133.   Lulka, M.F., et al., *Molecular imprinting of small molecules with organic silanes: Fluorescence detection.* Analytical Letters, 1997. **30**(13): p. 2301-2313.

134.   Turkewitsch, P., et al., *Fluorescent functional recognition sites through molecular imprinting. A polymer-based fluorescent chemosensor for aqueous cAMP.* Analytical Chemistry, 1998. **70**(10): p. 2025-2030.

135.   Chang, C.-P., et al., *Fluorescent conjugated polymer films as TNT chemosensors.* Synthetic Metals, 2004. **144**(3): p. 297-301.

136.   Matsui, J., O. Doblhoffdier, and T. Takeuchi, *2-(trifluoromethyl)acrylic acid: A novel functional monomer in non-covalent molecular imprinting.* Analytica Chimica Acta, 1997. **343**(1-2): p. 1-4.

137.   Bart, M., et al., *On the response of a label-free interferon-gamma immunosensor utilizing electrochemical impedance spectroscopy.* Biosensors & Bioelectronics, 2005. **21**(1): p. 49-59.

138.   Fernandez-Sanchez, C., C.J. McNeil, and K. Rawson, *Electrochemical impedance spectroscopy studies of polymer pegradation: application to biosensor development.* Trac-Trends in Analytical Chemistry, 2005. **24**(1): p. 37-48.

139.   Guan, J.G., Y.Q. Miao, and Q.J. Zhang, *Impedimetric biosensors.* Journal of Bioscience and Bioengineering, 2004. **97**(4): p. 219-226.

140.   Paenke, O., et al., *Impedance spectroscopy and biosensing.* Biosensing for the 21st Century, 2008. **109**: p. 195-237.

141.   Breselge, M., et al., *Comparison of the electrical characteristics of four 2,5-substituted poly(p-phenylene vinylene) derivatives with different side chains.* Thin Solid Films, 2006. **511**: p. 328-332.

142.   Lide, D.R., *Handbook of chemistry and physics.* 1998: CRC Press.

143.   Abdallah, T., et al., *Surface plasmons resonance technique for the detection of nicotine in cigarette smoke.* Sensors and Actuators a-Physical, 2003. **102**(3): p. 234-239.

144.   Svob Troje, Z., Z. Fröbe, and D. Perovic, *Analysis of selected alkaloids and sugars in tobacco extract.* Journal of Chromatography a, 1997. **775**(1-2): p. 101-107.

145.   Troje, Z.S., Z. Frobe, and D. Perovic, *Analysis of selected alkaloids and sugars in tobacco extract.* Journal of Chromatography a, 1997. **775**(1-2): p. 101-107.

146.   Sergeyeva, T.A., et al., *Porous molecularly imprinted polymer membranes and polymeric particles.* Analytica Chimica Acta, 2007. **582**(2): p. 311-319.

147.   Perez-Moral, N. and A.G. Mayes, *Comparative study of imprinted polymer particles prepared by different polymerisation methods.* Analytica Chimica Acta, 2004. **504**(1): p. 15-21.

Appendix 1: Nomenclature

ν	Freundlich heterogeneity parameter
θ	contact angle
A	Freundlich constant
AC	alternating current
ACN	acetonitrile
AIBN	azobisisobutyronitrile
C_b	bound concentration of target molecules
C_{dl}	double layer capacitance
C_f	free concentration of target molecules
C_i	initial concentration of target molecules
CPE	constant phase element
CVD	chemical vapor deposition
dH_2O	distilled water
DNA	deoxyribonucleic acid
EGDM	ethylglycol dimethacrylate
EIS	electrochemical impedance spectroscopy
ETD	Everhart and Thornley detector

HPLC	high-performance liquid chromatography
IBS	irritable bowel syndrome
Ig's	immunoglobulins
K	binding constant
LC	liquid chromatography
LD50	lethal dosage to kill 50% of the population
LEDs	light emitting diodes
LFD	large-field detector
LSCM	laser scanning confocal microscope
MAA	methacrylate
MIP	molecularly imprinted polymer
N	number of binding sites
NIP	non – imprinted polymer
NIR	near infrared
PBS	phosphate buffered saline
PDMS	polydimethylsiloxane
PLO	phase lock oscillator
PMAA	polymethacrylate
POC	point-of-care
ppm	parts per million
QCM	quartz crystal microbalance
R	radius
R_{ct}	charge transfer resistance

R_p	polarization resistance
R_s	solution resistance
S_0	electronic ground state
SAMs	self-assembled monolayers
Sb	amount of target molecules bound by the MIP per unit weight
SEM	scanning electron microscopy
SPR	surface plasmon resonance
TNT	trinitrotoluene
UV	ultraviolet
UV/Vis	ultraviolet/visible
wt%	weight percentage

Appendix 2: Publications and conference contributions

Publications:

- Electrical sensing of histamine based on molecular imprinted polymers, R. Thoelen, J. Alenus, J. Duchateau, F. Horemans, L. Lutsen, D. Vanderzande, T.J. Cleij, and P. Wagner, Biosensors & Bioelectronics, in preparation.

- A MIP-based impedimetric sensor for the detection of low-MW molecules, R. Thoelen, R. Vansweevelt, J. Duchateau, D. Vanderzande, M. Ameloot, T.J. Cleij, and P. Wagner, Biosensors & Bioelectronics 23 (6), 913-918 (2008).

- Application of functional PPV-derivatives prepared via the sulfinyl precursor route as transducers in impedimetric biosensors, I. Van Severen, P. Cooreman, R. Thoelen, L. Lutsen, P. Wagner, D. Vanderzande, and T. J. Cleij, Polymer Preprints 47 (1), 478-479 (2006).

- Impedimetric immunosensors based on the conjugated polymer PPV, P. Cooreman, R. Thoelen, J. Manca, M. vandeVen, V. Vermeeren, L. Michiels, M. Ameloot, and P. Wagner, Biosensors & Bioelectronics 20, 2151 – 2156 (2005).

- The influence of surface treatments on cathode formation and stability in polymer light emitting diodes, F.J.J. Janssen, A.W. Denier van der Gon, L.J. van IJzendoorn, R. Thoelen, M.J.A. de Voigt and H.H. Brongersma, Applied Surface Science 241 (3-4), 335-351 (2005).

Oral conference contributions:

- Belgian Physical Society (PBS) International Scientific Meeting, Vrije Universiteit Brussel, Brussel, Belgium, 21/05/2008, Piezoelectric and Electrochemical Sensing of Small Molecules using Synthetic MIP-based Receptors, R. Thoelen, J. Alenus, F. Horemans, J. Duchateau, L. Lutsen, D. Vanderzande, T.J. Cleij, and P. Wagner.

- Mikrosysteme in der Medizin (Ak BioMST), Technologiezentrum Dortmund, Germany, 19-20/06/2007, Impedimetrischer Nachweis von Nikotin mit MIPs – molekular geprägte Polymere als synthetische Rezeptoren, R. Thoelen. (invited lecture)

- Regionale ontwikkelingen op het gebeid van de (bio-)medische devices, Campus Technische Universiteit Eindhoven, Eindhoven, the Netherlands, 5/06/2007, Materialen op maat voor bio- en chemosensoren: van nicotine tot DNA, R. Thoelen, S. Wenmackers.

- Deutsches Biosensor Symposium (DBS), Ruhr-Universität Bochum, Bochum, Germany, 18-21/03/2007, Impedimetrische Sensoren auf der Basis von molekular geprägten Polymeren zum Nachweis von Nikotin, R. Thoelen, J. Duchateau, R. Vansweevelt, F. Horemans, J. D'Haen, L. Lutsen, T.J. Cleij, D. Vanderzande, and P. Wagner.

- The Ninth World Congress on Biosensors, Toronto, Canada, 10-12/05/2006, A MIP-based Impedimetric Sensor for the Detection of low-MW Molecules, R. Thoelen, R. Vansweevelt, J. D'Haen, J. Duchateau, F. Horemans, L. Lutsen, T.J. Cleij, D. Vanderzande, M. Ameloot, and P. Wagner.

- Belgian Physical Society (PBS) International Scientific Meeting, Université de Mons-Hainaut, Mons, Belgium, 25-26/05/2004, Using biologically activated polymer films as a biosensor, R. Thoelen, P. Cooreman, J. Manca, L. Lutsen, D. Vanderzande, R. Carleer, M. vandeVen, L. Michiels, and M. Ameloot and P. Wagner.

Poster conference contributions:

- BPG general meeting, De Haan, Belgium, 22-23/05/2008, Piezoelectric and Electrochemical Sensing of Small Molecules using Synthetic MIP-based Receptor, R. Thoelen, J. Alenus, F. Horemans, J. Duchateau, L. Lutsen, D. Vanderzande, T.J. Cleij, and P. Wagner.

- The Tenth World Congress on Biosensors, Shangai, China, 14-16/05/2008, Piezoelectric and Electrochemical Sensing of Small Molecules using Synthetic MIP-based Receptor, R. Thoelen, J. Alenus, F. Horemans, J. Duchateau, L. Lutsen, D. Vanderzande, T.J. Cleij, and P. Wagner.

- Joint general scientific meeting 2007 of the Belgian Physical Society and Belgian Biophysical Society, Universiteit Antwerpen, Antwerp, Belgium, 30/05/2007, Impedimetric sensing of small molecules using molecularly imprinted polymers, R. Thoelen, J. Duchateau, R. Vansweevelt, F. Horemans, L. Lutsen, J. D'Haen, D. Vanderzande, M. vandeVen, M. Ameloot, T.J. Cleij, and P. Wagner.

- Biomedica event 2007, Aachen, Germany, 21-22/03/2007, An Impedimetric Sensor based on Molecularly Imprinted Polymers for the Detection of Nicotine, J. Duchateau, R. Thoelen, R. Vansweevelt, , F. Horemans, J. D'Haen, L. Lutsen, T.J. Cleij, D. Vanderzande, M. vandeVen, M. Ameloot, and P. Wagner.

- 10th Bioforum, Bioliège, ULG, Luik, Belgium, 17/05/2006, Impedance Based Sensing of low MW Molecules Using Imprinted Nanocavities, R. Thoelen, R. Vansweevelt, J. Duchateau, D. Vanderzande, L. Lutsen, M. vandeVen, M. Ameloot, P. Wagner, and T.J. Cleij.

- Cargèse International School NanoSciencesTech, Cargèse, Corsica, France, 3-15/06/2006, Impedance Based Sensing of low MW Molecules Using Imprinted Nanocavities, R. Thoelen, R. Vansweevelt, J. Duchateau, L. Lutsen, T.J. Cleij, D. Vanderzande, M. vandeVen, M. Ameloot, and P. Wagner.

- Fysica 2006 Symposium (BNV-NNV), Leiden, The Netherlands, 28/04/2006, Electrical Sensing of Small Molecules with Molecularly Imprinted Nanocavities, R.

Thoelen, R. Vansweevelt, J. Duchateau, D. Vanderzande, P. Wagner, and T. J. Cleij.

- 3rd International Symposium on Sensor Science, Jülich, Germany, 18-21/06/2005, A polymer based impedimetric immunosensor, R. Thoelen, P. Cooreman, J. Manca, L. Lutsen, D. Vanderzande, R. Carleer, M. vandeVen, L. Michiels, and M. Ameloot and P. Wagner.

- Congrès general de la société Française de physique et de la Belgian Physical Society, Lille, France, 29/09/2005 – 2/11/2005, A polymer based impedimetric immunosensor, R. Thoelen, P. Cooreman, J. Manca, L. Lutsen, D. Vanderzande, R. Carleer, M. vandeVen, L. Michiels, and M. Ameloot and P. Wagner.

Appendix 3: Awards

- Best Poster Award, Biomedica event 2007, Aachen, Germany, 21-22/03/2007,

An Impedimetric Sensor based on Molecularly Imprinted Polymers for the Detection of Nicotine, J. Duchateau, R. Thoelen, R. Vansweevelt, , F. Horemans, J. D'Haen, L. Lutsen, T.J. Cleij, D. Vanderzande, M. vandeVen, M. Ameloot, and P. Wagner.

- BIO TECH Intl Award "From research to industrial application", 10th Bioforum 2006, Luik, Belgium. 17/05/2006,

Impedance Based Sensing of low MW Molecules Using Imprinted Nanocavities, R. Thoelen, R. Vansweevelt, J. Duchateau, D. Vanderzande, L. Lutsen, M. vandeVen, M. Ameloot, P. Wagner, and T.J. Cleij.

- Scientific Poster Award, Life Science Limburg, Cells at Work II congress 2004, Maastricht, the Netherlands.

An impedimetric immunosensor based on semiconducting polymerfilms, P. Cooreman, R. Thoelen, J. Manca, L. Lutsen, D. Vanderzande, R. Carleer, M. vandeVen, L. Michiels, and M. Ameloot and P. Wagner.

Appendix 4: List of figures

151

Appendix 5: List of tables